2018

Nano-engineered heated pavements

Ali Arabzadeh
Iowa State University

Nano-engineered heated pavements

by

Ali Arabzadeh

A dissertation submitted to the graduate faculty

in partial fulfillment of the requirements for the degree of

DOCTOR OF PHILOSOPHY

Major: Civil Engineering (Civil Engineering Materials)

Program of Study Committee:
Halil Ceylan, Co-major Professor
Kasthurirangan Gopalakrishnan, Co-major Professor
Sunghwan Kim
Peter C. Taylor
Sriram Sundararajan
Paul Spry

The student author, whose presentation of the scholarship herein was approved by the program of study committee, is solely responsible for the content of this dissertation. The Graduate College will ensure this dissertation is globally accessible and will not permit alterations after a degree is conferred.

Iowa State University

Ames, Iowa

2018

TABLE OF CONTENTS

Page

LIST OF FIGURES

Page

LIST OF TABLES

Page

ACKNOWLEDGMENTS

This thesis was made possible due to masterly guidance and support of my advisor, Professor Halil Ceylan, whose mentorship helped me find the way; his motivation inspired me to persevere when things were not working. I also would like to thank him for maintaining a positive, progressive environment in our research group.

I owe my deepest gratitude to Dr. Kim, first, by providing comments and advice whenever I faced a research challenge, and then for being such a great organizer in our research team. Had it not been for his guidance and patience, I would not have been able to finish my Ph. D. studies in a timely manner.

I am fortunate to have Dr. Kasthurirangan Gopalakrishnan as my co-major professor. His feedback during my Ph. D. studies has always been of huge help and his suggestions have always helped me add to the value of my research. It is also an honor for me to have had Drs. Peter C. Taylor, Sriram Sundararajan and Paul Spry on my program of study committee, and their comments and feedback throughout my research projects are greatly appreciated.

I am very grateful to Mr. Robert Steffes, our PCC lab manager, for always kindly assisting me with lab investigations and providing a very friendly environment at the lab. I owe a lot to Mr. Paul Kremer for allowing me access to the labs at the Town Engineering building at ISU. Had it not been for him, a major portion of my Ph. D. studies would have not been accomplished. I also would like to thank Therin Young, a graduate student from the Mechanical Engineering department at ISU, for helping me with my interdisciplinary research. Therin's findings set a milestone for accomplishing the portion of my Ph.D. studies that is related to nano-based materials. This study was

conducted at Iowa State University under the Federal Aviation Administration (FAA) Air Transportation Center of Excellence Cooperative Agreement 12-C-GA-ISU for the Partnership to Enhance General Aviation Safety, Accessibility and Sustainability (PEGASAS). I would like to thank the current project Technical Monitor, Mr. Benjamin J. Mahaffay, and the former project Technical Monitors, Mr. Jeffrey S. Gagnon (interim), Mr. Donald Barbagallo, and Dr. Charles A. Ishee, and the former program manager, Mr. Peter L. Sparacino for their invaluable guidance on this study. I also would like to thank the PEGASAS Industry Advisory Board members for their valuable support and feedback.

I would like to thank my friend and colleague Alireza Sassani for assisting me with joining Professor Ceylan's research group. I also would like to thank Alireza because of all his support during my Ph. D. studies and accompanying me in times of hardship. I also would like to thank my friend and colleague Sharif Gushgari for being such a good friend since the time we both joined ISU.

Last but not the least, I would like to acknowledge the people who mean a lot to me, my family. I thank my father for always being a role model for me and doing his best to encourage and support his children to achieve the highest levels of education, and I would like to mention here that he did not have the chance to go to school. I also would like to thank my mother for her guidance throughout my life. I also would like to thank my sister for taking care of my parents when I was away; it was because of her that I could pursue my graduate studies.

ABSTRACT

Millions of dollars are spent annually for removing ice and snow from paved surfaces using conventional techniques such as deployment of snow plowing equipment and use of deicing chemicals that are neither economical nor environmentally friendly. Alternative approaches such as producing superhydrophobic (super water-repellent) pavement surfaces and implementing electrically-conductive heated pavement systems, or even merging these two technologies to produce hybrid heated pavement systems, can alleviate many of the problems associated with conventional ice and snow removal techniques.

In this study, superhydrophobic concretes – including hot mix asphalt (HMA) and portland cement concrete (PCC) – and electrically-conductive asphalt matrices, including electrically conductive asphalt (ECAM) mastic and electrically-conductive cement paste (ECCP), were fabricated, and their characteristics evaluated. Water repellency of superhydrophobic HMA and superhydrophobic PCC was characterized through static water contact angle (WCA) measurements, and the frictional properties of these coated concrete were characterized using a microtribometer and a British pendulum tester. The electrical and thermal properties of ECAM and ECCP were characterized through volume resistivity measurements and active infrared thermography (IRT). These evaluations performed on superhydrophobic concretes and electrically-conductive matrices revealed that superhydrophobic HMA and superhydrophobic PCC are capable of repelling water, and possibly of repelling ice/snow. It was also found that ECAM and ECCP can generate enough heat for melting ice and snow at below freezing temperatures. Although it was found that ECCP can generate more heat than ECAM, this depends somewhat on the

design requirements for selecting a matrix for binding aggregate systems together to result in a concrete (either HMA or PCC), implemented in a heated pavement system, that can efficiently melt ice and snow.

CHAPTER 1. INTRODUCTION

Background

Ice and snow on the surface of airport pavements has always been a source of concern, and, millions of dollars are spent annually for removing ice and snow from pavement surfaces. Since the beginning of "all-weather" aircraft operations there have been landing and aborted takeoff incidents or accidents during each winter because of slippery and icy conditions on airport pavement surfaces. To overcome such problems, it is imperative to develop new technologies that can more effectively and efficiently remove or prevent the formation of ice and snow on asphalt cement concrete (ACC) and portland cement concrete (PCC) paved surfaces. Some of the newly emerged or emerging techniques for this purpose include application of superhydrophobic coatings on pavement surfaces to prevent ice formation or curb snow accumulation or implementation of electrically-conductive asphalt concrete (ECAC) or electrically-conductive portland cement concrete (ECON) for melting ice and snow or preventing their formation or accumulation.

ACC and PCC surfaces can be coated with nano-based materials to impart superhydrophobicity (super water-repellency) and icephobicity to these types of concrete. Such properties can be achieved by creating surface coatings made from low surface energy materials with embedded hierarchical structures. While there are many available low surface energy materials and many methods for synthesizing surface coatings for producing superhydrophobic/icephobic ACC and PCC, according to the reported literature, producing superhydrophobic coatings on ACC and PCC has not yet been attempted. Superhydrophobic ACC and PCC surfaces must also be able to maintain skid resistance when there is no ice/snow

present on these surfaces; such technology would be useless if it causes skidding problems during warm seasons.

Some recent studies have highlighted the potential for enabling electrically-conductive ACC and PCC through the addition of conductive materials (carbon fibers, graphite powder, etc.) to conventional ACC and PCC for electrical heating-based snow and ice removal applications. Such conductive materials could be used to improve the electrical conductivity of a pavement layer or improving the heat conductance of the pavement itself. The reported studies also seem to indicate that optimization of electrically-conductive asphalt concrete (ECAC) or electrically-conductive portland cement concrete (ECON) mix design to achieve the desired conductivity properties for practical applications without loss of mechanical performance and compaction properties is a highly challenging task.

Objective

The primary objectives of this research are as follow:

- To synthesize superhydrophobic ACC and PCC surfaces that can repel moisture and reduce ice adhesion, then investigate their tribological properties such as friction at microscale.
- To develop electrically-conductive asphalt mastic (ECAM) and electrically-conductive cement paste (ECCP) and characterize their electrical and thermal properties to investigate the heat generation efficiency of these matrices (both ECAM and ECCP) binding aggregate systems with respect to producing self-heating ACC and PCC.

The overall goal of this study is to investigate and produce materials to be used for producing water/ice-repellent and self-heating pavements to introduce state-of-the-art

methods/materials for mitigating winter-related maintenance problems in critical areas such as airports, bridge decks, etc. It is hoped that the findings of this study will suggest suitable substitutes for costly and non-environmental-friendly methods, such as deployment of snow removal equipment and use of deicing chemicals that are conventionally practiced for removing ice and snow from pavement surfaces.

Dissertation organization

This journal paper-based dissertation is organized as follows:

Chapter 1 includes a summarized background, research objectives, and dissertation organization.

Chapter 2 provides a state-of-the-art annotated bibliography, including a thorough literature review on different nano-materials, nano-coatings, coating methods, electrically-conductive materials, and methods for synthesizing and characterizing electrically-conductive asphalt-based materials.

Chapter 3 presents the first journal article: ***Superhydrophobic coatings on asphalt concrete surfaces: toward smart solutions for winter pavement maintenance*** that discusses methods for producing superhydrophobic coatings on ACC surfaces using spray deposition techniques, varying dosage rates of the selected low surface energy materials sprayed, and changing spray deposition duration. This article also describes the techniques used for characterizing water repellency and skid resistance of the synthesized coatings. In this article, the water repellency of coatings was characterized in terms of static water contact angle (WCA) measurements, with the tribological behavior of coatings measured with a microtribometer.

Chapter 4 presents the second journal article: ***Superhydrophobic coatings on Portland cement concrete surfaces*** that discusses methods for producing superhydrophobic coatings on PCC, then explains the characterization method used for evaluating water repellency and skid

resistance of the synthesized coatings using different low surface energy materials. In this article, water repellency was characterized by static WCA measurement and skid resistance was evaluated using a British pendulum tester with friction values reported in the form of British pendulum numbers (BPNs).

Chapter 5 presents the third journal article: ***Temperature-related anisotropic behavior of electrically-conductive asphalt mastic*** that describes a procedure for synthesizing single-phase and two-phase ECAMs and explains the volume resistivity characterization, highlights the influence of temperature change on volume resistivity measurements, and explains in detail the resistive-heating heat generation process in ECAM .

Chapter 6 presents the fourth journal article: ***Electrical and thermal properties of cement paste and asphalt mastic modified by electrically-conductive carbon-based materials*** that describes the method for synthesizing single-phase and two-phase matrices (both ECAM and ECC), compares the electrical behavior of ECAM and ECCP modified with the same carbon-based materials (at the same dosage rates), and discusses heat generation and propagation phenomena in both ECAM and ECCP.

Chapter 7 provides a summary along with conclusions and recommendations for future studies.

CHAPTER 2. LITERATURE REVIEW

This chapter provides a state-of-the-art annotated bibliography, including a thorough literature review on different nano-materials, nano-coatings and coating methods for producing superhydrophobic and icephobic ACC and PCC surfaces. This chapter also includes an extended literature review on electrically-conductive materials and methods for synthesizing and characterization of electrically-conductive asphalt-based materials. In addition to the information provided in this chapter, each journal article included in this study will have its own literature review, specific to its particular scope.

Review on Superhydrophobic ACC and PCC

Background and Motivation

Presence of ice and snow on the surface of ACC and PCC pavements has always been a source of concern for both users and agencies in charge of maintaining pavements. Millions of dollars are spent annually on removing ice and snow from roadways [1]. In airports, since the beginning of “all weather” aircraft operations, there have been numerous aborted landing and takeoff incidents or accidents each winter because of slippery and icy conditions on aprons, taxiways, and runways.

Ice accumulation on airplanes, power lines, wind turbines, etc. is another important concern for agencies that has drawn the attention of many researchers during the last decade. Conventional current approaches for ice/snow removal include spraying large quantities of anti-ice agents on paved areas and deploying a great number of snow plowing vehicles, etc. These are costly and time consuming [2], and research is underway around the world to develop pavements resistant to freezing-induced damages.

For mitigating problems associated with ice/snow formation on paved surfaces, superhydrophobic coating techniques [3]–[6] have received recent attention as alternatives to traditional ice and snow removal practices for reducing ice adhesion. The benefits of superhydrophobic coatings could also be combined with those of heated pavement systems in a hybrid heated pavement system (HPS) framework, potentially yielding greater water and ice repellency. Preventing or reducing ice/snow formation/accumulation is more desirable than fighting against their build-up, and a time-efficient method for mitigating problems associated with ice/snow accumulation is to use superhydrophobic coatings with icephobic properties.

An HPS houses electrodes inside the pavement surface, and the potential for moisture-related damage to ACC or PCC surfaces should be eliminated. There are severe downsides to water penetration, including electrode corrosion potential and other moisture damage potential of ACC and PCC such as increasing ice adhesion on the surface. Prevention of water penetration would essentially increase the lifecycle of ACC and PCC pavements and imbedded electrodes in HPS.

Hydrophobicity

A surface is classified as hydrophobic if it repels water and as hydrophilic if it absorbs water [2], [6]. The magnitude of cohesive forces within water molecules and adhesive forces associated with the interaction between water and surface determine the wettability of a surface. If cohesive forces within the water molecule are greater than adhesive forces enveloped between water and surface, water droplets will bead up without wetting the surface.

Two distinct models are proposed to explain the roughness effect [7]. On one hand, according to Wenzel model, roughness increases the surface area of a solid and geometrically improves its hydrophobicity. The Cassie model, on the other hand, explains that air trapped beneath the droplets can lead to further enhancement of hydrophobicity. Tiny entrapped air

pockets reduce the solid-liquid contact area, making the surface superhydrophobic. If these two aforementioned roughness induction methods are applied on certain types of hydrophobic materials with low surface energy, the final products will be superhydrophobic.

Static WCA (i.e., θ_{CA} in *Figure 2.1*) can be used to characterize the wetting behavior of a surface; it is the angle a static water droplet makes with the surface, and, based on measured WCA, surfaces are classified as [8]: (a) hydrophilic ($0 < WCA < 90$), hydrophobic ($90 < WCA < 150$) and superhydrophobic ($150 < WCA < 180$).

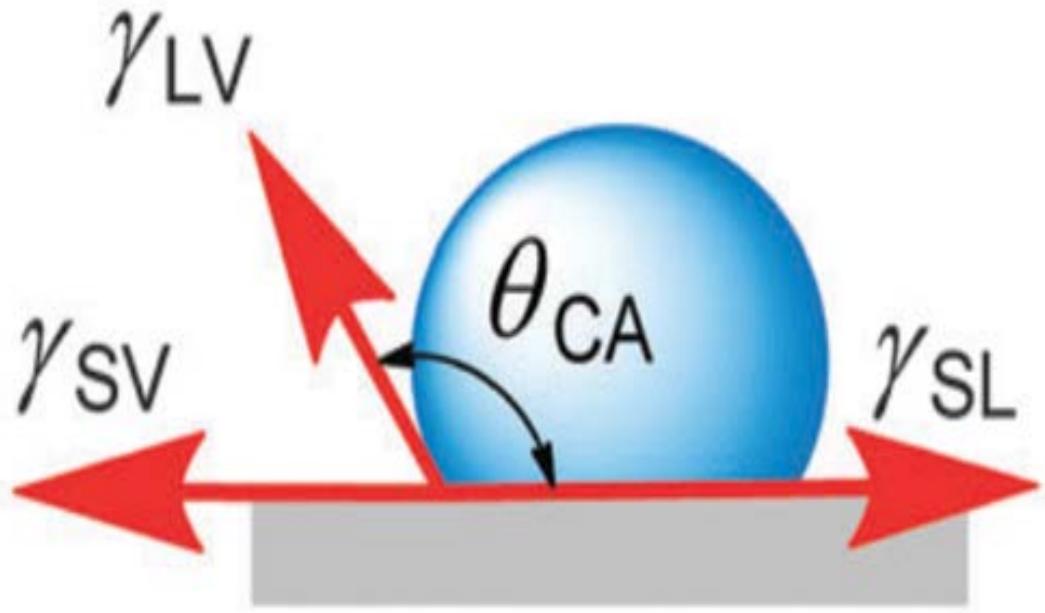

Figure 2.1 *Schematic of static WCA measurement and interfacial forces between solid, liquid and vapor phases* [8].

In addition to the WCA, the work of adhesion can also be considered as a criterion for showing how water-repellent a nano-coated ACC or PCC can be [2], [6].. The lower the work of adhesion, the more ice/snow repellent a surface becomes. The work of adhesion can be calculated using Equation (1).

$$W_A = \gamma_{LV}(1 + cos\theta) \quad (1)$$

Where: W_A = work of adhesion at contact angle θ, and γ_{LV} is the surface tension of water, 72.8 mN/m.

Hydrophobicity and Icephobicity

Icephobicity has long been a subject of debate [9] (Hejazi, et al. 2013), and icephobic surfaces are believed to both delay the formation of ice nuclei and reduce adhesive forces (both shear and normal) between ice and surface [9]–[12]. According to the literature, superhydrophobic coatings can possess ice-repellent properties [13], and early studies of icephobic surfaces have focused on droplet-on-liquid interactions that can affect ice formation.

Methods for Producing Superhydrophobic Surfaces

Several physical and chemical modifications have been developed in various disciplines to identify suitable methods for producing superhydrophobic surfaces. Methods for synthesizing superhydrophobic surfaces include wax solidification, lithography, polymer conformation, vapor deposition, sublimation, plasma techniques, etc., [14]. According to Young [15], who did a fundamental investigation to identify suitable superhydrophobic materials for ice-and snow-free airport concrete pavements, a layer-by-layer (LBL) spray deposition technique can be used for producing superhydrophobic ACC and PCC. However, research still continues to find other scalable coating materials and coating methods for producing ice-repellent coatings on the airfield paved area surfaces . The findings of Young during his Ph.D. studies [15] had a huge impact on investigating the feasibility of fabricating superhydrophobic ACC and PCC in this study [2], [3], [6].

Review on Electrically-conductive Asphalt-based Materials

Background and Motivation

According to FAA AC 150/5200-30D, Airport Winter Safety and Operations [16], presence of contaminants such as ice, snow, or slush on paved areas of airfields causes hazardous conditions that can lead to airplane incidents or even accidents. Moreover, snowstorms often reduce airport traffic volume through flight delays or cancellations, or, in the worst case scenario, airport closure [16]. To mitigate such winter-related problems, an airport operator attempts to select an appropriate time-saving approach to minimize the costs and efforts associated with ice and snow removal from the surface of runways, taxiways, aprons, etc. [16]. One such method previously mentioned in this study is the use of superhydrophobic coatings. Another alternative is to use a HPS made of ECAC that can be used for anti-icing and de-icing purposes by generating heat through resistive heating.

Conventional asphalt concrete is not electrically conductive but rather highly resistive owing to the high electrical resistivity of its components that can include aggregate, asphalt binder, and mineral filler. Electrical resistivity of asphalt concrete can be significantly reduced through the addition of conductive materials such as powders, fibers, and solid particles [17]. Experimental studies on ECAC reported in the literature indicate that optimization of ECAC mix design to achieve high conductivity (for pavement de-icing applications), and at the same time maintain adequate mechanical properties, is a challenging task warranting thorough and detailed experimental investigation [18], [19]. According to the existing literature [17], conductive materials incorporated into ECAC can broadly be categorized as: (a) powders, e.g., graphite or carbon black (CB); (b) fibers , e.g., carbon fiber (CF), steel fiber, or carbon nano-fiber (CNF) (SF); (c) shavings, e.g., steel shaving (SS); and (d) solid particles (substituting for coarse aggregate in part) . e.g., steel slag (SS) and marconite. Considering the wide variety of available

conductive materials, it is of paramount importance to consider conductive materials in terms of their associated costs and rate them with respect to their potential for achieving economic and efficient heated pavements based on literature review results, experimental results, and material supplier recommendations. Through such a rating system, the highest ranked conductive materials can be selected for development of ECAC. It is also important to note that steel-based conductive materials should not be given priority in the evaluation process, since they generate several concerns, e.g., producing foreign object debris (FOD), causing safety-related issues, availability, etc., associated with their use in airport pavements.

It is also inferred that the use of large quantities of a single conductive material to achieve higher conductivity in asphalt mixtures is not only cost-prohibitive, but can also degrade mechanical performance. To overcome such problems, the combined use of conductive powders and fibers in asphalt concrete can potentially lead to achieving a cost-effective and well-performing ECAC with adequate electrical and mechanical properties [20].

Although several mixing procedures have been randomly explored by previous research studies, there is no systematic guidance or specification available on optimal mixing technology for ECAC. One study [17], for example, indicated that a desirable mixing procedure would be one that can disperse conductive fillers uniformly in asphalt mixture without excessively increasing the mixing temperature and asphalt content. Two mixing procedures, dry and wet, have typically been employed for preparing ECAC specimens at the lab. In the dry mixing procedure [21], conductive materials are either mixed with dry aggregate before adding asphalt binder or added directly to the asphalt and aggregate mixture. The wet mixing procedure [22], on the other hand, entails introducing the conductive materials into the asphalt binder matrix, then adding the modified binder into the aggregate for final mixing. Comparing these two mixing

methods can provide useful information regarding their practicality for achieving the ultimate goal, optimum field implementation.

The quality of conductivity enhancement in asphalt concrete can be evaluated by resistivity measurements. Among different methods for measuring resistivity, the two-probe method is more common for measuring the conductivity of ECAC [18], [23], [24]. Based on the literature, the resistivity of asphalt concrete has been measured at different temperatures, including 15ºC [23], 20ºC [18], and 25ºC [24]. Asphalt is a highly temperature-dependent material [25]–[27] and its behavior in terms of resistivity should be studied over a wider temperature range. Moreover, ECAC, in the context of ice and snow melting, should be able to maintain high electrical conductivity at low temperatures.

Concepts behind Electrical Conductivity

Resistance and resistivity

Resistance (R) is an electrical property defined as the ratio of applied voltage to the electric current. The resistance of an object depends on its dimensions and its materials' composition. With respect to dimensions, increasing length increases the R value and increasing the cross-sectional area section results in reduction of the R value. To eliminate the effect of an object's geometry, one can alternatively consider resistivity (ρ) that is representative of intrinsic property of materials. The electrical resistivity of asphalt-based materials can be obtained using Ohm's law [18]:

$$\rho = \frac{RS}{L} \quad (2)$$

Where:

ρ = electrical resistivity measured in Ω cm,

R = electrical resistance measured in Ω,

S = electrode conductive area measured in cm^2, and

L = the distance between electrodes within or on the surface of concrete.

Conductance, denoted by G, is the inverse of resistance, i.e., 1/R.

Within the context of composite materials, there are two types of resistance: composite and contact [28]. Composite resistance is defined as the resistance of individual fibers that depends on their material properties and aspect ratios. Contact resistance, on the other hand, deals with passage of electrons between adjacent fibers that are in contact (*Figure 2.2*). Such contact resistance solely depends on the common surface area between the fibers in contact, because the matrix is almost electrically-insulating.

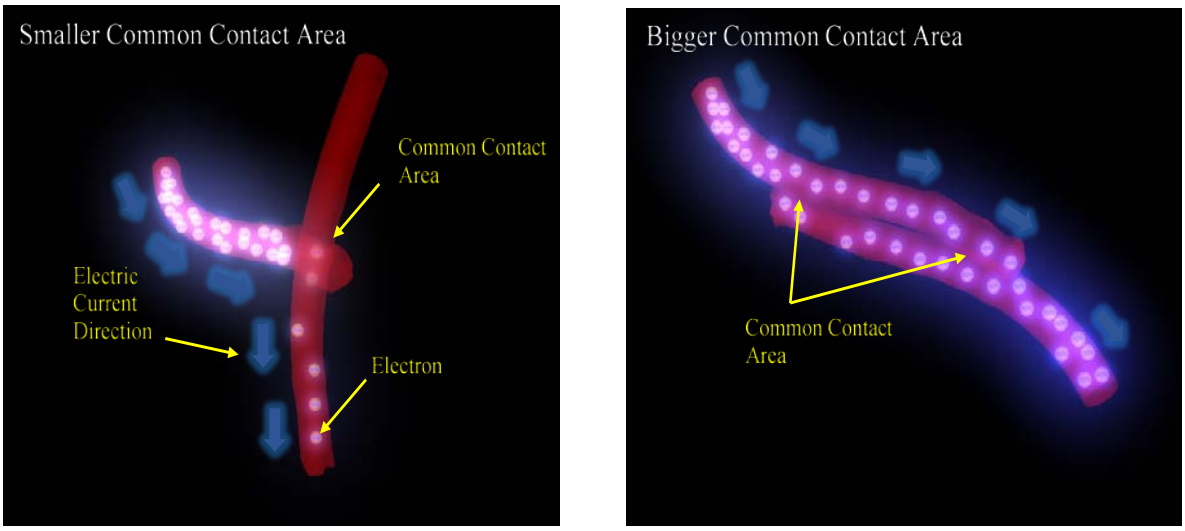

Figure 2.2 *Mechanism of electron passage through common contact area of fibers.*

Percolation threshold

Percolation theory, in essence, is used to define how a given set of regularly or randomly positioned sites is interconnected in a space [29]. Based on this theory, at some critical probability - referred to as percolation threshold -, an interconnected network of sites is formed

that causes the system to percolate at the span of the material under study [30]. Percolation theory has been utilized in a broad range of applications, such as spread of disease in a population, flow of a fluid in a porous medium, quarks in nuclear matter, etc.. Percolation theories, in the context of conductivity, are applied to explain insulator-to-conductor transitions in materials composed of conductive filler(s) and an insulating matrix [31]. The sudden transition (from insulator to conductor) within these materials is evidence of a percolation threshold [30].

When a small amount of conductive material is added within an insulating matrix, they are completely isolated and electrons cannot travel through the added conductive materials rendering the composite to continue as an insulator. However, an increase in percentage of conductive materials allows them to contact one another.

The greater the amount of conductive materials, the greater the amount of contact, and hence the greater the conductivity of the composite (*Figure 2.3*). Addition of conductive materials causes a gradual increase in conductivity, i.e., a gradual decrease in resistivity. When the conductive material content reaches a threshold value, a first few continuous conductive paths will be formed within the composite, enabling the travel of electrons through the sample [32]. Beyond this percolation threshold, addition of conductive materials results in gradual development and spreading of a conductive network in all three dimensions [32]. In other words, at this stage the addition of more conductive materials results in a sharp decrease in electrical resistivity. Adding conductive materials can continue up to an optimum value at which point the conductive materials are in contact with one another in all directions and many conductive networks and electron passages are formed [32]. As a result, after this stage, adding more conductive materials would have little effect in decreasing the resistivity, and of course would not be economical.

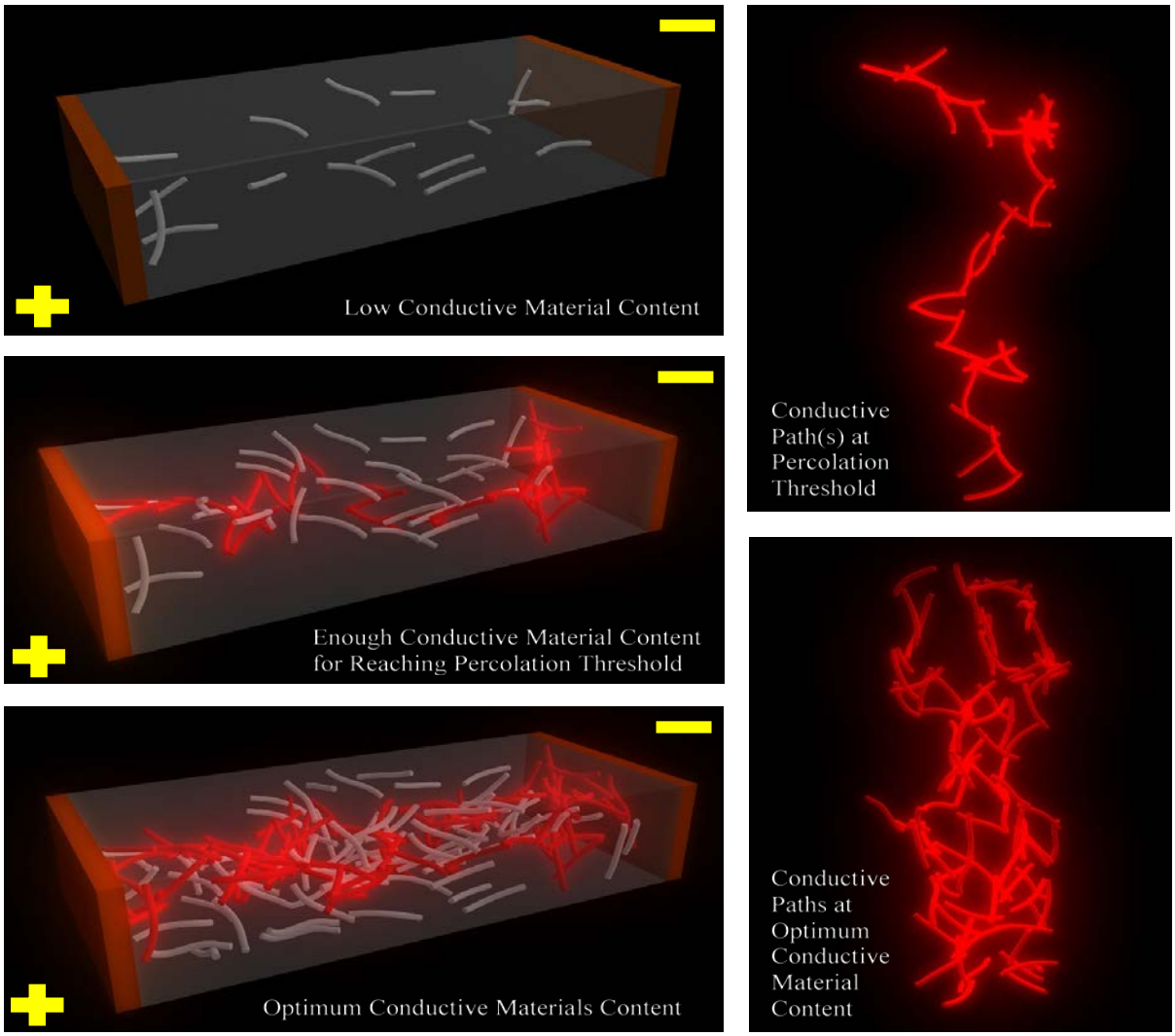

Figure 2.3 *Effect of conductive materials' volume content on the quality of conductivity in composite systems.*

Tunneling effect

The electron conduction mechanism in semiconductors depends on [33], [34]: intrinsic conductance of the conductive fillers, the direct contact of conductive fillers, and the traveling of electrons, at close proximities, between conductive fillers explained through the tunneling effect. Tunneling, a quantum-mechanical effect, occurs when electrons pass through an insulating material or barrier. In the context of classical physics, there is no way for electrons to travel through such a barrier if they do not have enough energy, but in the quantum-mechanical world,

unlike in classical physics, electrons possess wavelike properties. These waves taper off quickly rather than merely ending abruptly when they hit a wall or barrier. It is believed that electron tunneling, sometimes called hopping, is highly dependent on the barriers of chemical composition, temperature [35], and, most importantly, distances between the conductive fillers [36], [37]. According to Simmons [38], the resistivity of tunneling in a low-voltage range can be explained by the following equation:

$$\rho_{tunl} = \frac{h^2}{e^2\sqrt{2m\lambda}} \exp\left(\frac{4\pi d}{h}\sqrt{2m\lambda}\right) \quad (3)$$

Where:

P_{tunl} = electron tunneling resistance,

h = Planck's constant,

d = tunneling distance,

m= the mass of an electron,

λ = the barrier height of insulator, and

e= the quantum of electricity.

Referring to Simmons' equation, one can easily see that distance – among other variables - has a strong influence on tunneling resistance (**Error! Reference source not found.**), or alternatively, conductivity [39].

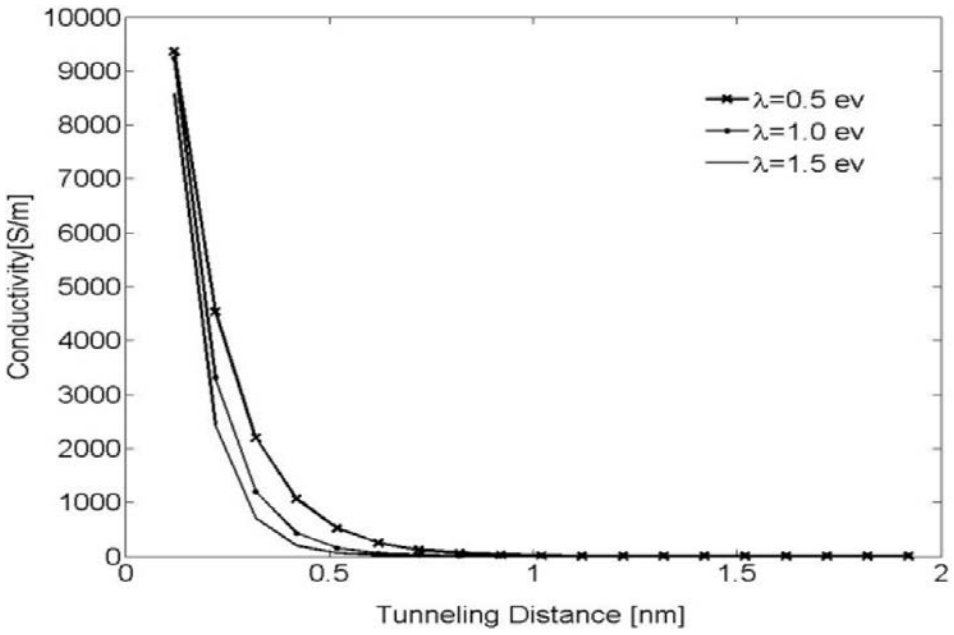

Figure 2.4 *The influence of distance on tunneling conductivity* [39].

Increasing Temperature in ECAC through Electrical Currents

ECAC temperature can be increased either through induction heating [32], [40]–[42] or conduction heating [20]. Conduction heating is used for melting ice and snow on the surface of areas paved with asphalt concrete [20], while induction heating is used for accelerating the self-healing process in asphalt concrete. Unlike induction heating, in conduction method, electrodes are in direct contact with ECAC [20]. As a result, for heat conduction, electrodes can be embedded in ECAC. It is worth noting that all the underlying concepts of conductivity enhancement in asphalt concrete are the same for both conduction and induction heating.

Electrical Resistivity Measurement in Asphalt Mixtures

Wu, et al., [24] measured volume resistivity at room temperature of 25ºC using a two-probe method. They used stainless steel disk-shaped electrodes with diameters of 120 mm and thicknesses of 25 mm. To ensure perfect contact between the asphalt concrete specimens and the electrodes, they used a dispersed type of graphite to fill the electrode-specimen gaps. Wu, et al., [24] reported contact resistance between the electrode and asphalt concrete to be less than 1Ω, a

negligible value compared with the measured resistance values, greater than 100 Ω, obtained from their specimens.

Garcia, et al., [18] performed resistivity measurements at room temperature, i.e. 20 ºC. They used nickel electrodes and connected them at the short ends of test specimens. Dry graphite powder was utilized to fill the gaps between each specimen and the electrodes to guarantee perfect contact. Garcia, et al., reported a contact resistance between the graphite and electrode of less than 0.1 Ω, much lower than the resistance of each specimen that was generally higher than 20 Ω. Garcia, et al., used a multimeter for measuring resistance values below 36×10^6 Ω and a resistance tester for measuring resistance values higher than 36×10^6 Ω.

Wang, et al., [23] used the two-probe method for measuring the resistivity of asphalt concrete specimens at a room temperature of 15 ºC. They used highly conductive silver paint to stick two copper plates/electrodes to the ends of each cylindrical specimen. Wang, et al., used a UNI-T modern digital multimeter to measure resistance values below 40×10^6 Ω, and a resistance meter for measuring values higher than 40×10^6 Ω. They reported that contact resistance between the two electrodes was lower than 1 Ω, much lower than the resistance values obtained from the specimens, generally greater than 0.1×10^6 Ω.

Huang, et al., [19], following the standard two-wire method, used a Keithley 2000 digital multimeter for measuring electrical resistivity of high-conductivity asphalt concrete. For measuring the resistivity of conventional asphalt concrete or asphalt concrete specimens with low conductive-material volume content, they used the external voltage power method because the Keithley 2000 digital multimeter was not able to measure such high resistance values.

Following the external voltage power method, the electrical resistance can be calculated using the following formula [19]:

$$R_0 = -\frac{V_2}{V_1 - V_2} R_{st} \quad (4)$$

Where:

R_0 = is the calculated value of resistance,

V_1 and V_2 = are the voltage values that can be precisely measured by the Keithley 2000, and

R_{st} = is the resistance of a standard resistor, 22 M Ω.

Huang, et al., covered the electrical contact areas of each specimen with a highly conductive silver paint, then glued copper tapes onto the painted areas so that a perfect contact between the specimen and each electrode could be guaranteed [19]. Huang, et al., did not report any contact resistance value.

Cong, et al., [43] used the two-probe method for measuring the resistivity of 90×10×10 mm specimens made of bitumen modified with electrically-conductive materials, e.g., different types of CB. They used silver paint for sticking copper wires to each specimen's ends (10×10 mm cross section), and measured the resistance at a room temperature of 20 ºC.

Temperature is another factor affecting resistivity, and it can considerably influence electrical conductivity of materials made of asphalt [44].

Conductive Materials Used for Increasing the Electrical Conductivity of Asphalt Mixtures

Carbon fiber

Carbon fiber produced from either poly acrylonitrile (PAN) or pitch precursors [45] is very compatible with asphalt concrete because, like asphalt, it is made of carbon. The melting point of carbon fiber is approximately 1000ºC, making it suitable for use in hot-mix asphalt (HMA) [46]. In addition to chemical and thermal compatibility, the high tensile strength of carbon fibers contributes to an increased tensile strength in asphalt concrete [46], including

resistance to thermal cracking [47], [48]. With regards to stiffening effects, carbon fibers increase the fatigue life of asphalt concrete [46]. It has been reported that the presence of CF can increase the fatigue life of asphalt concrete by approximately 10-25 orders of magnitude [49]. It is believed that CF is the best conductivity enhancement material for use in asphalt concrete [24] because high aspect ratio carbon fibers produce the longest conductive paths compared with other types of conductive fillers [24]; a fiber-to-fiber contact mechanism facilitates the conductive network formation and hence increases the electron transmission rate through the asphalt concrete [24]. Although carbon fiber, with a resistivity of approximately 10-3 Ω cm [24], can considerably increase the electrical conductivity of asphalt mixtures, it has one major drawback, i.e., poor dispersion; CF has a high tendency to agglomerate into small or large clusters [24]. Preparation of a well-dispersed CF modified asphalt concrete with more than 8% CF is not an easy task, especially if conventional mixing techniques are followed [24]. It is reported in the literature that high aspect ratio CFs, even at very low volume contents, can substantially increase the electrical conductivity [50].

Steel fiber and steel wool

Fatigue life of asphalt concrete can be extended by 10-25 times by addition of steel fibers (SFs) [49]. SF, with a resistivity of 7×10^{-3} Ω cm [41], has not been widely used in asphalt concrete compared with its application in portland cement concrete (PCC). Both SF and steel wool (SW) have been used in asphalt mastic [51] and asphalt concrete for increasing electrical conductivity and generating heat through induction [32], [40], [52]. Liu, et al., [32] stated that incorporation of SW into porous asphalt concrete increases its conductivity, and that percolation threshold and optimum conductive materials content can be reached at volume contents of 2.54% and 3.81% respectively.

Graphite

Graphite has a basic two-dimensional hexagonal crystalline structure, but the shape and size of graphite can vary according to the source from which it is obtained from and/or its manufacturing process [53]. Graphite is classified into flake type, amorphous, artificial, ultra-high surface, etc.[54]. Flake graphite has resistivity values ranging from 0.03 Ω.cm to 0.05 Ω.cm [54]. Amorphous graphite has a 0.13 Ω.cm resistivity [54]. Artificial graphite has a 0.047 Ω.cm resistivity [54]. Artificial nanoplatelet graphite has resistivity values ranging from 0.184 Ω.cm to 0.289 Ω.cm [54]. It is believed that flake type graphite is the best candidate among these types [53]. Graphite absorbs oil and hence results in increasing the optimum asphalt content [50]. Graphite has a carbon-based layered structure with weakly bonded layers, rendering the graphite lubricant and slippery [50]. Because of its intrinsic lubricating characteristic, graphite, if used beyond a certain limit, can significantly influence the mechanical strength of asphalt concrete [50]. Graphite reduces the indirect tensile (IDT) strength [19], Marshal stability [50], resilient modulus [50], and rutting dynamic stability of asphalt concrete [50]. To enhance the conductivity of asphalt concrete using graphite, a substantial amount of this conductive material must be added to the asphalt mixture, significantly influencing the performance of HMA [19].

Carbon black

CB is an amorphous carbon solid produced by deposition of solid carbon particles that are formed in a gaseous state [54]. CB - a material with the finest particle size among all the common industrial carbons - is manufactured by thermal cracking or combustion of a hydrocarbon-based fuel under reducing conditions [54]. Most formed CB particles have nanometer sizes [54]. CB, with a typical resistivity value of 0.341 Ω cm, can be used as a conductivity enhancing agent [55]. It is believed that CB, like bitumen, helps improve anti-aging, and conductivity (both thermal and electrical) of polymer-based matrixes at relatively low

dosages [56]. CB increases the complex modulus and increases the elasticity of asphalt mixtures [57]. CB can be used for stabilizing asphalt against oxidative degradation [58]. It is believed that CB with its higher surface area can also more effectively serve as an anti-oxidation agent [58]. Increasing the concentration of CB results in increasing the stiffness in asphalt binder [58].

Aluminum chips

Aluminum, with a resistivity of 2.65×10^{-6} Ω.cm, is one the best electrically-conductive materials, but when aluminum is solely incorporated in asphalt concrete in the form of chips, it does not effectively improve the electrical conductivity of concrete [53]. It is believed that aluminum is easily oxidized when exposed to air and its conductivity therefore decreases [53]. It is possible to use other conductive materials such as microscale steel fibers and graphite together with aluminum chips to obtain good electrical conductivity in asphalt concrete [53].

Steel slag

Steel slag is a byproduct of the stainless steel manufacturing process [59]. Production of three tons of stainless steel yields one tone of stainless steel slag [60], a relatively huge amount. For example, in Europe, twelve million tons of steel slag are produced on an annual basis [61].

Steel slag used as coarse aggregate improves the mechanical properties of asphalt concrete [59]. Replacing up to 75% of limestone coarse aggregate by steel slag improves the mechanical properties of asphalt concrete, including indirect tensile strength, resilient modulus, fatigue life, rutting resistance, and creep modulus [62]. If steel slag is used in stone mastic asphalt (SMA), it can make the SMA more cost-effective in terms of having accessibility to appropriate aggregate [63], [64]. It is recommended to replace steel slag only with either fine or coarse aggregate, because hot mix asphalt (HMA) containing 100% steel slag is more susceptible to bulking and formation of higher voids [65] due to the angular shape of steel slag. [65]. It is claimed that asphalt concrete mixtures containing more than 30% steel slag exhibit improved

skid resistance [62], and it is also reported that steel slag has the ability to retain heat more than other types of aggregates conventionally used in asphalt concrete [59]. Utilizing steel slag aggregate as the only conductive material in asphalt concrete, can improve the electrical resistivity by approximately one order of magnitude [59].

Multiplex ECAC

ECAC conductivity is highly dependent on the electrical resistivity of the conductive materials used, i.e., the lower the resistivity of the conductive materials the higher the electrical conductivity of the asphalt concrete [24].A combination of conductive fillers can result in a remarkably higher conductivity compared with single powder fillers at the same total content [24]. It is also believed that a combination of graphite and carbon fiber in asphalt concrete can result in an effective self-monitoring system for controlling strain [50]. The amount of conductive filler used in the mix can be calculated based on the volume percentage of the binder phase constituting of bitumen and conductive filler(s) [24], i.e., mastic.

ECAC for Anti-icing and De-icing Purposes

ECAC can be used for winter pavement maintenance purposes [20] as an alternative approach (Figure *2.5*) to conventional ice and snow removal techniques such as the use of deicing chemicals, deployment of snow removal equipment, etc. Deicing chemicals have detrimental effects on pavements [66], and the use of snow plowing equipment is time-consuming and costly. ECAC can serve as a heater [20] that, through resistive heating, is capable of melting ice and snow in an efficient manner.

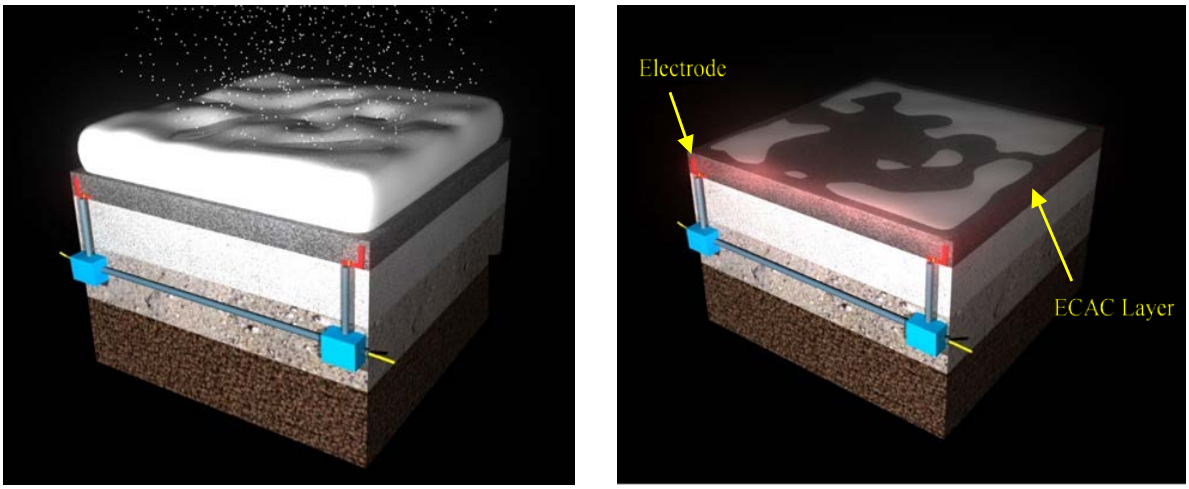

Figure 2.5 *Snow melting capability of ECAC.*

Wu, et al., [20] prepared a test slab made of two-lift asphalt concrete with each layer having a thickness close to 50 mm. They simulated the snow/ice melting process on a bridge deck paved with ECAC. In that study, Wu et al., used AC-13 aggregate gradation in the surface asphalt course, and used AC-16 aggregate gradation in the conductive asphalt layer (second layer). They made the third layer (base) with portland cement concrete. For producing ECAC (second layer), they added SF, CF and graphite at 7% of total asphalt mixture weight. Steel slag was also substituted for basalt in the ECAC. Wu, et al., used a thermal insulating layer between the base layer and the ECAC and kept the ECAC layer at a constant temperature of -15°C for 24 h. They then applied 200 volts to the ECAC specimen and performed thermography for a duration of 30 minutes. They reported the temperature at one specific point, and based on their observation, the temperature rose from -15°C to 16.6°C.

Derwin, et al. investigated the performance efficiency of Snowfree ®, a commercial name for their ECAC system [67]. Snowfree ® was formulated by Superior Graphite Co., and developed with the cooperation of the FAA Technical Center and Flood Testing Laboratories [67]. The Snowfree ® system uses a combination of graphite, asphalt, and electricity to melt ice and snow [67].

According to Derwin, et al., [67] a demonstration section was installed in November 1994 at Chicago O'Hare Airport on a heavily-used departure taxiway (Figure 2.6). The system was powered by a 120-volt electrical source operated automatically with the aid of embedded temperature and moisture sensors [67]. Durability, safety, and performance of the Snowfree ® system was measured in a pilot study over a three-year and a half period.

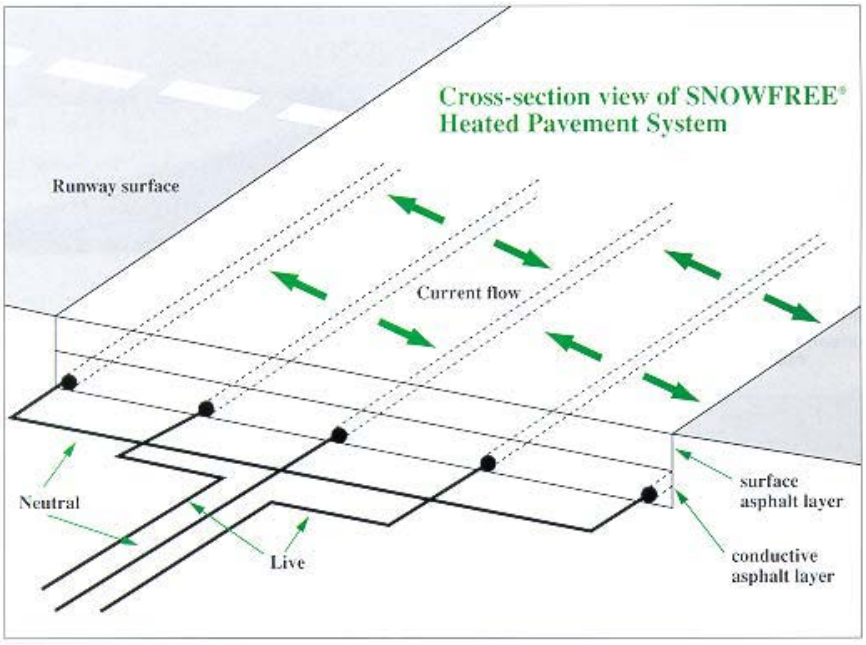

Figure 2.6 S*chematic of the Snowfree ® system installed on a taxiway in O'Hare International Airport* [67].

Derwin, et al., reported that cables, aconductive asphalt layer (ECAC), and a surface asphalt concrete layer were placed during an 18-hour time window [67]. The heated pavement section covered an area with dimensions of 70 ft×90 ft. The total system power requirement was approximately 300 kW [67]. Derwin, et al., reported that the spacing between each two-cable pair (electrodes) was 16 ft, and the system was designed to operate at 120 V, with each cable having a current carrying capacity of 830 A.

After the test section at O'Hare International Airport was ready to operate, a current leakage test was conducted by Underwriters Laboratories, and no safety-related concerns were identified [67]. The HPS was able to successfully melt a 2-inch snow layer in early March. The test section at the O'Hare International airport could increase the temperature by up to 9 degrees in 2.5 h [67]. The temperature of the Snowfree ® HPS increased at the rate of 3-5 degrees per hour during the period in which Derwin, et al., conducted their study.

As mentioned earlier, the HPS test section constructed at the O'Hare International Airport was made of asphalt concrete. The ECAC layer was designed to meet FAA P401 specifications for the paved areas of airfields. According to Derwin, et al., using the correct proportions of graphite and aggregate helped in maintaining the durability of the ECAC Snowfree ® HPS equal to that of normal asphalt concrete [67]. According to a report prepared by Derwin, et al., in 2003, the test section had been in place and exposed to traffic-related and environmental stresses for four years, and the study revealed no differences, in terms of presence of cracks, between heated and normal asphalt concrete.

ECAC for Anti-icing and De-icing Purposes

The ultimate goal of this study is to produce highly efficient superhydrophobic coatings and an ECAC capable of generating enough sufficient heat that, when these technologies are combined, the result would be a hybrid heated pavement system capable of fighting ice formation and snow accumulation far better than each individual technology. Figure 2.7 presents a schematic of a hybrid heated systems that combines ECAC, embedded hydronic pipes, and a superhydrophobic coating.

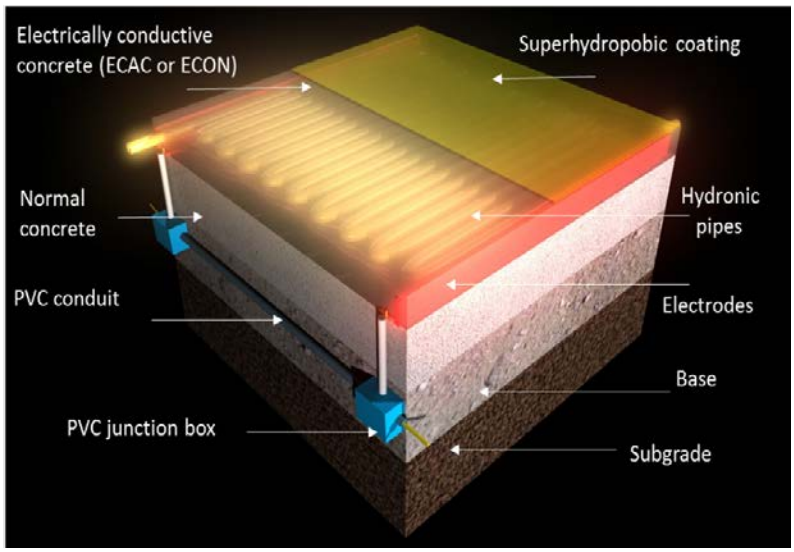

Figure 2.7 S*chematic of a hybrid heated pavement system* [67].

References

[1] W. Shen, H. Ceylan, K. Gopalakrishnan, S. Kim, and A. Nahvi, "Sustainability assessment of alternative snow-removal methods for airport apron paved surfaces," No. DOT/FAA/TC-17/34, 2017.

[2] A. Arabzadeh, H. Ceylan, S. Kim, K. Gopalakrishnan, A. Sassani, S. Sundararajan, and P. C. Taylor, "Superhydrophobic coatings on Portland cement concrete surfaces," *Constr. Build. Mater.*, vol. 141, pp. 393–401, 2017.

[3] A. Arabzadeh, H. Ceylan, S. Kim, K. Gopalakrishnan, and A. Sassani, "Fabrication of Polytetrafluoroethylene-Coated Asphalt Concrete Biomimetic Surfaces: A Nanomaterials-Based Pavement Winter Maintenance Approach," in *International Conference on Transportation and Development*, 2016, pp. 54–64.

[4] H. Ceylan, A. Arabzadeh, A. Sassani, Kim, and K. Gopalakrishnan, "Innovative nano-engineered asphalt concrete for ice and snow controls in pavement systems," in *6th Eurasphalt &Eurobitume Congress*.

[5] A. Arabzadeh, H. Ceylan, S. Kim, S. Gopalakrishnan, K Sassani, A Sundararajan, P. C. Taylor, and A. Abdullah, "Influence of Deicing Salts on the Water-Repellency of Portland Cement Concrete Coated with Polytetrafluoroethylene and Polyetheretherketone," in *Airfield and Highway Pavements*, 2017, pp. 217–227.

[6] A. Arabzadeh, H. Ceylan, S. Kim, K. Gopalakrishnan, and A. Sassani, "Superhydrophobic coatings on asphalt concrete surfaces," *Transp. Res. Rec. J. Transp. Res. Board*, vol. 2551, pp. 10–17, 2016.

[7] A. Lafuma and D. Quéré, “Superhydrophobic states.,” *Nat. Mater.*, vol. 2, no. 7, pp. 457–460, 2003.

[8] Z. Chu and S. Seeger, “Superamphiphobic surfaces,” *Chem. Soc. Rev.*, vol. 43, no. 8, p. 2784, 2014.

[9] V. Hejazi, K. Sobolev, and M. Nosonovsky, “From superhydrophobicity to icephobicity: forces and interaction analysis.,” *Sci. Rep.*, vol. 3, p. 2194, 2013.

[10] A. J. Meuler, J. D. Smith, K. K. Varanasi, J. M. Mabry, G. H. McKinley, and R. E. Cohen, “Relationships between water wettability and ice adhesion,” *ACS Appl. Mater. Interfaces*, vol. 2, no. 11, pp. 3100–3110, 2010.

[11] S. Jung, M. Dorrestijn, D. Raps, A. Das, C. M. Megaridis, and D. Poulikakos, “Are superhydrophobic surfaces best for icephobicity?,” *Langmuir*, vol. 27, no. 6, pp. 3059–3066, 2011.

[12] R. Menini and M. Farzaneh, “Elaboration of Al2O3/PTFE icephobic coatings for protecting aluminum surfaces,” *Surf. Coatings Technol.*, vol. 203, no. 14, pp. 1941–1946, 2009.

[13] L. Cao, A. K. Jones, V. K. Sikka, J. Wu, and D. Gao, “Anti-icing superhydrophobic coatings,” *Langmuir*, vol. 25, no. 21, pp. 12444–12448, 2009.

[14] X. Zhang, F. Shi, J. Niu, Y. Jiang, and Z. Wang, “Superhydrophobic surfaces: from structural control to functional application,” *J. Mater. Chem.*, vol. 18, no. 6, p. 621, 2008.

[15] T. J. Young, “Development of durable superhydrophobic materials for ice-and snow-free airport concrete pavements,” Iowa State University, 2016.

[16] U. S. Terminal, U. S. Terminal, E. Route, and E. Route, “Advisory Circular,” 2016.

[17] P. Pan, S. Wu, F. Xiao, L. Pang, and Y. Xiao, “Conductive asphalt concrete: A review on structure design, performance, and practical applications,” *J. Intell. Mater. Syst. Struct.*, vol. 26, no. 7, pp. 755–769, 2015.

[18] Á. García, E. Schlangen, M. Van De Ven, and Q. Liu, “Electrical conductivity of asphalt mortar containing conductive fibers and fillers,” *Constr. Build. Mater.*, vol. 23, no. 10, pp. 3175–3181, 2009.

[19] B. Huang, X. Chen, and X. Shu, “Effects of electrically conductive additives on laboratory-measured properties of asphalt mixtures,” *J. Mater. Civ. Eng.*, vol. 21, no. 10, pp. 612–617, 2009.

[20] S. Wu, P. Pan, M. Chen, and Y. Zhang, “Analysis of characteristics of electrically conductive asphalt concrete prepared by multiplex conductive materials,” *J. Mater. Civ. Eng.*, vol. 25, no. 7, pp. 871–879, 2012.

[21] Y. Zhang, “Preparation and properties investigation of multiplex electrically conductive asphalt concrete,” Wuhan University of Technology, 2010.

[22] M. Jamal, A. Khattab, H. R. Rizvi, and P. Zhang, “The impact of carbon nano-fiber modification on asphalt binder rheology,” *Constr. Build. Mater.*, vol. 30, pp. 257–264, 2012.

[23] H. Wang, J. Yang, H. Liao, and X. Chen, “Electrical and mechanical properties of asphalt concrete containing conductive fibers and fillers,” *Constr. Build. Mater.*, vol. 122, pp. 184–190, 2016.

[24] S. Wu, L. Mo, Z. Shui, and Z. Chen, “Investigation of the conductivity of asphalt concrete containing conductive fillers,” *Carbon N. Y.*, vol. 43, no. 7, pp. 1358–1363, 2005.

[25] A. Bozorgzad, Y. Kim, and H. Lee, “Determining the optimum content and stirring time of emerging dry polymer for asphalt using rotational viscometer, dynamic shear rheometer, and atomic force microscopy,” *Adv. Civ. Eng. Mater.*, vol. 7, no. 1, 2018.

[26] D. J. Mensching, R. Rahbar-Rastegar, B. S. Underwood, and J. Sias Daniel, “Identifying indicators for fatigue cracking in hot-mix asphalt pavements using viscoelastic continuum damage principles,” *Transp. Res. Rec. J. Transp. Res. Board*, vol. 2576, pp. 28–39, 2016.

[27] M. Bazzaz, M. K. Darabi, D. N. Little, and N. Garg, “A straightforward procedure to characterize nonlinear viscoelastic response of asphalt concrete at high temperatures,” *Transp. Res. Rec. J. Transp. Res. Board*, 2018.

[28] N. Kwok and H. T. Hahn, “Resistance heating for self-healing composites,” *J. Compos. Mater.*, vol. 41, no. 13, pp. 1635–1654, 2007.

[29] G. E. Pike and C. H. Seager, “Percolation and conductivity: A computer study. I*,” *Phys. Rev. B*, vol. 10, no. 4, pp. 1421–1434, 1974.

[30] M. Weber and M. R. Kamal, “Estimation of the volume resistivity of electrically conductive composites,” *Polym. Compos.*, vol. 18, no. 6, pp. 711–725, 1997.

[31] J. K. W. Sandler, J. E. Kirk, I. A. Kinloch, M. S. P. Shaffer, and A. H. Windle, “Ultra-low electrical percolation threshold in carbon-nanotube-epoxy composites,” *Polymer (Guildf).*, vol. 44, no. 19, pp. 5893–5899, 2003.

[32] Q. Liu, E. Schlangen, and M. Van De Ven, “Induction Healing of Porous Asphalt,” *Transp. Res. Rec. J. Transp. Res. Board*, vol. 2305, pp. 98–101, 2012.

[33] S. Paschen, M. N. Bussac, L. Zuppiroli, E. Minder, and B. Hilti, “Tunnel junctions in a polymer composite,” *J. Appl. Phys.*, vol. 78, no. 5, pp. 3230–3237, 1995.

[34] W. S. Bao, S. A. Meguid, Z. H. Zhu, and G. J. Weng, “Tunneling resistance and its effect on the electrical conductivity of carbon nanotube nanocomposites,” *J. Appl. Phys.*, vol. 111, no. 9, 2012.

[35] J. Siegel, O. Lyutakov, V. Rybka, Z. Kolská, and V. Svorčík, “Properties of gold nanostructures sputtered on glass.,” *Nanoscale Res. Lett.*, vol. 6, no. 1, p. 96, 2011.

[36] F. P. Zamborini, L. E. Smart, M. C. Leopold, and R. W. Murray, “Distance-dependent electron hopping conductivity and nanoscale lithography of chemically-linked gold monolayer protected cluster films,” *Anal. Chim. Acta*, vol. 496, no. 1–2, pp. 3–16, 2003.

[37] C. Yeh and K. Najafi, “A low-voltage tunneling-based silicon microaccelerometer,” *IEEE Trans. Electron Devices*, vol. 44, no. 11, pp. 1875–1882, 1997.

[38] J. G. Simmons, “Generalized formula for the electric tunnel effect between similar electrodes separated by a thin insulating film,” *J. Appl. Phys.*, vol. 34, no. 6, pp. 1793–1803, 1963.

[39] A. B. Oskouyi, U. Sundararaj, and P. Mertiny, “Tunneling conductivity and piezoresistivity of composites containing randomly dispersed conductive nano-platelets,” *Materials (Basel).*, vol. 7, pp. 2501–2521, 2014.

[40] Q. Liu, Á. García, E. Schlangen, and M. Van De Ven, “Induction healing of asphalt mastic and porous asphalt concrete,” *Constr. Build. Mater.*, vol. 25, no. 9, pp. 3746–3752, 2011.

[41] Q. Liu, E. Schlangen, Á. García, and M. van de Ven, “Induction heating of electrically conductive porous asphalt concrete,” *Constr. Build. Mater.*, vol. 24, no. 7, pp. 1207–1213, 2010.

[42] Á. García, “Self-healing of open cracks in asphalt mastic,” *Fuel*, vol. 93, pp. 264–272, 2012.

[43] P. Cong, P. Xu, and S. Chen, “Effects of carbon black on the anti aging, rheological and conductive properties of SBS/asphalt/carbon black composites,” *Constr. Build. Mater.*, vol. 52, pp. 306–313, 2014.

[44] S. P. Wu, L. T. Mo, and Z. H. Shui, “Piezoresistivity of graphite modified asphalt-based composites,” *Key Eng. Mater.*, vol. 249, pp. 391–395, 2003.

[45] D. C. Chung, Deborah DL, *Carbon fiber composites*. 2012.

[46] S. M. Abtahi, M. Sheikhzadeh, and S. M. Hejazi, “Fiber-reinforced asphalt-concrete - a review,” *Constr. Build. Mater.*, vol. 24, no. 6, pp. 871–877, 2010.

[47] A. Arabzadeh, “The influence of different mixture design variables on thermal fatigue cracking of asphalt concrete pavements,” Middle East Tecnical University, 2015.

[48] A. Arabzadeh and M. Güler, “Influence of mixture design variables on thermal coefficient of asphalt concrete,” in *Proceedings of Conference on Advances in Civil Engineering*, 2014, pp. 1–6.

[49] S. J. Lee, J. P. Rust, H. Hamouda, Y. R. Kim, and R. H. Borden, “Fatigue cracking resistance of fiber-reinforced asphalt concrete,” *Text. Res. J.*, vol. 75, no. 2, pp. 123–128, 2005.

[50] X. Liu and S. Wu, “Study on the graphite and carbon fiber modified asphalt concrete,” *Constr. Build. Mater.*, vol. 25, no. 4, pp. 1807–1811, 2011.

[51] A. Mokhtari and F. M. Nejad, “Comparative Study on Performance of Wax-Modified and Typical SMA Mixtures,” *J. Mater. Civ. Eng.*, vol. 25, no. 3, pp. 419–427, 2013.

[52] Á. García, E. Schlangen, M. Van De Ven, and D. Vliet, “Induction heating of mastic containing conductive fibers and fillers,” *Mater. Struct.*, vol. 44, no. 2, pp. 499–508, 2011.

[53] P. Park, Y. Rew, and A. Baranikumar, “Controlling conductivity of asphalt concrete with graphite,” Southwest Region University Transportation Center, 2014.

[54] “Asbury Carbons Inc.” [Online]. Available: www.asbury.com.

[55] N. Guo and M. C. Leu, “Effect of different graphite materials on electrical conductivity and flexural strength of bipolar plates fabricated by selective laser sintering,” *Carbon N. Y.*, vol. 37, no. 4, pp. 482–492, 2010.

[56] M. Le Guern, E. Chailleux, F. Farcas, S. Dreessen, and I. Mabille, “Physico-chemical analysis of five hard bitumens: Identification of chemical species and molecular organization before and after artificial aging,” *Fuel*, vol. 89, no. 11, pp. 3330–3339, 2010.

[57] S. Wen and D. D. L. Chung, “Effects of carbon black on the thermal , mechanical and electrical properties of pitch-matrix composites,” vol. 42, pp. 2393–2397, 2004.

[58] A. K. Apeagyei, “Laboratory evaluation of antioxidants for asphalt binders,” *Constr. Build. Mater.*, vol. 25, no. 1, pp. 47–53, 2011.

[59] P. Ahmedzade and B. Sengoz, “Evaluation of steel slag coarse aggregate in hot mix asphalt concrete,” vol. 165, pp. 300–305, 2009.

[60] D. M. Proctor, K. A. Fehling, E. C. Shay, J. L. Wittenborn, C. Avent, R. D. Bigham, M. Connolly, B. Lee, T. . Shepker, M. . Zak, D. M. Proctor, K. a Fehling, E. C. Shay, J. L. Wittenborn, J. J. Green, C. Avent, R. D. Bigham, M. Connolly, B. Lee, T. O. Shepker, and M. A. Zak, "Physical and chemical properties of blast furnace, basic oxygen furnace and electric arc furnace steel industry slag," *Environ. Sci. Technol.*, vol. 34, no. No 8, pp. 1576–1582, 2000.

[61] H. Motz and J. Geiseler, "Products of steel slags an opportunity to save natural resources," *Waste Manag.*, vol. 21, no. 3, pp. 285–293, 2001.

[62] I. M. Asi, "Evaluating skid resistance of different asphalt concrete mixes," *Build. Environ.*, vol. 42, no. 1, pp. 325–329, 2007.

[63] S. Wu, Y. Xue, Q. Ye, and Y. Chen, "Utilization of steel slag as aggregates for stone mastic asphalt (SMA) mixtures," *Build. Environ.*, vol. 42, no. 7, pp. 2580–2585, 2007.

[64] Y. Xue, S. Wu, H. Hou, and J. Zha, "Experimental investigation of basic oxygen furnace slag used as aggregate in asphalt mixture," *J. Hazard. Mater.*, vol. 138, no. 2, pp. 261–268, 2006.

[65] P. S. Kandhal and G. L. Hoffman, "The use of steel slag as bituminous concrete fine aggregate," Pennsylvania, 1982.

[66] K. Wang, D. E. Nelsen, and W. A. Nixon, "Damaging effects of deicing chemicals on concrete materials," *Cem. Concr. Compos.*, vol. 28, no. 2, pp. 173–188, 2006.

[67] D. Derwin, P. Booth, P. Zaleski, and W. Marsey, "Snowfree ® Heated Pavement System To Eliminate Icy Runways," *Asphalt*, no. 724, pp. 1–10, 2003.

CHAPTER 3. SUPERHYDROPHOBIC COATINGS ON ASPHALT CONCRETE SURFACES: TOWARD SMART SOLUTIONS FOR WINTER PAVEMENT MAINTENANCE

A journal paper published in Transportation Research Record: the journal of Transportation Research Board

Ali Arabzadeh[1], Halil Ceylan[2], Sunghwan Kim[3], Kasthurirangan Gopalakrishnan[4] and Alireza Sassani[5]

Abstract

Millions of dollars are spent annually for ice or snow removal from roadways and airport paved surfaces in cold regions. Snow or ice on such paved areas can cause traffic accidents and financial loss through flight cancellations or delays. For mitigating such winter pavement maintenance issues, the use of superhydrophobic (super water-repellent) coating techniques is gaining attention as a smart and cost-effective alternative to traditional snow and ice removal practices. This study focused on creating, characterizing, and evaluating innovative superhydrophobic coatings on asphalt concrete surfaces for ice- and snow-free flexible-pavement applications. The Layer by layer (LBL) method was utilized to create asphalt concrete surface coating with the polytetrafluoroethylene (PTFE) as a well-known super ice/water-repellent material. Superhydrophobicity and skid resistance of the coated asphalt concrete surface were characterized in terms of the water-contact angle, the work of adhesion, and the coefficient of friction at the micro-texture level. These properties were evaluated for different test variables,

[1] Graduate Research Assistant, Civil, Construction and Environmental Engineering (CCEE), Iowa State University (ISU), Ames, IA, E-mail: arab@iastate.edu
[2] Professor, Director, Program for Sustainable Pavement Engineering and Research (PROSPER), CCEE, ISU, Ames, IA, E-mail: hceylan@iastate.edu
[3] Research Scientist, Institute for Transportation, ISU, Ames, IA, E-mail: sunghwan@iastate.edu
[4] Research Associate Professor, CCEE, ISU, Ames, IA, E-mail: rangan@iastate.edu
[5] Graduate Research Assistant, CCEE, ISU, Ames, IA, E-mail: asassani@iastate.edu

including spray times and dosage rates of PTFE, under a statistical design based experimental test program. The measurement results indicate that uses of the LBL method for spray depositing the PTFE particles and the micro-tribometer for measuring coefficient of friction in micro-texture level are promising methods for creating and characterizing superhydrophobic coatings on asphalt concrete. The results of statistical analyses indicate that spray time and dosage of PTFE significantly affect the ability of a coated flexible pavement to be icephobic/superhydrophobic and skid resistant.

Introduction

Research is underway around the world to enhance pavements resistant to freezing-induced damage. Each year America's harsh winters cost the nation's economy billions of dollars in snow and ice removals, weather damage to roadways, and revenue lost by closed businesses. More than 76,300 flights in 2014 were cancelled because of snow and ice accumulation on the airport surfaces, leaving millions of travelers in the lurch and costing airports and airlines millions in revenue (*1*). For mitigating the problems associated with ice/snow formation on paved surfaces, both heated-pavement systems (*2, 3*) and/or superhydrophobic (super water-repellent) coating techniques (*3*) have received recent attention as alternatives to traditional snow and ice removal practices. The former is used for melting the ice or snow on the surface, while the latter can be used for preventing or curbing ice or snow formation. Moreover, the benefits of superhydrophobic coatings could be combined with those of heated pavement systems in a hybrid heated pavement system framework, yielding potentially greater water and ice repellency.

A surface is called superhydrophobic when the contact angles of droplets deposited on it are equal to or bigger than 150° (*4*). In such a case, the water droplets do not tend to wet the surface and can be easily rolled off the surface either when they are blown or when the surface is

tilted. Superhydrophobicity is achieved through a combination of surface roughness and low surface energy (*5*). Two distinct models are proposed to explain the roughness effect (*6*). On one hand, according to Wenzel model, roughness increases the surface area of the solid, geometrically improving the hydrophobicity. The Cassie model, on the other hand, asserts that air can remain trapped beneath the droplets, leading to further enhancement of hydrophobicity. Tiny entrapped air pockets reduce the solid-liquid contact area making the surface superhydrophobic. If these two roughness induction methods are applied to certain types of hydrophobic materials with low surface energy, the final products will be superhydrophobic. Polytetrafluoroethylene (PTFE) with a water-contact angle of 108° (*7,8*) is a hydrophobic material with low surface energy; PTFE particles created with diameters at submicron scales using an appropriate deposition technique can readily become superhydrophobic (*7*).

Ice formation on airplanes, power lines, wind turbines, etc. is an important concern for agencies and over the last decades has drawn the attention of many researchers trying to remedy associated problems. Likewise, ice formation on pavements has been a major source of concern, and various conventional approaches have been employed for ice/snow removal, including spraying large quantities of anti-ice agents on paved areas and deploying many snow-plowing vehicles, etc., costly and time-consuming methods. Since preventing or reducing ice/snow formation/accumulation is more desirable than fighting against their build-up, a more economical and time-efficient method for mitigating problems associated with ice/snow accumulation is to use superhydrophobic coatings with icephobic properties (*9, 10, 11, 12, 13)*. After coating the pavements with such materials, the rate of ice formation decreases, and because of the low work of adhesion of super ice/water repellent materials, the bond strength developed between the

ice/snow and the coated pavement surface decreases, so that by applying small mechanical forces the ice/snow can be removed.

To the best of our knowledge, there is a very limited body of literature dealing with applying nanomaterials on asphalt concrete to make it ice/water repellent. The first such attempt, using wet methods, used a copolymer fluoroacrylate previously modified with CaO nanoparticles was sprayed over the asphalt concrete, and the results revealed that the coated asphalt concrete was able to curb the formation of ice on the surface (*14*). In addition to making a surface superhydrophobic, PTFE is one of the well-known materials for reducing ice adhesion strength because of its low surface energy and chemical stability (*15*). While PTFE's icephobicity has been widely investigated on different substrates like plastic (*16*) and aluminum (*17*) for decreasing ice formation on outdoor structures like ground wires, phase conductors of overhead power lines, aircraft wings and fuselages, telecommunication antennas, and conductors (*18.19*), the ice/water repellency of PTFE has never been evaluated for asphalt concrete.

After super water-repellent (superhydrophobic) materials has been applied on a pavement surface, skid resistance must be controlled. The main intention of applying these materials on the paved areas is either to curb the formation of ice/snow or facilitate their removal. However, the application of nano-materials will be of no avail if they endanger passengers by making the roadways/runways more slippery under dry conditions. There are two components affecting tire-pavement friction (*20*): the adhesion developed between the pavement surface and a tire, and the aggregate micro-asperities penetrating into the tire rubber. The former develops due to electrostatic attraction between the rubber molecules and the asperities on the pavement surface, while the latter is the result of rubber deformation hysteresis. The asperities of the pavement surface are classified into three orders: micro-texture, macro-texture, and mega-

texture (*20*). Micro-texture, including the aggregate mineralogy and bitumen texture, is classified as corresponding to irregularities between 0.005 and 0.3 mm; a harsh pavement surface has an average micro-texture depth of 0.05 mm. Macro-texture - attributed to the size, angularity, shape and distribution of coarse aggregate - is classified as corresponding to irregularities between 0.3 and 4.0 mm; a pavement is considered rough if the average depth of macro-texture is greater than 1.0 mm. Mega-texture is classified as irregularities greater than 4.0 mm; mega-texture deals with major surface irregularities like cracks and potholes. It is believed that micro-texture is the most important among these three orders of roughness (*21, 22*). Moreover, pavement friction is governed by micro-texture at low speed, while both micro-texture and macro-texture are responsible for skid resistance at high speeds.

While a modified British pendulum test can be performed to measure the skid resistance of asphalt concrete samples at micro-texture level in laboratory (*23*), to characterize skid resistance of a nano-coated substrate, the use of devices providing higher resolution in measuring the coefficient of friction (COF) can yield more accurate and reliable results. The COF measured on the coated and uncoated cut surface of asphalt concrete can be quite representative of the skid resistance over coated and uncoated flexible pavements, respectively; COF measured at micro-texture level makes contributions to skid resistance at both low and high speeds, while the physical properties of aggregate are the predominant factor at high speeds whether or not the surface is coated.

In this study, a statistical design-based experimental test program was developed to create and evaluate superhydrophobic coatings on asphalt concrete for ice- and snow-free flexible pavement applications. The Layer by layer (LBL) method was utilized to coat the asphalt concrete specimens/substrates with PTFE nano-particles using different spray times and variable

dosages of PTFE. The coated substrates' superhydrophobicity was evaluated by measuring the water contact angle, and the COF was then measured for both the coated and uncoated substrates. To this end, a micro-tribometer based COF measurement method, another novel feature of this research, was designed and used. Finally, statistical analyses were conducted to determine significant parameters affecting superhydrophobicity and skid resistance of the coated asphalt concrete substrates. The findings of this study will be discussed to provide some guidance on actual implementation of the use of superhydrophobic coated asphalt concrete for ice- and snow-free flexible pavement applications.

Materials and Methodology

To investigate the effect of different variables on the superhydrophobicity and skid resistance of nano-coated asphalt concrete substrates, a statistical design was developed and performed prior to the start of experiments. The selected variables were spray times (3, 6, 9 and 12 seconds) and dosages (10, 20, 30 and 40%) of PTFE. As the result of this statistical design, 16 disk-shaped asphalt concrete substrates were prepared. Each asphalt concrete substrate was divided into four quarters for the sake of obtaining replicates. Three replicates were used for coating and one used for control purposes, i.e., forty-eight (16×3) samples were coated and 16 (16×1) samples were used for control purposes. Each coated sample's superhydrophobicity was evaluated by measuring the water-contact angle and the skid resistance of each sample was measured using a micro-tribometer.

Preparation of Asphalt Concrete Substrates

The asphalt concrete samples used in this study consisted of limestone, with a gradation (See Figure 3.1) consistent with Superpave mix design and Federal Aviation Administration's (FAA) advisory circular (*24*), and bitumen at optimum content. The physical properties of both the limestone and the bitumen are presented in Table *3.1*.

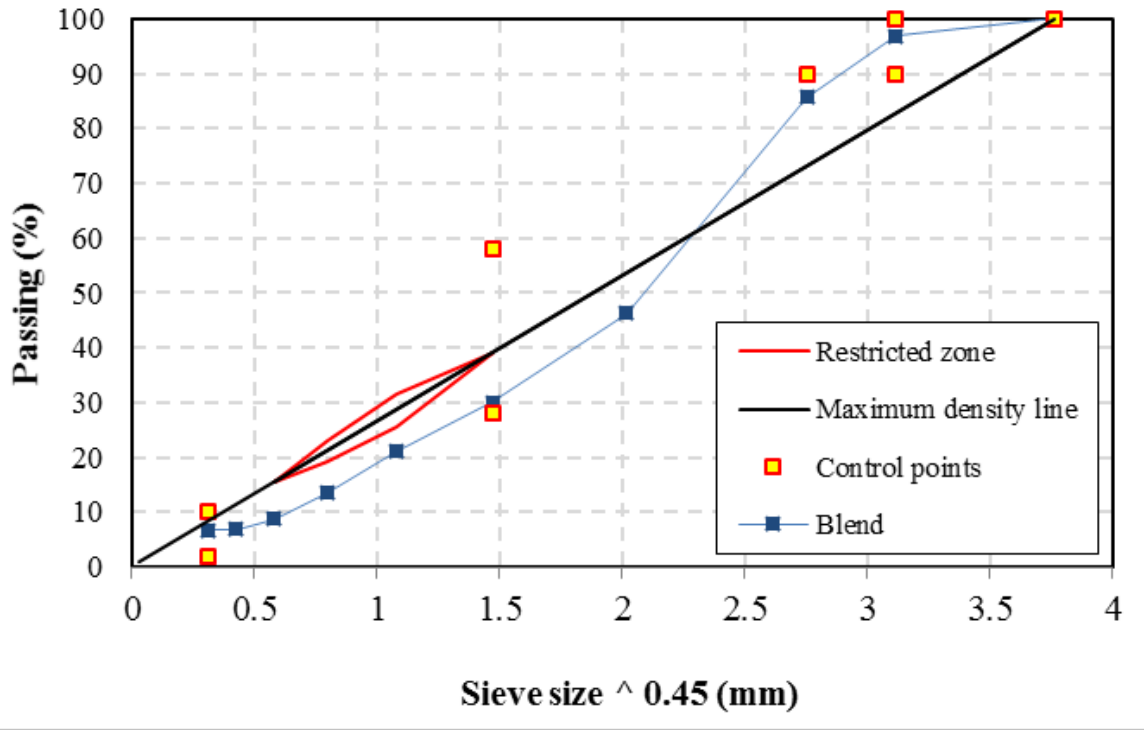

Figure 3.1 *Aggregate gradation.*

Table 3.1 *Aggregate and bitumen properties.*

Aggregate	**Specific gravity (g/cm^3)**	**Absorption (%)**
Limestone	2.76	1.44
Asphalt binder	**Specific gravity (g/cm^3)**	**Penetration value (0.1mm)**
PG58-28	1.028	75

Using a gyratory compactor, mixtures with a diameter of 10 cm and a height of 15 cm were compacted in a cylindrical mold, achieving a 4% air void in the Superpave gyratory compactor. After compaction, a diamond table saw was used to make 5 cross-sectional cuts through each cylindrical asphalt concrete specimen to obtain four 1cm-thick substrates. To minimize effects of compaction-related non-uniformities adjacent to the ends, disk-shaped specimens were obtained from the core of each cylindrical sample. Again, each specimen was cut into four quarters. Hereinafter, a quarter disk-shaped asphalt concrete specimen will be referred to as an asphalt concrete specimen/substrate.

Coating the Asphalt Concrete Substrates

There are different methods, including layer by layer (LBL), wax solidification, lithography, polymer conformation, vapor deposition, sublimation, plasma technique, and others, for synthesizing the superhydrophobic surfaces (*25*). Because of the asphalt concrete non-planar surface, the specimens used in this study were coated using the LBL method (*25*). To achieve LBL coating, a two-part epoxy resin dissolved in xylene was first sprayed for three seconds on the top surface of each asphalt concrete specimen. Two-part epoxy was used for adhering the PTFE to the asphalt concrete substrate, after which PTFE dispersed in acetone was sprayed over the epoxy resin. PTFE was added to the acetone based on different weight percentages of epoxy resin.

The epoxy (EP 1224), acquired from ResinLab, consisted of two parts: part A - a polymer resin - and part B - a curing agent. For coating each asphalt concrete specimen, 10 mL of part A, 5 mL of part B and 15 mL of xylene were introduced into a beaker. The obtained batch was magnetically stirred for 5 minutes at 500 rpm at ambient temperature. Hereinafter, this mixture is referred to simply as epoxy. After the stirring time was over, the epoxy was immediately introduced into a spray gun (Figure *3.2*a) set up for epoxy, and immediately sprayed over an

asphalt concrete substrate for three seconds. In order to eliminate the hardening effect of the epoxy over time, the remaining amount in the paint cup was discarded and, for each spray deposition, a fresh batch was prepared

Note that this research highlights the application of superhydrophobic materials on asphalt concrete. Zynol® MP 1300 PTFE obtained from DuPont has a melting point of 325-342 °C and an average particle size of 12 microns. This product was dispersed in acetone at different dosage levels; the dosages were based on the percent weight (10, 20, 30 and 40%) of the two-part epoxy. PTFE at each dosage, was introduced into acetone to obtain a 50-mL mixture, the mixture magnetically stirred for 15 minutes at 500 rpm at ambient temperature, then immediately introduced into a spray gun specifically dedicated to spraying the PTFE/acetone mixture. The mixtures of acetone and PTFE were sprayed on the asphalt concrete substrates for time durations of 3, 6, 9 and 12 seconds (Figure *3.2*a). It should be mentioned that two separate spray guns for spraying PTFE and epoxy were used to prevent contamination of the spray materials with one another.

Note that, Figure *3.2*b depicts two different scenarios that might occur during the PTFE and epoxy deposition. If the dosage of PTFE is low and the spraying time too short, either the amount of PTFE nanoparticles sticking to the surface will be very small or the PTFE nanoparticles will sink into the epoxy. When the spraying time is too long and the dosage of the PTFE particles is high, some nanoparticles will accumulate on the surface without binding to the substrate, and the nanoparticle deposition will be uneconomical.

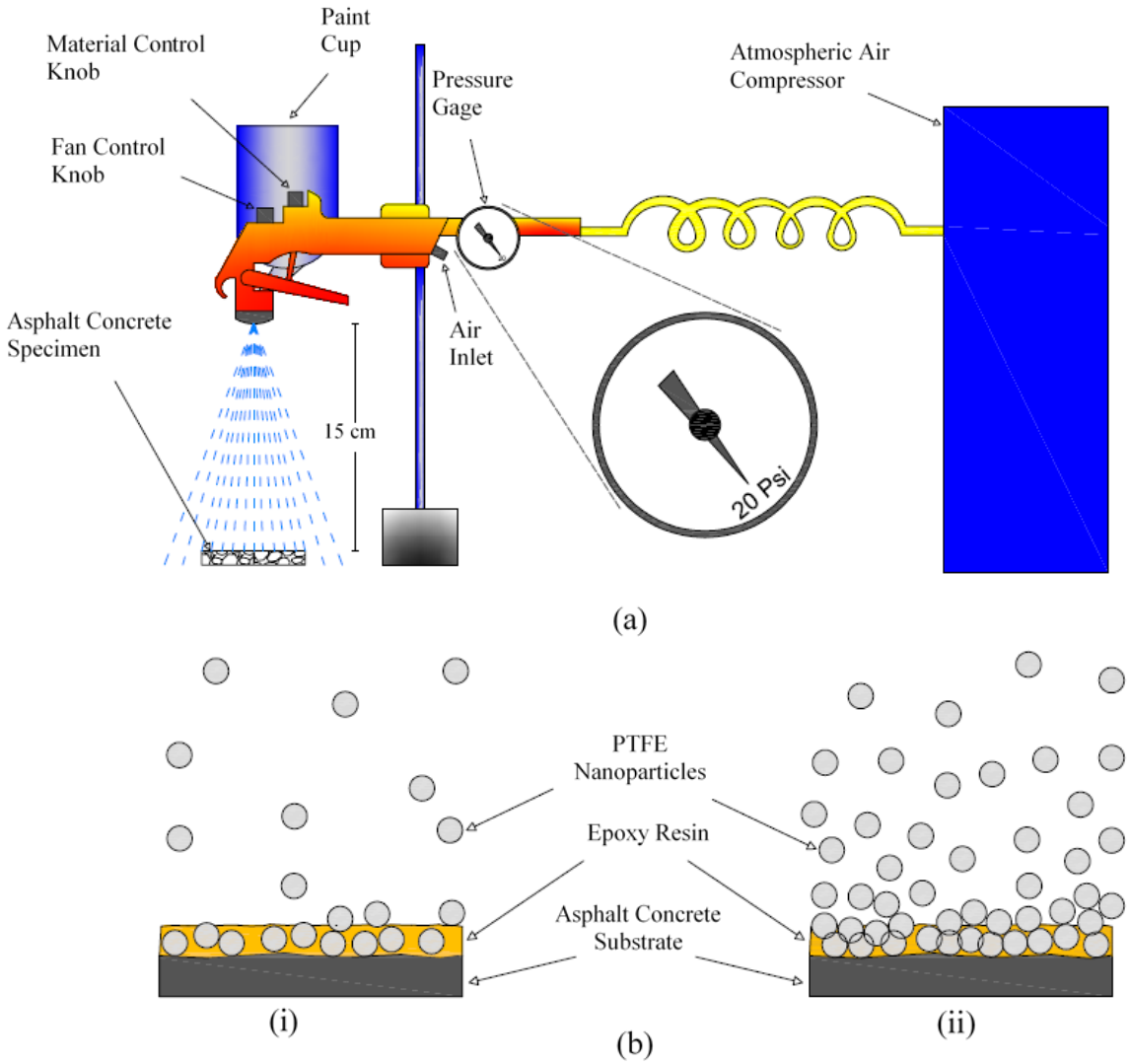

Figure 3.2 *LBL deposition method: (a) spray gun set up for spraying the epoxy and the PTFE and (b) deposition of nanoparticles when the amount of PTFE is low (i) and high (ii).*

Magnifying and Capturing the Water Droplets

To measure the contact angle, 4 µL water droplets, using a micropipette, were deposited on three spots on the surface of each coated specimen. The droplets were big enough to enable the deposition yet small enough to decrease the effect of gravity on their shapes. While it was possible to obtain smaller droplets by evaporating 5 µL droplets under ambient conditions for 40 minutes to obtain 0.3 µL water droplets over the specimens (*25*), this approach was difficult to

control. Rather than using an evaporation method, after deposition the 4 µL droplets were allowed to relax for 30s to reach equilibrium (*26*), then magnified and imaged by a high-magnification Sony camera. Before capturing the droplets' images, it was ensured that the source of light located around the lens of camera emitted an appropriate intensity of light. This level of illumination guaranteed obtaining images with high contrast so that solid-liquid (SL) and liquid-gas (LG) interfaces could easily be distinguished. Tangent lines were then drawn on the two aforementioned interfaces so that the water contact angles could be easily measured. Figure *3.3* illustrates the test setup used for magnifying and capturing the water droplets to measure the water contact angles. The test was performed under controlled environmental conditions of 25° C and relative humidity of 60%.

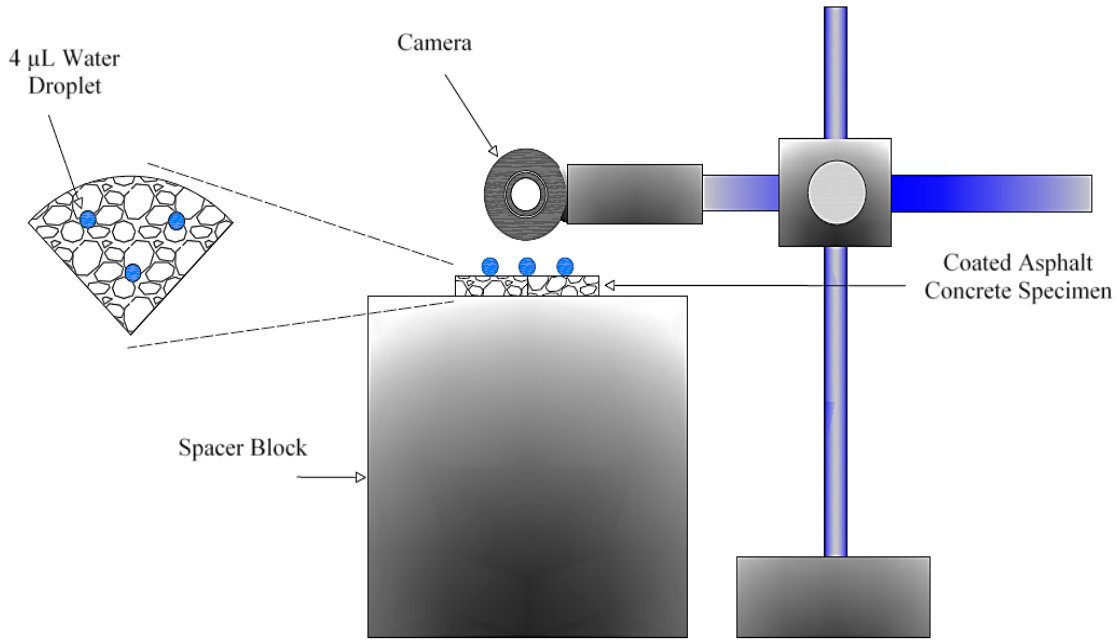

Figure 3.3 *Set-up used for measuring the contact angles.*

Data Collection for Measuring the Coefficients of Friction

Coating the asphalt concrete with PTFE to make it water repellent was just the first step in this study. Before coating a runway or roadway with superhydrophobic coatings, it is necessary to evaluate skid resistance, because if vehicles slide on the coated pavements, spraying PTFE will be to no avail.

In the current state of practice, according to ASTM E274, the skid resistance of asphalt concrete is usually measured at 65 km/h using the locked-wheel method (*27*). According to FAA's advisory circular, the skid resistance of asphalt concrete can be measured at either 65 or 95 km/h using continuous friction-measuring equipment (CFME) (*24*).

One of the most important contributions of this study was measuring the skid resistance at the surface of nano-coated asphalt concrete using a micro-tribometer. The COF values of the coated samples were investigated by performing ramp load tests with a ball-on-flat micro-tribometer. It is worth noting that there were other available methods for studying micro-tribology such as: block-on-ring (*28*), pin-on-disk (*29*), etc. A probe (steel ball) with a tip radius of 2.55 mm was fixed on a probe arm. The sample was mounted on the sample stage and moved horizontally with a DC motor. The load on the probe arm was applied by lowering the vertical stage. Frictional and normal forces were measured with semiconductor strain gauges mounted on the probe arm. All the movements and data collection efforts were controlled with a computer and a data acquisition system connected to the micro-tribometer. A schematic diagram of the device used for measuring the COF is presented in Figure *3.4*.

For data collection, a code was written in the LabView® environment; the probe arm applied a variable normal load - starting from 20 mN and ending at 45 mN - along a 10-mm distance. The speed of the lateral stage was 5 mm/s during application of an increasing normal load. The data were logged along three paths for each specimen.

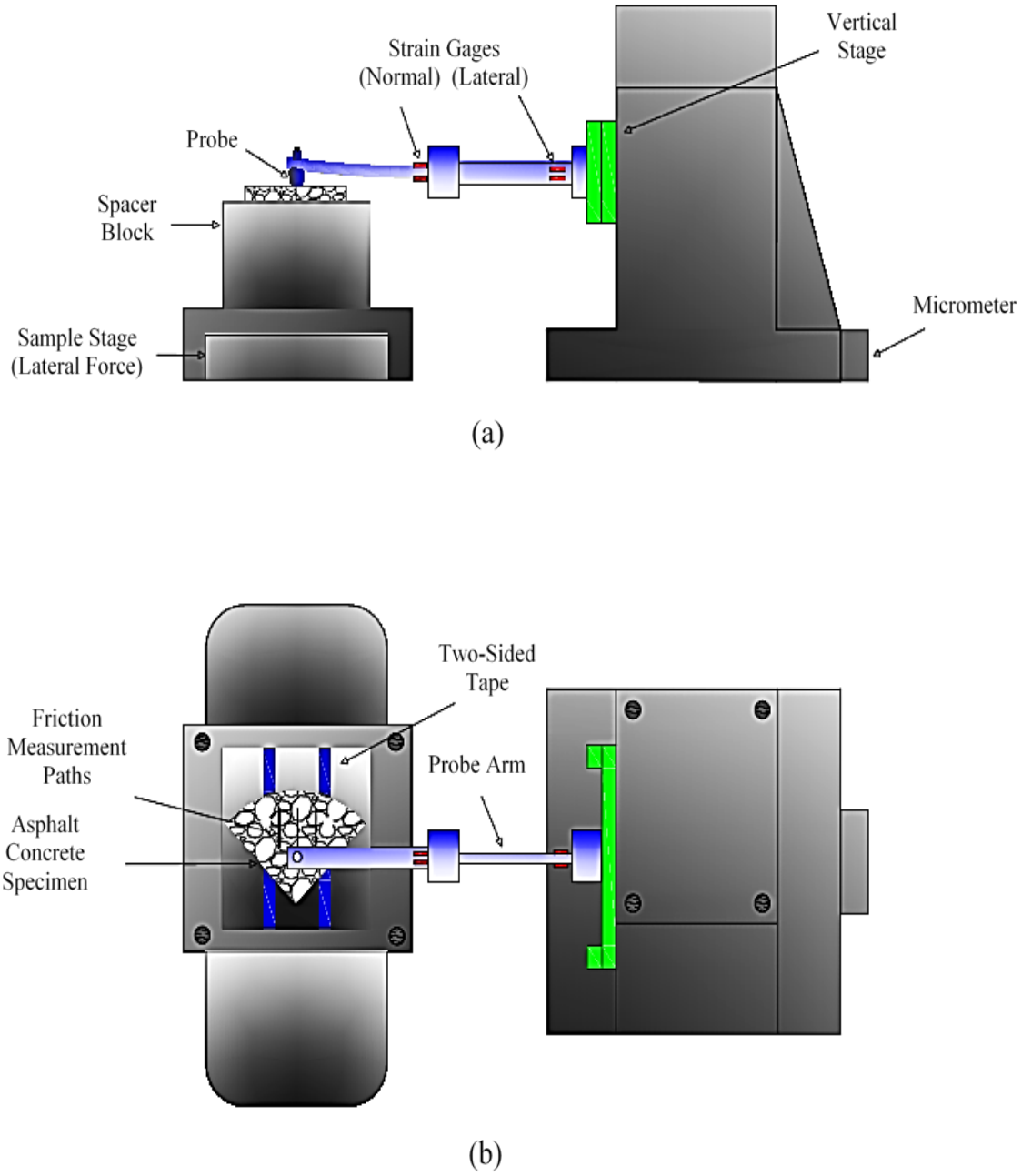

Figure 3.4 *Schematic of the ball-on-flat micro-tribometer; (a) side view and (b) top view.*

Results and Discussion

Contact Angle Measurements

Using the sessile-drop and tangent line method - among the available methods (*25*), the static contact angles of the three deposited water droplets were measured with an on-screen protractor (Figure *3.5*a). The sessile-drop method is the most commonly-employed technique for measuring the contact angle of droplets on liquid repellent surfaces, and it is always coupled with digital image analysis (*30*). In this technique, a liquid droplet of a known volume is gently deposited on the surface from above and the droplet profiles captured using a high-resolution camera. Tangent lines are drawn on the SL and LG interfaces, and the contact angle is measured. After performing measurements using this method, the three measured values were averaged for each specimen. It is worth noting that each specimen had three replicates on each of which three water contact angle measurements were performed. The averaged values for each spraying time and PTFE dosage are presented in Table *3.2*. To depict the behavior of larger droplets resembling rain droplets in terms of size, a portion of paved asphalt concrete was coated with PTFE using the LBL method (Figure *3.5*b). Note that in Figure *3.5*b the water droplets form a spherical shape on the coated side, i.e., they do not tend to wet the surface. However, on the right side not coated with superhydrophobic material, the water cannot form a spherical shape and it wets the surface.

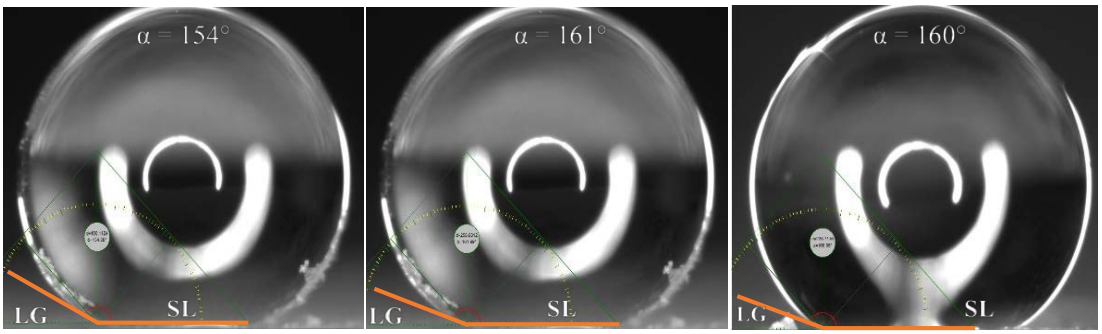

(a)

(b)

Figure 3.5 *Water droplet-asphalt concrete interaction; (a) an example of water contact angle measurement for three droplets and (b) the behavior of water droplet on the coated (left) and uncoated paved asphalt concrete (right).*

A statistical analysis of variance test (ANOVA) was conducted on forty-eight averaged water contact angles (See Table *3.2*). For the selected confidence level of (1-α) = 0.05, a spray time with probability (P) of 0.0002 became the most significant factor. It is worth noting that in the ANOVA analysis method a factor becomes significant if its measured P-value becomes less than a selected confidence level, i.e., the smaller the P-value the more significant the factor. The percentage of PTFE also turned out to be important with a P value of 0.016.

Table 3.2 *Measured contact angles (degrees).*

Spray Time (s)	PTFE (%)							
	10		20		30		40	
	Ave.[1]	SE[2]	Ave.	SE	Ave.	SE	Ave.	SE
3	125	8.3	152	5.4	155	2.6	150	4.8
6	156	2.9	157	3.1	156	2.5	155	1.7
9	161	3.2	154	5.8	165	2.5	158	2.1
12	156	9.0	156	3.9	161	1.6	166	1.5

Note: [1]Ave stands for the average and [2]SE stands for the standard error.

It is important to note that, in Table *3.2*, superhydrophobicity is achieved at a 6-scond spray time for all different percentages of PTFE, and increasing the spray time from 3 to 6 seconds resulted in a proportional increase in hydrophobicity. Increasing the spray time to more than 6 seconds did not significantly increase the superhydrophobicity for different percentages of PTFE except for 40%.

The highest contact angle of 166° was achieved at a spray time of 12 seconds and a PTFE percent of 40. While the reason for such a high contact angle can be attributed to the thorough distribution of nanoparticles over the sample, it should be kept in mind that, for the purposes of ice/snow removal from the pavement/runway, achieving 150-degree contact angles is sufficient (*14*). Increasing the amount of PTFE by either increasing the spray time more than 6 seconds or the dosage of PTFE to more than 20% is not an economical approach.

The reason for obtaining low hydrophobicity (i.e., the lowest contact angle of 125°) at a 3-second spray time and 10% of PTFE can be attributed to the way PTFE particles are deposited on the epoxy layer. When the amount of PTFE particles is low, they sink into the adhesive layer and the accumulation of nanoparticles on the sunken ones is not enough to uniformly cover the whole surface of the specimen.

In addition to the water-contact angle, the work of adhesion can also be considered as a criterion for showing how much a nano-coated asphalt concrete can achieve ice/snow repellence (*14*). The lower the work of adhesion, the more ice/snow repellent a surface becomes. The work of adhesion can be calculated using Equation (1) (*14*).

$$W_A = \gamma_{LV}(1 + cos\theta) \quad (1)$$

Where: W_A = work of adhesion at contact angle θ; and γ_{LV} is the surface tension of water, equal to 72.8 mN/m.

The values of work of adhesion were calculated based on the data of Table *3.2*, and the results are presented in Table *3.3*. Note that, in Table *3.3* the work of adhesion is considerably low for all of the spray times and dosages of PTFE, except for the specimens coated with a spray time of 3 seconds and a PTFE dosage of 10%. It is worth noting that, because of the sensitive nature of Equation (1), increasing the spray time and the dosage of PTFE results in considerable changes in the calculated values of work of adhesion (See Table *3.3*).

Table 3.3 *Measured values of work of adhesion (mN/m).*

Spray Time (s)	**PTFE (%)**			
	10	**20**	**30**	**40**
3	31.3	8.6	6.8	9.5
6	6.4	5.8	6.1	6.8
9	4.1	7.6	2.4	5.3
12	6.5	6.3	4.1	2.1

Coefficient of Friction Measurements

The data from the ramp load test were plotted and straight lines were fit to them, with the slope of the line equal to the kinetic coefficient of friction (μ_k). The COF was measured over the three paths on each replicate, then the three measured values were averaged for each replicate. It

is worth noting that since each specimen had three replicates, to compare the skid resistance of the coated and uncoated asphalt concrete, the COF was also measured over three paths on sixteen uncoated control specimens - each specimen had one replicate for control purposes. Figure *3.6* represents the data gathered from one of the ramp load tests for a coated specimen. The kinetic COF for this specimen is 0.25.

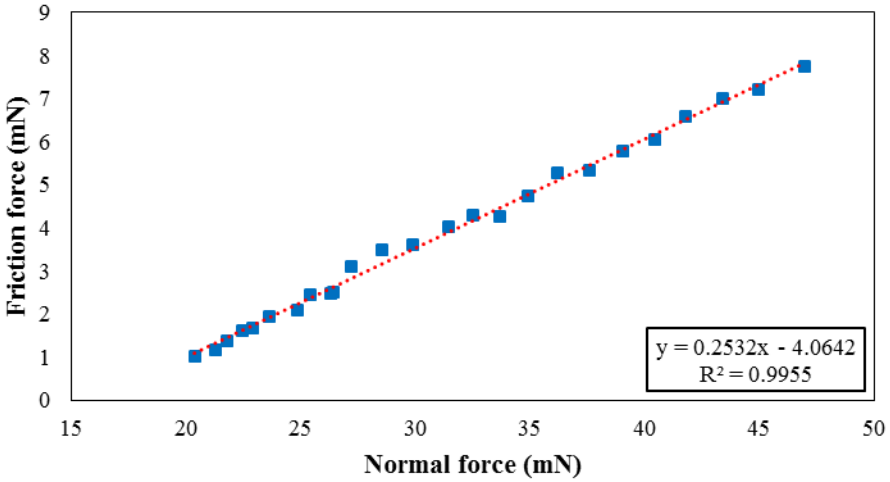

Figure 3.6 *The data obtained from the ramp load test.*

After calculating the coefficients of friction for all 16 coated specimens, each having three replicates, a two-way ANOVA was conducted. For the selected confidence level of (1-α) = 0.05, spray time, with a P-value of 0.0001, became the most significant factor, and the percentage of PTFE, with a P value of 0.001, also turned out to be important. The results of the ANOVA performed on the measured contact angles and coefficients of friction were compatible, with spray time the most significant factor in both types of tests.

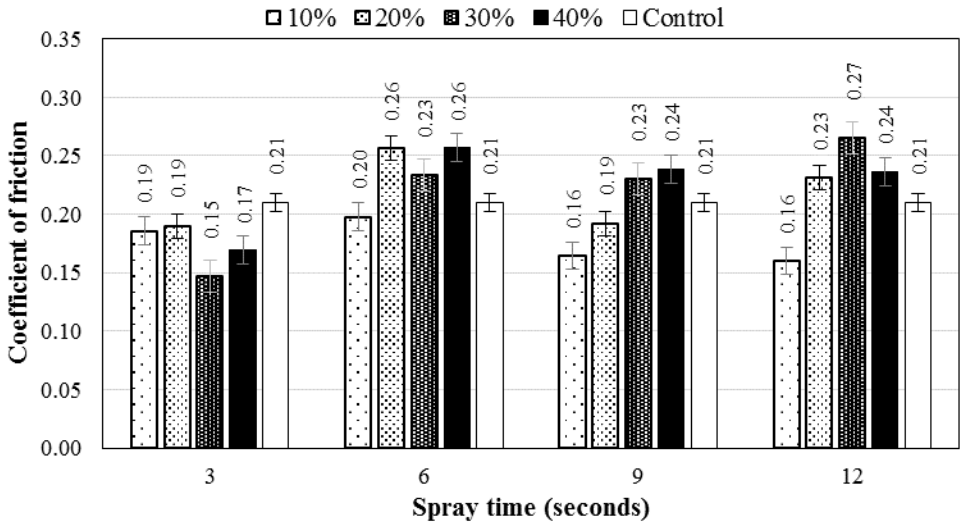

Figure 3.7 *Averaged coefficient of friction values.*

Note that, in Figure *3.7*, increasing the spray time from 3 seconds to 6 seconds considerably increases the COF values, and the results obtained in this section are in agreement with the result obtained for the contact angle measurements. Increasing the spray time from 3 seconds to 6 seconds resulted in achieving superhydrophobic surfaces, while the 6-second spray time with more than the 10% of PTFE dosage resulted in obtaining more skid-resistant surfaces than for the uncoated control sample. The 6-second spray time with the 10% of PTFE dosage still resulted in obtaining skid-resistant surfaces comparable to those of the uncoated control sample.

In fact, the 10% of PTFE dosage under different spray times achieved less skid-resistant surfaces than the uncoated control sample, with the reason for obtaining such relatively low COF values at this PTFE dosage can be attributed to the non-uniform distribution of the PTFE nanoparticles over the adhesive layer of epoxy. A considerable number of nanoparticles could have sunken into the epoxy layer, so while performing the ramp load test, the probe may have passed over the areas covered with epoxy on which no PTFE particles were present. The COF of epoxy is lower than that of an asphalt concrete surface.

Conclusions and Recommendations

The goals of this study were to create, characterize, and evaluate superhydrophobic coated asphalt concrete surfaces for ice- and snow-free flexible pavement applications. The layer by layer (LBL) method and the micro-tribometer based coefficient of friction measuring method was employed to create superhydrophobic coatings and to characterize skid resistance of superhydrophobic coated substrates at micro-texture level. A statistical design based experimental test program was developed and conducted to evaluate the effects of different test variables, including spray times and dosage rates of PTFE. The major conclusions drawn from test procedures and results are summarized along with recommendations as follows:

- Using a LBL method for spray-depositing the PTFE particles seems to be a promising method for achieving ice-repellent surfaces having potential to mitigate problems associated with ice accretion or snow accumulation on roadways or airfield areas paved with nano-coated asphalt concrete.
- The micro-tribometer based coefficient of friction method designed and demonstrated in this study can be a promising method for characterizing skid resistance of nano-coated asphalt concrete at micro-texture level.
- Spray time is a significant factor affecting superhydrophobicity. Increasing the spray duration from 3 seconds to 6 seconds resulted in achieving contact angles higher than 150°, and at the other spray times of 9 and 12 seconds, the superhydrophobicity remained. However, the super water-repellency did not uniformly increase for all of the specimens after 6 seconds. Up to a certain level, increasing the amount of PTFE in nano-coating of asphalt concrete also increases the ice/snow repellency, and above that level, adding to the PTFE deposition

amount is uneconomical, and does not significantly increase the superhydrophobicity.

- Similarly to superhydrophobicity, spray time had a significant influence on the coefficient of friction. While increasing the spray time from 3 seconds to 6 seconds drastically increased the skid resistance of the asphalt concrete samples, when PTFE is sprayed on epoxy in the field, it should be kept in mind that long enough deposition durations should be used for spraying or else the epoxy not covered with PTFE can slightly decrease the skid resistance over the roadway/runway.
- In the context of micro-texture, PTFE results in obtaining comparable or even higher skid resistances measured on the nano-coated asphalt concrete at 6-second spray time for all PTFE dosages. If the spray time and dosage of PTFE are wisely selected, the nano-coated pavements can provide high coefficients of friction at low speeds.
- In the context of macro-texture, the main contributors to improving skid resistance are shape, distribution and the angularities of the coarse aggregate in the asphalt concrete. In other words, the physical properties of aggregate and its particle distribution should be the main concern in pavements coated with the super-ice/water repellent nanomaterials like PTFE at high speeds. It is recommended that this issue be further studied before using of superhydrophobic coatings in actual snow and ice removal strategies for flexible pavement systems.
- The contact angle and friction coefficient measurements were all performed at ambient temperature. Since flexible pavements coated with icephobic PTFE must

curb the formation of ice/snow in cold climatic conditions, it is recommended to perform these tests at lower temperatures so that the effect of temperature on spray deposition, water/ice repellency, and skid resistance can be determined.

Acknowledgements

The authors thank Dr. Sriram Sundararajan and Therin Young of The Department of Mechanical Engineering at Iowa State University for technical support and assistances. Special thanks to DuPont for providing PTFE utilized in this study. The contents of this paper reflect the views of the authors who are responsible for the facts and accuracy of the data presented within. This paper does not constitute a standard, specification, or regulation.

References

1. The Wall Street Journal. The Case for Heated Runways. Mccartney S. http://www.wsj.com/news/article_email/SB10001424052702304914204579392883809689994-lMyQjAxMTA0MDIwMDEyNDAyWj. Accessed Jul. 2015.

2. Gopalakrishnan, K., H. Ceylan, S. Kim, S. Yang, and H. Abdullah. Self-Heating Electrically Conductive Concrete for Pavement Deicing: A Revisit. In Transportation Research Board 94th Annual Meeting Compendium of Papers, DVD-ROM, TRB Paper 15-4764, Transportation Research Board of the National Academies, Washington, DC, 2015.

3. Ceylan, H., K. Gopalakrishnan, S. Kim, and W. Cord. Heated Transportation Infrastructure Systems: Existing and Emerging Technologies. Proceedings of the 12th International Symposium on Concrete Roads, DVD-ROM, Prague, Czech Republic, September 23 - 26, 2014.

4. Feng, X., and L. Jiang. Design and Creation of Superwetting/Antiwetting Surfaces. Advanced Materials, Vol. 18, No. 23, 2006, pp. 3063-3078.

5. Onda, T., S. Shibuichi, N. Satoh, and K. Tsujii. Super-Water-Repellent Fractal Surfaces. Langmuir, Vol. 12, No. 9, 1996, pp. 2125-2127.

6. Lafuma, A., and D. Quéré. Superhydrophobic States. Nature Materials, Vol. 2, No. 7, 2003, pp. 457–460.

7. Miller, J. D., S. Veeramasuneni, J. Drelich, M. R. Yalamanchili, and G. Yamauchi. Effect of Roughness as Determined by Atomic Force Microscopy on the Wetting Properties of PTFE Thin Films. Polymer Engineering & Science, Vol., No. 14, 1996, pp.1849-1855.

8. Zhang, J., J. Li, and Y. Han, Macromol. Superhydrophobic PTFE Surfaces by Extension. Macromolecular Rapid Communications, Vol. 25, No. 11, 2004, pp. 1105-1108.

9. Cao, L., A. K. Jones, V. K. Sikka, J. Wu, and D. Gao. Anti-Icing Superhydrophobic Coatings. Langmuir, Vol. 25, No. 21, 2009, pp. 12444-12448.

10. Mishchenko, L., B. Hatton, V. Bahadur, J. A. Taylor, T. Krupenkin, and J. Aizenberg. Design of Ice-Free Nanostructured Surfaces Based on Repulsion of Impacting Water Droplets. ACS Nano, Vol. 4, No. 12, 2010, pp. 7699-7707.

11. Farzaneh. M., and C. C. Ryerson. Anti-Icing and Deicing Techniques. Cold Regions Science and Technology, Vol. 65, No. 1, 2011, pp. 1-4.

12 Boinovich, L. B., and A. M. Emelyanenko. Anti-Icing Potential of Superhydrophobic Coatings. Mendeleev Communications, Vol. 23, No. 1, 2013, pp. 3-10.

13. Hejazi, V., K. Sobolev, and M. Nosonovsky. From Superhydrophobicity to Icephobicity: Forces and Interaction Analysis. Scientific Reports, No. 3, Article number 2194, 2013, pp. 1-6.

14. Nascimento, J. H. O. D., P. A. Pereira, E. F. Freitas, and F. Fernandes. Development and Characterization of a Superhydrophobic and Anti-Ice Asphaltic Nanostructured Material for Road Pavements. Proceedings of the 7th International Conference on Maintenance and Rehabilitation on Pavements and Technological Control, DVD-ROM, Auckland, New Zealand, 2012.

15. Menini, R., and M. Farzaneh. Elaboration of Al2O3/PTFE Icephobic Coatings for Protecting Aluminum Surfaces. Surface and Coatings Technology, Vol. 203, No. 14, 2009, pp. 1941-1946.

16. Yamauchi, G., K. Takai, and H. Saito. PTEE Based Water Repellent Coating for Telecommunication Antennas. IEICE Transactions on Electronics, Vol. 83, No.7, 2000, pp. 1139-1141.

17. Jafari, R., R. Menini, and M. Farzaneh. Superhydrophobic and Icephobic Surfaces Prepared by RF-Sputtered Polytetrafluoroethylene Coatings. Applied Surface Science, Vol. 257, No. 5, 2010, pp. 1540-1543.

18. Song, H. J., Z. Z. Zhang, and X. H. Men. Superhydrophobic PEEK/PTFE Composite Coating. Applied Physics A, Vol. 91, No. 1, 2008, pp. 73-76.

19. Menini, R., Z. Ghalmi, and M. Farzaneh. Highly Resistant Icephobic Coatingd on Aluminum Alloys. Cold Regions Science and Technology, Vol. 65, No. 1, 2011, pp. 65-69.

20. Panagouli, O. K., and A. G. Kokkalis. Skid Resistance and Fractal Structure of Pavement Surface. Chaos, Solitons & Fractals, Vol. 9, No. 3, 1998, pp. 493-505.

21. Kokkalis, A. G., and O. K. Panagouli. Fractal Evaluation of Pavement Skid Resistance Variations. II: Surface Wear. Chaos, Solitons & Fractals, Vol. 9, No. 11, 1998, pp. 1891-1899.

22. Goodman, S., Y. Hassan, and A. E. Halim. Preliminary Estimation of Asphalt Pavement Frictional Properties from Superpave Gyratory Specimens and Mix Parameters. In Transportation Research Record: Journal of the Transportation Research Board, No. 1949, Transportation Research Board of the National Academies, Washington D.C., 2006, pp. 173-180.

23. Asi, I. M. Evaluating Skid Resistance of Different Asphalt Concrete Mixes. Building and Environment, Vol. 42, No. 1, 2007, pp. 325-329.

24. FAA. Measurement, Construction, and Maintenance of Skid-Resistant Airport Pavement Surfaces. FAA Advisory Circular (AC) No. 150/5320-12C. FAA, U.S. Department of Transportation, Washington, D.C., 2007.

25. Zhang, X, F. Shi, J. Niu, Y. Jiang, and Z. Wang. Superhydrophobic Surfaces: From Structural Control to Functional Application. Journal of Materials Chemistry, Vol. 18, No. 6, 2008, pp. 621-633.

26. Kwok, D. Y., and A. W. Neumann. Contact Angle Measurement and Contact Angle Interpretation. Advances in Colloid and Interface Science, Vol. 8, No. 3, 1999, pp. 167-249.

27. ASTM E274. Standard Test Method for Skid Resistance of Paved Surfaces Using a Full-Scale Tire. Annual book of ASTM standards, ASTM International, PA, 2011.

28. Zhang, Z., C. Breidt, L. Chang, F. Haupert, and K. Friedrich. Enhancement of the Wear Resistance of Epoxy: Short Carbon Fibre, Graphite, PTFE and Nano-TiO 2. Composites Part A: Applied Science and Manufacturing, Vol. 35, No. 12, 2004, pp. 1385-1392.

29. Liu, X. X., T. S. Li, X. J. Liu, R. G. Lv, and P. H. Cong. An Investigation on the Friction of Oriented Polytetrafluoroethylene (PTFE). Wear, Vol. 262, No. 11, 2007, pp. 1414-1418.

30. Srinivasan, S., G.H. McKinley, and R.E. Cohen. Assessing the Accuracy of Contact Angle Measurements for Sessile Drops on Liquid-Repellent Surfaces. Langmuir, Vol. 27, No. 22, pp. 13582-13589.

1

CHAPTER 4. SUPERHYDROPHOBIC COATINGS ON PORTLAND CEMENT CONCRETE SURFACES

A journal paper published in Construction and Building Materials

Ali Arabzadeh[1], Halil Ceylan[2], Sunghwan Kim[3], Kasthurirangan Gopalakrishnan[4], Alireza Sassani[5], Sriram Sundararajan[6] and Peter C. Taylor[7]

Abstract

The objective of this study was to synthesize, characterize, and evaluate use of nanomaterials-based superhydrophobic (super water-repellent) coatings on portland cement concrete (PCC) surfaces. These coatings are synthesized with nanomaterials such as polytetrafluorethylene (PTFE), polyether ether ketone (PEEK) and silanized diatomaceous earth (DE). Using a layer-by-layer (LBL) deposition technique, each coating type was deposited at four different spray durations, and the resulting water-repellency of the coated surfaces were characterized by measuring static water contact angles (WCAs). These measurements were evaluated through a statistical design-based experimental test program that revealed that spray duration and coating type are significant variables. A skid-resistant coating composed of PTFE and PEEK was utilized to evaluate the impact of superhydrophobic coatings on pavement skid resistance.

[1] Graduate Research Assistant, Civil, Construction and Environmental Engineering (CCEE), Iowa State University (ISU), Ames, IA, E-mail: arab@iastate.edu
[2] Professor, Director, Program for Sustainable Pavement Engineering and Research (PROSPER), CCEE, ISU, Ames, IA, E-mail: hceylan@iastate.edu
[3] Research Scientist, Institute for Transportation, ISU, Ames, IA, E-mail: sunghwan@iastate.edu
[4] Research Associate Professor, CCEE, ISU, Ames, IA, E-mail: rangan@iastate.edu
[5] Graduate Research Assistant, CCEE, ISU, Ames, IA, E-mail: asassani@iastate.edu
[6] Professor, Department of Mechanical Engineering, ISU, Ames, IA, E-mail: srirams@iastate.edu
[7] Director, National Concrete Pavement Technology Center, SU, Ames, IA, E-mail: ptaylor@iastate.edu

Introduction

Presence of ice and snow on the surface of rigid pavements and penetration of water into portland cement concrete (PCC) have always been constant sources of concern. During the wintertime, slippery conditions on sidewalks and critical areas of roadways - such as steep slopes and intersections - impose injuries on pedestrians and traveling passengers. Each year, agencies spend millions of dollars removing ice and snow from these surfaces, and in airports, particularly since the beginning of "all-weather" aircraft operations, each winter there have been landing and aborted takeoff incidents or accidents because of slippery and icy conditions on aprons, taxiways, and runways. In addition to pavement winter maintenance issues due to presence of ice and snow, penetration of surface water into PCC causes durability-related problems like freezing-induced damage [1] and sulfate attack [2] leading to expansion, cracking, scaling, and crumbling of the concrete. To overcome winter maintenance related problems, the use of heated pavements [3,4] and superhydrophobic (super water-repellent) coating techniques [5,6] have received recent attention as alternatives to costly and time consuming conventional ice and snow removal practices. Superhydrophobic surfaces, typically icephobic (ice-repellent) [7], can make concrete more durable [8] by repelling surface water.

Lotus leaf is the most famous superhydrophobic surface in nature [9], and there have been biomimetic approaches to mimicking the "lotus effect" for producing hydrophobic (water-repellent) surfaces [10, 11]. Hydrophobicity is governed by chemical properties of the materials - or surface energy and a nano to micro scale hierarchical topographical or surface roughness structure [12]. Although transferring the fascinating "lotus effect" to artificial surfaces has been widely researched, there is very limited literature dealing with bio-inspired superhydrophobic concrete.

So far, superhydrophobic PCC that can also be icephobic [7] has been produced by either applying siloxane-based coatings or emulsions either on concrete with an integrated microtexture [13] or on concrete with embedded hierarchical structure [14]. In both these methods, while the micro roughness and hierarchical structures were produced in fresh concrete, PCC can become superhydrophobic without changing concrete's original structure of [15]. For example, there are cases in which super water-repellent asphalt concrete was created using only polymeric nanostructured coatings like fluoroacrylate [11] or fluorocarbon [5]. There are numerous low surface energy materials like polytetrafluoroethylene (PTFE) [16], polyetheretherketone (PEEK) [17] and perfluorodecyltrichlorosilane (PFDTS) [18] that can become nanostructured using appropriate techniques at the laboratory, and they can then can be utilized for producing super ice/water-repellent coatings on concrete.

Superhydrophobic pavements should maintain skid resistance at an acceptable level in the absence of ice or snow. Two components affect tire-pavement friction: adhesion and hysteresis [19–21]. Adhesion results from molecular bonds developed between the pavement surface and the tire, while the hysteresis component is related to rubber deformation due to pavement surface asperities. While superhydrophobic coatings can slightly decrease skid resistance by changes in surface chemistry, producing the correct surface texture (asperity pattern) on PCC can solve this problem [22]. Among the causes of pavement surface asperities, micro texture (irregularities between 0.005 and 0.3 mm) and macro texture (irregularities between 0.3 and 4 mm) are the most influential in terms of skid resistance [19]. The frictional property of PCC at microtexture level, can be measured using a British pendulum tester (BPT), either at the laboratory or in the field [23].

The purpose of this study was to investigate the feasibility of producing superhydrophobic concrete, at laboratory scale, for ice-and snow-free pavement applications. To this end, a statistical design-based experimental test program was developed to create and evaluate nanostructured superhydrophobic coatings on PCC substrates. The layer-by-layer (LBL) method of spray deposition was utilized to coat the PCC substrates with PTFE, PTFE/PEEK, and diatomaceous earth (DE) silanized with PFDTS. The superhydrophobicity of the coated samples was evaluated by measuring water contact angles (WCAs), followed by a statistical analysis so that the significant design variables could be identified. PTFE/PEEK was selected for coating PCC specimens with different surface textures at the laboratory. After coating the specimens, the effect of different asperity patterns on enhancing the skid resistance was evaluated. It is hoped that the findings of this study will provide guidance with respect to field implementation of superhydrophobic PCC.

Materials and Methodology

To investigate the effects of different variables on the superhydrophobicity of nano-coated PCC substrates, a statistical design was developed prior to their preparation. The selected design variables include the types of water-repellent materials (PTFE, PTFE/PEEK, and silanized DE) and spray durations (4, 6, 8, and 10 seconds). After preparing and coating the substrates, superhydrophobicity levels of the samples were characterized by measuring the static WCAs. For evaluating the effect of nanotechnology-based materials on skid resistance, seven different types of surface textured PCC specimens were prepared. The textured specimens were coated with PTFE/PEEK and their skid resistance measured using a British pendulum tester (BPT) both before and after the coating.

Preparation of Water Contact Angle (WCA) Measurement Substrates/Specimens

The concrete used in this study was prepared in accordance with Iowa DOT mix design (Materials I.M.529) for constructing PCC pavements similar to that described by the FAA advisory circular [24] for construction of airports. The selected water-to-cement ratio was 0.43, and the cement utilized was ASTM C 150 type I/II [25] manufactured by Holcim. The coarse aggregate was limestone - conforming to ASTM C 33's D-57 gradation category [26] - with nominal maximum aggregate size of 25 mm. The fine aggregate was river sand conforming to ASTM C 33 specifications. After preparing the concrete, it was cast into cylindrical molds (100 mm in diameter and 200 mm in height); the specimens were demolded after one day and cured for 28 days at 23ºC and 100% relative humidity. The cylindrical concrete specimens were then cut using a diamond saw to obtain twelve 10-mm-thick disk-shaped specimens with smooth cut surfaces. To obtain replicates, each specimen was further cut to obtain quarters (Figure *4.1*).

Figure 4.1 *Preparation of PCC substrates at the laboratory.*

Preparation of Skid Resistance Measurement Specimens

Microtexture is fine-scale roughness resulting from the presence of fine aggregates and pores in the concrete. On the other hand, macrotexture results from measureable striations that are formed through texturization on fresh or hardened concrete [27]. To investigate the influence of superhydrophobic coatings on PCC skid resistance, it was decided to prepare different surface

textures on fresh concrete specimens cast in beam molds, with concrete mixture and curing regimes identical to those used in preparation of cylindrical specimens. In this way, the effect of surface texture (see Figure *4.2*) on enhancing a potential drop in skid resistance of coated PCC could be evaluated. The surface areas of the specimens were large enough to accommodate the required width and length (78×127 mm) for measuring the skid resistance by BPT. It is worth noting that a smooth control surface was also prepared by finishing the surface of fresh concrete with a steel trowel.

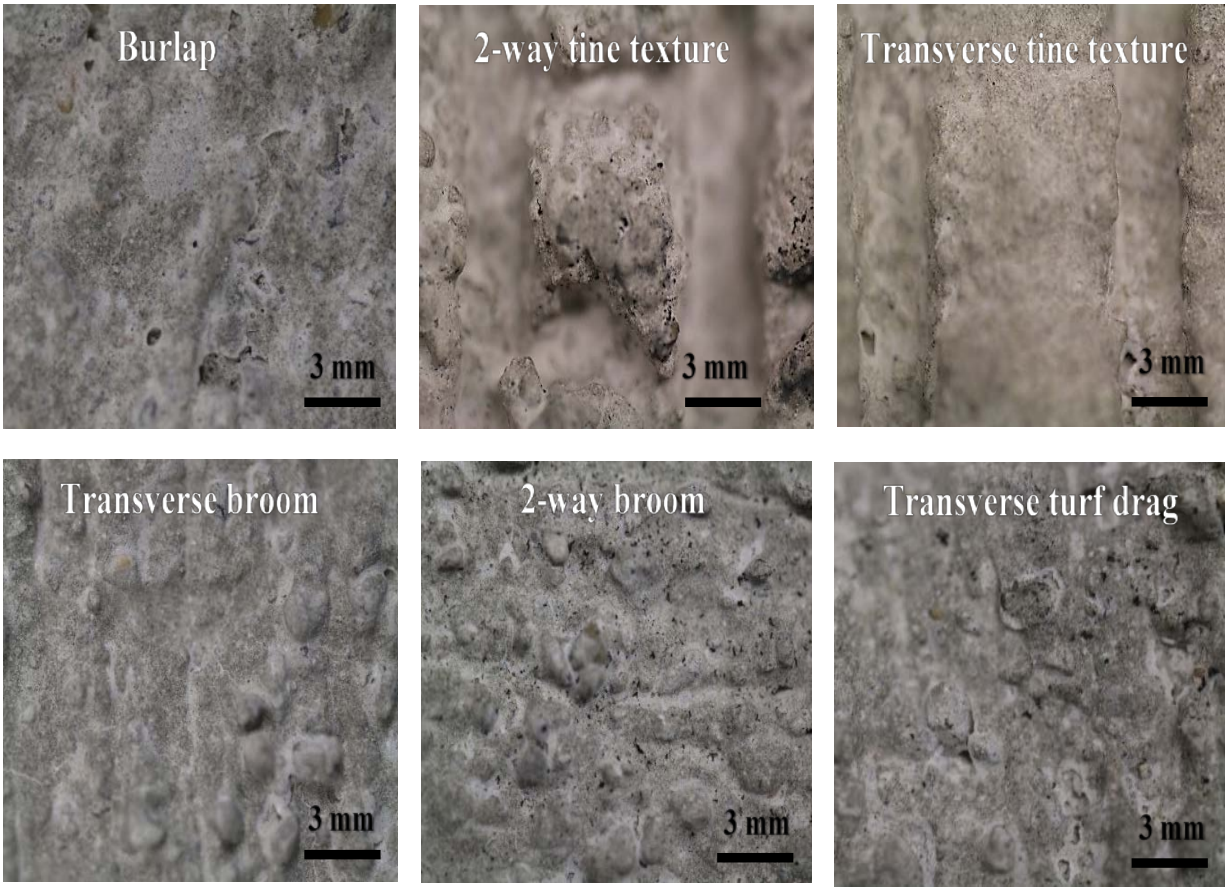

Figure 4.2 *Magnified images of different surface textures produced using burlap, tine, broom and turf.*

Burlap, broom and turf drag surfaces usually have 1.5-3 mm deep striations [27]. The tine depth, width and spacing of the tine texture surfaces produced in this study were 5, 3, and 10 mm, respectively, all within the recommended ranges [27].

Coating the Substrates/Specimens

This research mostly highlights the production of three different nanostructured superhydrophobic coatings on the surface of PCC for ice-and snow-free rigid pavement applications. The water-repellent materials used in this study were PTFE, PEEK, and DE. DE, being hydrophilic, was silanized with PFDTS to render it hydrophobic. These materials were chosen based on their promising water-repellency and tribological behavior on aluminum surfaces reported in an earlier study [28]. According to that study [28], any of the coatings synthesized with PTFE, PTFE, PEEK, or silanized DE resulted in satisfactory durability against grinding action, tested by rubbing 240-grit silicon carbide paper against the coated aluminum surfaces. In other words, there was not a considerable drop in water-repellency after reducing the coating thicknesses by approximately 30% [28]. In addition to these tests, a ball-on-flat micro tribometer was used for performing reciprocal wear tests on the coatings by applying a contact pressure of 24 MPa. The results revealed that PTFE coating had the highest wear resistance, followed by the PTFE/PEEK coating and then the silanized DE coating [28].

Zynol MP 1300 PTFE obtained from DuPont had an average particle size of 12 microns, and Vestakeep PEEK acquired from HT Polymers had an average particle size of 50-80 microns. DE obtained from Fisher Scientific had an average particle size of 5-100 microns and a porous structure with openings no smaller than 0.1 micron. PFDTS was acquired from Sigma Aldrich and used for silanizing the DE.

Diatomaceous earth is a chalky sedimentary material made of skeletal remains of prehistoric micro-organisms [29]. This hydrophilic material can become hydrophobic after silanizing it with a low surface energy solution like PFDTS [30]. To this end, 0.6 grams of PFDTS and 6 grams of DE were introduced into a beaker, followed by hexane added to the beaker in such a way that the total volume of all the components became 50 ml. The batch was magnetically stirred at 500 rpm and 25°C until the hexane had evaporated in about 30 hours. After that, to dry the silanized DE, the beaker was placed in an oven set at 150ºC for 2 hours.

Because of the non-planar surface of PCC, all the substrates were coated using the layer-by-layer (LBL) method [10], a top-down coating technique. In this method, a binding layer is first sprayed on the substrate (first layer), and then the water-repellent material is spray-deposited (second layer). In this study, the binding layer was EP 1224 epoxy acquired from ResinLab. This epoxy is commercially available in two parts: part A, a polymer-based resin, and part B, a curing agent. Part A was mixed with part B at the volume ratio of 2:1, and to decrease viscosity it was mixed with acetone at a volume ratio of 1:1. The whole batch was then magnetically stirred for 5 minutes at 500 rpm and 25ºC. At the end of the stirring process, the prepared binder was immediately introduced into the paint cup of a spray gun specifically intended for spraying the binder, and sprayed over the PCC substrate for three seconds (Figure *4.3*a). After covering the surface of PCC substrates with the fresh binding agent, they were immediately coated with either PTFE, PTFE/PEEK, or silanized DE dispersed in acetone.

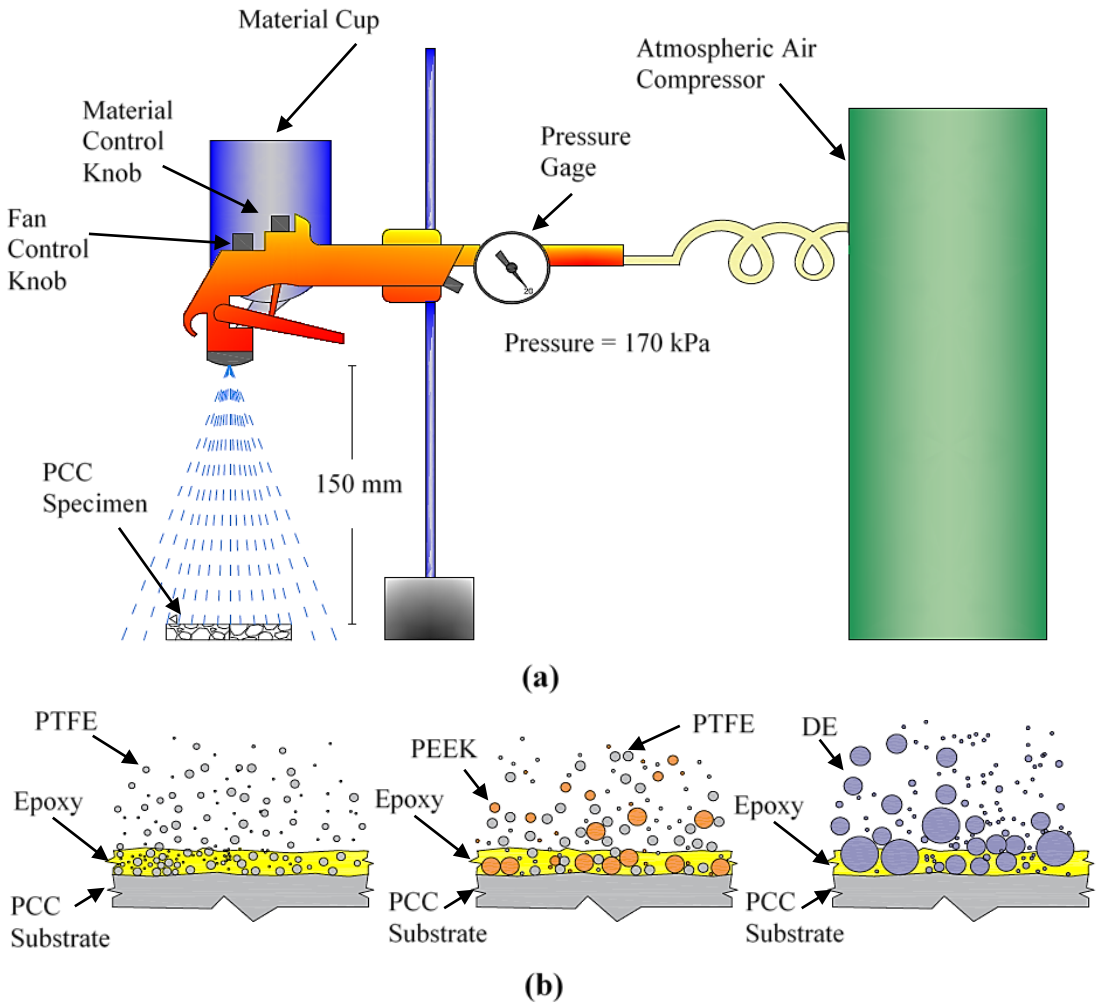

Figure 4.3 *LBL deposition method: (a) spray gun set-up and (b) production of different types of coatings.*

For coating the substrates with PTFE or silanized DE, 6 grams of each of the mentioned materials were mixed with acetone in such a way such that the total volume of PTFE and acetone or the total volume of silanized DE and acetone was 60 ml. For coating the specimens with PTFE/PEEK, 5 grams of PTFE and 1 gram of PEEK were mixed with acetone to obtain a 60 ml batch.

Since a PEEK/PEEK coating provides reasonable friction on a concrete surface [28], all the skid resistance measurement specimens were coated with PTFE/PEEK. Each of the obtained

batches (PTEF + acetone, PTFE/PEEK + acetone, or silanized DE + acetone) were magnetically stirred for 15 minutes at 500 rpm and 25ºC, the prepared batches introduced into the paint cup of a completely clean spray gun used only for spraying the hydrophobic materials (Figure *4.3*a), and then sprayed on the PCC substrates covered with fresh binder. Based on the execution of statistical design, the WCA measurement specimens were coated with PTFE, PTFE/PEEK, and silanized DE at spray durations of 4, 6, 8, and 10 seconds. Based on the statistical analysis performed on the measured WCAs, the specimens used for skid resistance measurement were coated only with PTFE/PEEK for 6 seconds. After the specimens were coated, they were allowed to rest for 5 hours so that the epoxy could cure before measuring skid resistance.

Figure *4.3*b depicts a closer view of the spray deposition mechanism of different water-repellent materials on the portland cement concrete. After deposition, all the low surface energy materials utilized provide a hierarchical structure with particle sizes ranging from nanoscale to microscale. The LBL deposition technique allows the particles to cover the surface and produce the desired roughness.

WCA Measurement

Using a micropipette, 4 µL water droplets were deposited on three spots over each replicate (quarter disk-shaped substrate) at 25 °C and 65% relative humidity. Since each specimen had 4 replicates, 12 water droplets were deposited for measuring the WCAs on each specimen. After placing each water droplet on the surface, it was allowed to relax for 30 seconds to reach equilibrium [31], after which each water droplet was magnified with a macro lens and imaged using a Canon EOS 70D camera (Figure *4.4*).

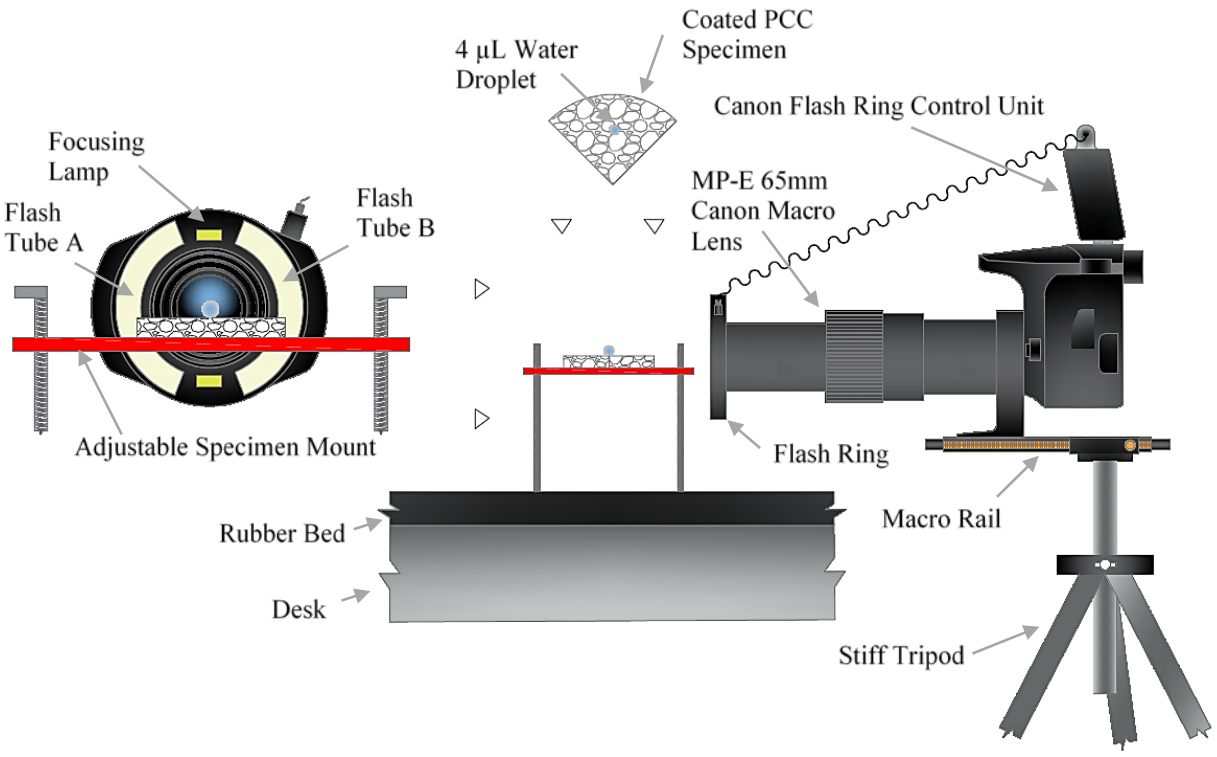

Figure 4.4 *The set up used for magnifying and capturing the tiny water droplets.*

A proper level of illumination was established to facilitate detection of the solid-liquid (SL) and liquid-gas (LG) interfaces. After obtaining the images, tangent lines were drawn on the SL and LG interfaces (Figure 4.5a), and the water contact angles measured with an on-screen protractor. Figure 4.5a also shows the effect of different materials and variation in spray duration on the measured WCAs. The procedure utilized for measuring the WCAs in this study is referred to as a sessile-drop and tangent line method [31]. It is worth noting that a surface is called superhydrophobic when the measured WCA is equal to or larger than 150° [32].

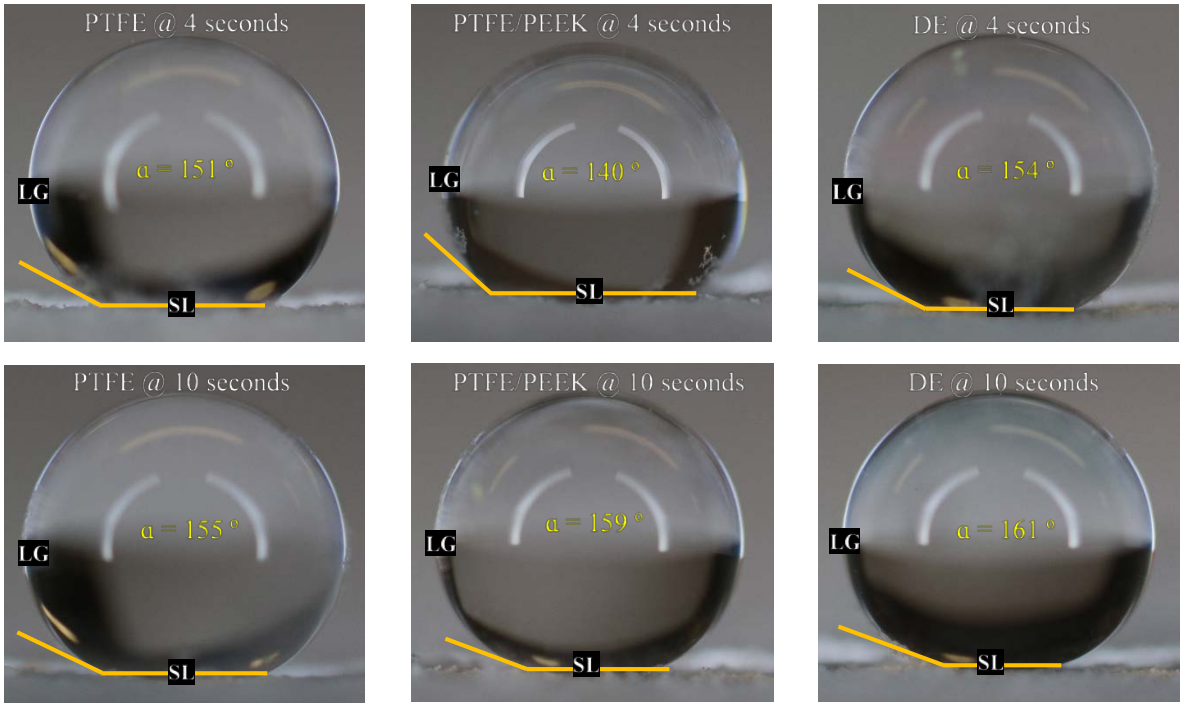

(a)

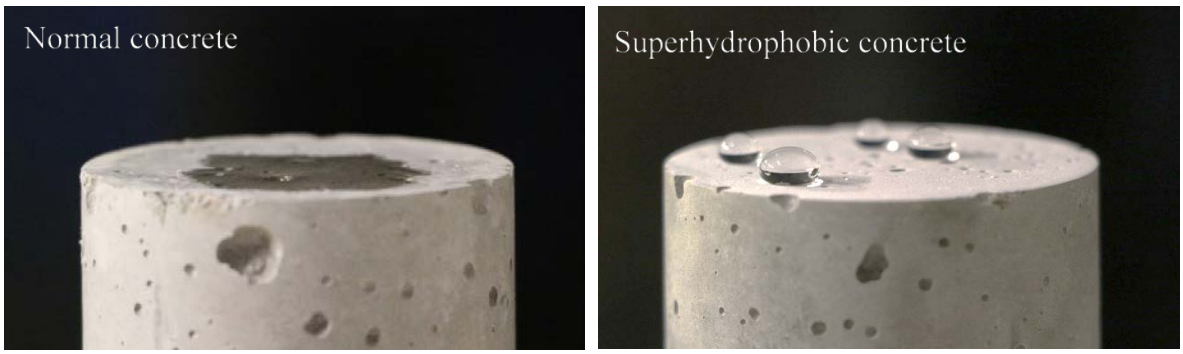

(b)

Figure 4.5 *Water droplet deposition: (a) deposition of 4 µL water droplets using the sessile-method and measuring the WCAs and (b) water-repellency of uncoated (left) and coated (right) PCC specimens.*

Figure 4.5b depicts the behavior of water droplets on the uncoated and coated PCC cylindrical specimens of 50 mm diameter. The sizes of these droplets are much greater than the ones used for WCA measurements.

Skid Resistance Measurement

The British pendulum number (BPN) is representative of the lost amount of kinetic energy after one pass of the British pendulum tester (BPT) rubber slider on a test surface [33]. Although BPT (Figure *4.6*a) is mainly used for measuring skid resistance at microtexture level, it can also be used for measuring the influence of macrotexture on the obtained BPN values [34]. In other words, macrotexture can also be influential at low speeds. Investigating the effect of macrotexture on enhancing the skid resistance of coated surfaces was another novel feature of this study.

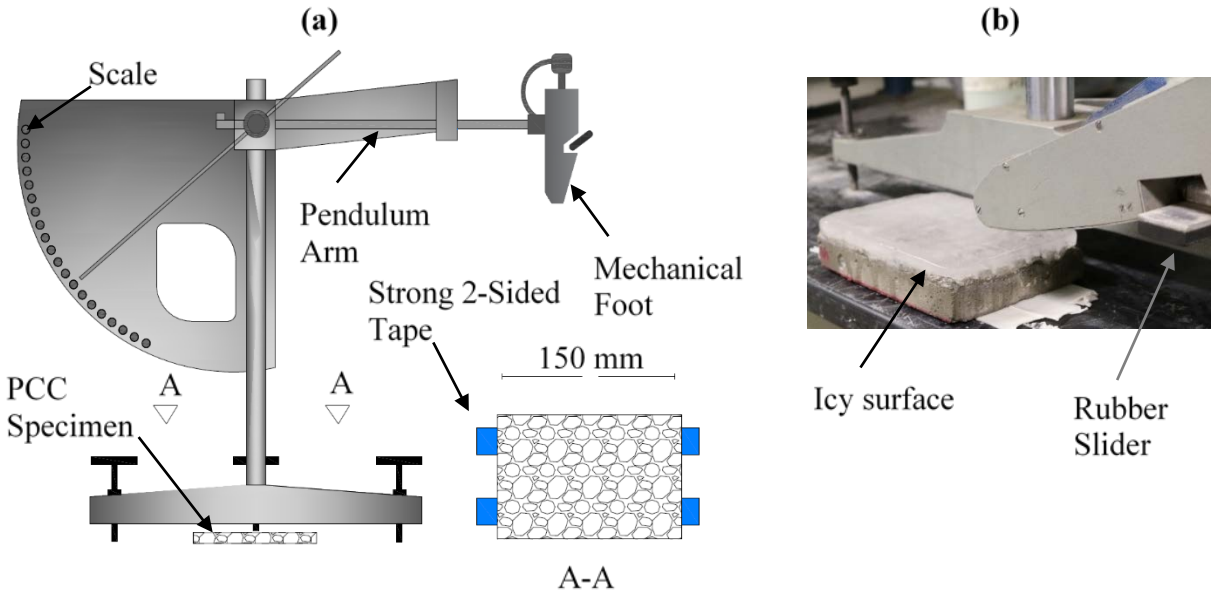

Figure 4.6 *Skid resistance test: (a) schematic of the BPT device and (b) measurement of BPN on an icy surface.*

In accordance with ASTM E303-93 standard [35], the skid resistance under wet conditions was measured. Although a level was used to ensure that the coated specimens and the BPT were completely horizontal, keeping the water on the coated surfaces was not easy due to high water repellency of the surfaces, causing the water droplets to bead up each time surface wetting was attempted. In addition to measuring the BPN values under wet conditions - was in

accordance with the ASTM E303-93 standard - it was decided to measure the BPN values under dry conditions for the sake of comparison. While the BPNs were measured on the uncoated samples at 25°C and relative humidity of 65%, due to delay in the measurements on the coated samples, their BPNs were measured at 35°C and relative humidity of 73%. To make a comprehensive study regarding winter maintenance of paved areas, a 5-mm thick layer of ice was produced on one of the samples at -10°C, and its skid resistance was measured (Figure *4.6*b).

Results and Discussion

WCA Data Analysis

The water contact angle was measured at 12 different positions on each specimen and the measured values were averaged (Figure 4.7).

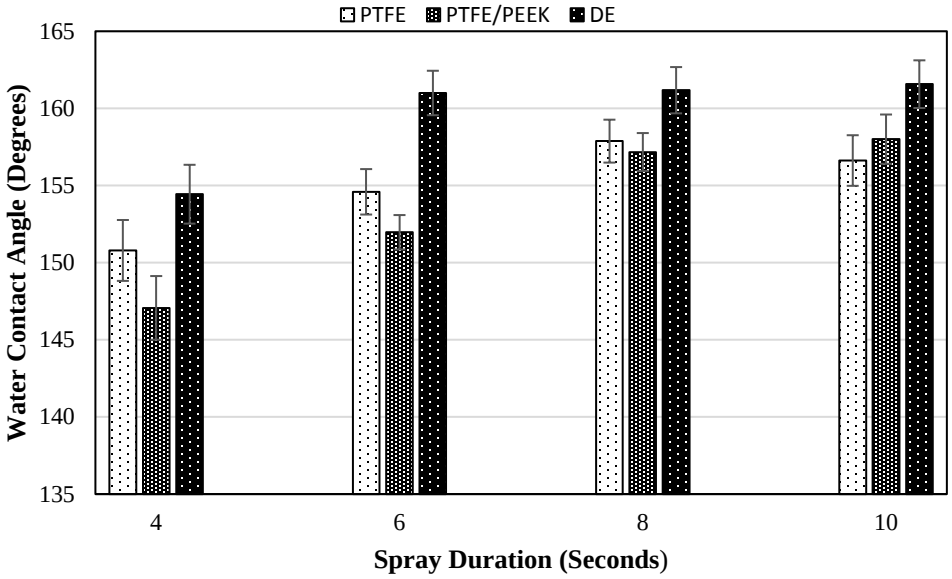

Figure 4.7 *Measured and averaged WCAs.*

It is worth noting that each specimen had four replicates on each of which three WCAs were measured, so each bar in Figure 4.7 represents averaged values for 12 WCA measurements.

A two-way analysis of variance (ANOVA) with the WCAs as responses was conducted. For the selected confidence interval of (1- α) = 0.95, the spray duration and the type of water-repellent material turned out to be significant factors (P-values of 3.2×10^{-09} and 9.9×10^{-07}, respectively). In the ANOVA analysis, a factor becomes significant if its P-value is less than α (0.05 in this study). The smaller the P-value, the more significant the factor. Although both factors became significant, it is possible to say that, because of its smaller P-value, spray duration had more influence on the responses obtained .

Note that in Figure 4.7 all of the specimens coated with PTFE and silanized DE are superhydrophobic because all of their measured WCAs are greater than 150 º. These types of particulate systems have been shown to produce the hierarchical structure necessary to exhibit superhydrophobicity [28]. As the spray duration increases, while the hydrophobicity increases steadily for the specimens coated with silanized DE and PTFE/PEEK, the samples coated with PTFE do not exactly follow this trend. Adding two more seconds to the spray duration of 8 seconds results in a slight reduction in superhydrophobicity of PTFE at 10 seconds. The reason for this behavior can be attributed to the saturation of the PCC substrate with the PTFE particles in such a way such that excess particles cannot stick to the binder and are blown away during the spraying process. While this phenomenon might have been observed on the surfaces coated with PTFE/PEEK and silanized DE at spray durations of 10 seconds, it is possible to postulate that the silanized DE and the PEEK present in PTFE/PEEK coating have a higher affinity for sticking to the epoxy utilized in this study.

For the spray duration range of 4-8 seconds, the substrates coated with PTFE have higher WCAs compared to those of the PCC substrates coated with PTFE/PEEK. The reason for this behavior stems from the fact that PTFE with a WCA of 108° [16] is more hydrophobic than

PEEK having a WCA of 88° [36]. Since this comparison has been made based on measurements performed on solid pieces of these materials, not when they are tiny particles at nano and micro scales, when the hierarchical structure is formed with the aid of the LBL spray deposition technique, PTFE outperforms the PTFE/PEEK coating. Another important aspect of Figure 4.7 is the decrease in differences between the WCAs measured on PTFE and PTFE/PEEK coatings as the spray duration increases from 4 to 8 seconds. This phenomenon can be explained by considering the sizes and specific gravities of PTFE and PEEK particles. The specific gravity of PTFE is almost 1.5 times greater than that of PEEK, and the average particle size of PEEK is almost 5 times greater than that of PTFE. As a result, PTFE particles approach the surface and penetrate into the binder in quicker fashion when they are sprayed using the LBL method. As a result, for short spray durations, the difference between the WCA measured for PTFE and PTFE/PEEK is bigger, and this difference diminishes as more PTFE particles accumulate and spread over the surfaces at longer spray durations of PTFE/PEEK. For the same reason, while the PTFE/PEEK is not superhydrophobic, it is still more than just hydrophobic [37] at a spray duration of 4 s. In that short amount of time, most of the PTFE particles sink into the binder, and only a small number bind to the surface and their presence is dwarfed by that of PEEK particles.

As expected, the highest hydrophobicity for all spray durations was achieved when silanized DE was used for coating the surface of PCC [30]. The reason for this excellent superhydrophobicity (WCAs > 160°) for spray durations of 6,8 and 10 seconds can be attributed to the nanoscale porous silica-rich structure of DE providing a high surface area [30]. Moreover, the relatively bigger particle average size of silanized DE (see Figure *4.3*b) enhances its superhydrophobicity [17]. It is worth noting that the highest contact angle was achieved when

the silanized DE was sprayed for 10 seconds on the PCC, and, to the author's knowledge, this was the first time that a measured WCA on the concrete exceeded 160°.

Skid Resistance Data Analysis

The specimens used for skid resistance measurement were coated with the skid resistant PTFE/PEEK coating for a duration of 6 seconds. The PCC substrates coated with PTFE/PEEK approached superhydrophobicity at a spray duration of 6 seconds (see Figure 4.7), so the use of longer spray durations would not be practically economical.

As expected, under both wet and dry conditions, the control surface achieved the lowest BPN values both before and after coating (Table 4.1& Table 4.2). Since this control surface was made by simply troweling the surface of fresh concrete, no considerable macrotexture was produced.

Under wet conditions, the coated and uncoated specimens with transverse turf drag texture exhibited the highest BPN values (Table 4.1). Because of the sharp edges of the asperities formed on this type of surface, the rubber is easily trapped in its striations and hence deforms more easily (see Figure *4.2*). It is also believed that the turf drag surface provides a surface friction equivalent to that of concrete pavements [38]. While the measured BPN value on the wet uncoated turf drag surface was 83.25, after measuring the skid resistance on the coated surface, the BPN value dropped by approximately 36%, resulting in the obtained value of 52.75. This behavior can be attributed to the completely horizontal state of the surface that did not allow the water droplets (beaded up on the coated surface) to easily flow.

Table 4.1 *Measured BPN values in wet condition.*

Types of Surface Texture	Before Coating		After Coating		RSR
	Ave.	SE	Ave.	SE	%
Control	58.50	0.28	34.50	0.86	41.02
Burlap	72.12	0.51	43.75	0.47	39.34
Transverse and longitudinal Tine	77.75	0.14	52.50	0.64	32.47
Transverse Broom	75.97	0.14	51.50	0.64	32.21
Transverse and longitudinal Broom	72.50	0.64	48.75	0.85	32.75
Transverse Tine	64.37	0.47	41.50	0.35	35.53
Transverse Turf Drag	83.25	0.47	52.75	0.25	36.63

Note: Ave = Average, SE = Standard Error and RSR = Reduction in Skid Resistance.

Unlike the other surface textures, the turf drag surface did not have interconnected tiny channels on the surface (see Figure *4.2*), and as a result, after each surface wetting, some water remained trapped on the completely horizontal surface of the specimen. In addition to this drainage problem, the striations on the turf drag surface were possibly somewhat shallower than other surface textures - excluding the control and burlap - so that the BPT foot could be lubricated by the water remaining in the tiny dips and lead to a considerable drop in the measured BPN. Among all of the coated surfaces investigated in this study, broom (both types), and transverse and longitudinal tine textures exhibited better surface drainage qualities with less reduction in skid resistance, approximately 32%.

Under dry conditions (Table 4.2), the highest value of BPN was achieved for the uncoated turf drag surface but, compared with wet conditions, the dry coated turf drag surface caused a smaller drop in BPN (approximately 20 %), resulting in the obtained value of 79.25. Among all the investigated coated surfaces, transverse and longitudinal tine texture provided the lowest reduction in skid resistance, 2.48%.

Table 4.2 *Measured BPN values in dry condition.*

Types of Surface Texture	Before Coating		After Coating		RSR
	Ave.	SE	Ave.	SE	%
Control	65.25	0.25	49.50	0.328	24.13
Burlap	72.50	0.28	65.87	0.87	9.13
Transverse and longitudinal Tine	85.50	0.28	83.37	0.55	2.48
Transverse Broom	86.5	0.28	71.00	0.41	17.91
Transverse and longitudinal Broom	88.00	0.08	69.00	0.71	21.59
Transverse Tine	89.25	0.41	68.12	0.31	23.66
Transverse Turf Drag	98.75	0.25	79.25	0.48	19.74

Note: Ave = Average, SE = Standard Error and RSR = Reduction in Skid Resistance.

Actual concrete pavements are designed and constructed with a crown or slope to facilitate the drainage of water from their surfaces, and superhydrophobic coated surfaces in this condition (i.e. slightly tilted surface) would help the water droplets flow out immediately, so it would be more realistic to consider the skid resistance data only for the dry condition. By following this assumption, data analysis complexity will be reduced, and the effect of surface texture on enhancing the skid resistance of superhydrophobic PCC pavements could be interpreted in a simpler way.

It is worth noting that the skid resistance was measured on the uncoated surfaces at 25° C, and for the coated specimens the BPNs were measured at 35° C. Since hysteresis changes with temperature, and for each 1°C increase in temperature, the skid resistance would drop by approximately 0.35 BPN [20]. Due to this phenomenon, the obtained BPN values measured on the coated surfaces could be a little higher than those presented in Table 4.1 and Table 4.2.

The average BPN value measured on the icy surface turned out to be 16, drastically lower than the lowest obtained values measured on the coated control surface under both dry (BPN = 49.5) and wet (BPN = 34.5).

Findings and Conclusions

The objective of this study was to investigate the feasibility of producing super water/ice-repellent portland cement concrete in a laboratory environment. The LBL spray deposition technique was utilized to produce three different nano-based superhydrophobic coatings on concrete surfaces. A statistical design-based experimental test program was conducted on the measured responses (WCAs) to evaluate the effect of different test variables, including spray durations and coating types. A British pendulum tester was used for investigating the influence of different concrete surface textures on enhancing the skid resistance of surfaces coated with the most wear-resistant coating. The efforts made in this study lead to the following conclusions:

- Low surface energy materials like PTFE, PEEK and silanized DE can help achieve water/ice-repellent surfaces with potential to mitigate the winter maintenance issues on roadways and airfield areas paved with PCC.
- The Layer-by-layer (LBL) spray deposition technique was for the first time utilized to create superhydrophobic PCC for ice-and snow-free rigid pavement applications. The detailed procedure was clearly documented in a step-by-step manner so that other researchers and practitioners can study and implement this technology.
- Spray duration significantly affects superhydrophobicity. The WCA increased for all the specimens (except the ones coated with PTFE) as the spray duration increased from 4 to 10 seconds. The specimens coated with PTFE showed the same trend for durations of 4 to 8 seconds, meaning that this type of coating, among the selected spray durations for this study, reaches its best performance at a spray duration of 8 seconds.

- Similar to spray duration, the choice of type of low surface energy material had an important impact on the degree of hydrophobicity. Within the spray duration range of 4-8 seconds, the PCC specimens coated with silanized DE were the most superhydrophobic, followed by the PTFE. While the 4-second spray deposition of PTFE/PEEK resulted in obtaining an overhydrophobic but not superhydrophobic surface, for this type of coating, all other spray durations resulted in obtaining superhydrophobic PCC specimens. The silanized DE reached excellent superhydrophobicity with a measured WCA greater than 160° at a spray duration of 10 seconds. This is the first time that a superhydrophobic PCC with such a high degree of superhydrophobicity has been demonstrated.
- Texturizing the PCC surface can considerably enhance diminished skid resistance on super water/ice-repellent rigid pavements. Transverse turf drag texture and transverse and longitudinal tined surfaces are good candidates for enhancing the skid resistance of superhydrophobic rigid pavements.

Recommendations

There are a huge number of different types of water-repellent materials and spray deposition techniques that should be investigated in further studies for finding smart solutions for winter pavement maintenance. Although, according to the reported literature superhydrophobicity leads to ice-repellency, it is recommended that the force required to detach the ice from the surface of superhydrophobic concrete be directly measured to see if any ice will attach to this type of concrete. Another issue that requires investigation is the durability of these nano-coatings on paved areas. There is a need for producing a standard test setup for measuring the wear resistance of these coatings on PCC surfaces. After performing such ab investigation, the most appropriate materials resulting in the most economical approach should be utilized for

spray deposition on PCC surfaces. Producing superhydrophobic concrete is all about making a balance between cost and performance, i.e., one must decide between either increased lifespan and increased cost, or decreased lifespan and lower cost. It would also be possible to nano-treat the surface of heated PCC pavements, then investigate the combined effect of these technologies with respect to removing ice and snow.

Acknowledgements

This paper was prepared from a study conducted at Iowa State University under the Federal Aviation Administration (FAA) Air Transportation Center of Excellence Cooperative Agreement 12-C-GA-ISU for the Partnership to Enhance General Aviation Safety, Accessibility and Sustainability (PEGASAS). The authors would like to thank the current project Technical Monitor, Mr. Benjamin J. Mahaffay, and the former project Technical Monitors, Mr. Jeffrey S. Gagnon (interim), Mr. Donald Barbagallo, and Dr. Charles A. Ishee for their invaluable guidance on this study. The authors also would like to thank the PEGASAS Industry Advisory Board members for their valuable support and feedback. The assistance and efforts of Mr. Robert F. Steffes, ISU PCC Lab Manager, with the lab investigations are greatly appreciated. Although the FAA has sponsored this project, it neither endorses nor rejects its findings. The presentation of this information is in the interest of invoking comments by the technical community on the results and conclusions of the research.

References

[1] M. Şahmaran, M. Lachemi, V. Li, Assessing the durability of engineered cementitious composites under freezing and thawing cycles, J. ASTM Int. 6 (2009) 1–13. doi:10.1520/JAI102406.

[2] S.U. Al-Dulaijan, Sulfate resistance of plain and blended cements exposed to magnesium sulfate solutions, Constr. Build. Mater. 21 (2007) 1792–1802. doi:10.1016/j.conbuildmat.2006.05.017.

[3] H. Abdualla, H. Ceylan, S. Kim, K. Gopalakrishnan, P.C. Taylor, Y. Turkan, System requirements for electrically conductive concrete heated pavements, Transport. Res. Rec. 2569 (2016) 70–79. doi:10.3141/2569-08.

[4] J. Gomis, O. Galao, V. Gomis, E. Zornoza, P. Garcés, Self-heating and deicing conductive cement. Experimental study and modeling, Constr. Build. Mater. 75 (2015) 442–449. doi:10.1016/j.conbuildmat.2014.11.042.

[5] A. Arabzadeh, H. Ceylan, S. Kim, K. Gopalakrishnan, A. Sassani, Superhydrophobic coatings on asphalt concrete surfaces, Transp. Res. Rec. 2551 (2016) 10–17. doi:10.3141/2551-02.

[6] A. Arabzadeh, H. Ceylan, S. Kim, K. Gopalakrishnan, A. Sassani, Fabrication of polytetrafluoroethylene-coated asphalt concrete biomimetic surfaces: a nanomaterials-based pavement winter maintenance approach, in: Proceedings of ASCE ICTD, 2016: pp. 54–64.

[7] L. Cao, A.K. Jones, V.K. Sikka, J. Wu, D. Gao, Anti-icing superhydrophobic coatings, Langmuir. 25 (2009) 12444–12448. doi:10.1021/la902882b.

[8] L. Schueremans, D. V Gemert, S. Giessler, Chloride penetration in RC-structures in marine environment - Long term assessment of a preventive hydrophobic treatment, Constr. Build. Mater. 21 (2007) 1238–1249. doi:10.1016/j.conbuildmat.2006.05.006.

[9] H.C. Baeyer, The Lotus Effect, The Sciences. 40 (2000) 12–15. doi:10.1002/j.2326-1951.2000.tb03461.x.

[10] X. Zhang, F. Shi, J. Niu, Y. Jiang, Z. Wang, Superhydrophobic surfaces: from structural control to functional application, J. Mater. Chem. 18 (2008) 621-633. doi:10.1039/b711226b.

[11] J.H.O. Nascimento, P. Pereira, E. Freitas, F. Fernandes, Development and characterization of a superhydrophobic and anti-ice asphaltic nanostructured material for road pavements, in: Proceedings of 7th Internationa COnference on Maitenance and Rehabilitation on Pavements and Technological Control, August 28-30, 2012, Aukland, New Zealand.

[12] T. Onda, S. Shibuichi, N. Satoh, K. Tsujii, Super-water-repellent fractal surfaces, Langmuir. 12 (1996) 2125–2127. doi:Doi 10.1021/La950418o.

[13] M. Horgnies, J.J. Chen, Superhydrophobic concrete surfaces with integrated microtexture, Cem. Concr. Compos. 52 (2014) 81–90. doi:10.1016/j.cemconcomp.2014.05.010.

[14] I. Flores-Vivian, V. Hejazi, M.I. Kozhukhova, M. Nosonovsky, K. Sobolev, Self-assembling particle-siloxane coatings for superhydrophobic concrete, ACS Appl. Mater. Interfaces. 5 (2013) 13284–13294. doi:10.1021/am404272v.

[15] S. Weisheit, S.H. Unterberger, T. Bader, R. Lackner, Assessment of test methods for characterizing the hydrophobic nature of surface-treated High Performance Concrete, Constr. Build. Mater. 110 (2016) 145–153. doi:10.1016/j.conbuildmat.2016.02.010.

[16] J. Zhang, J. Li, Y. Han, Superhydrophobic PTFE surfaces by extension, Macromol. Rapid Commun. 25 (2004) 1105–1108. doi:10.1002/marc.200400065.

[17] R. Ourahmoune, M. Salvia, T.G. Mathia, B. Berthel, S. Fouvry, N. Mesrati, Effect of sandblasting substrate treatment on single lap shear strength of adhesively bonded PEEK and its composites, ICCM Int. Conf. Compos. Mater. (2011) 2–7.

[18] W. Zhou, J. Zhang, Y. Liu, X. Li, X. Niu, Z. Song, G. Min, Y. Wan, L. Shi, S. Feng, Characterization of anti-adhesive self-assembled monolayer for nanoimprint lithography, Appl. Surf. Sci. 255 (2008) 2885–2889. doi:10.1016/j.apsusc.2008.08.045.

[19] O.K. Panagouli, a. G. Kokkalis, Skid resistance and fractal structure of pavement surface, Chaos, Solitons & Fractals. 9 (1998) 493–505. doi:10.1016/S0960-0779(97)00085-4.

[20] S.M. Bazlamit, F. Reza, Changes in asphalt pavement friction components and adjustment of skid number for temperature, J. Transp. Eng. 131 (2005) 470–476. doi:10.1061/(ASCE)0733-947X(2005)131:6(470).

[21] R.B. Kogbara, E.A. Masad, E. Kassem, A. Scarpas, K. Anupam, A state-of-the-art review of parameters influencing measurement and modeling of skid resistance of asphalt pavements, Constr. Build. Mater. 114 (2016) 602–617. doi:10.1016/j.conbuildmat.2016.04.002.

[22] M.A. Ahammed, S.L. Tighe, Early-life, long-term, and seasonal variations in skid resistance in flexible and rigid pavements, Transp. Res. Rec. 2094 (2009) 112–120. doi:10.3141/2094-12.

[23] ASTM E274/E274M, Standard Test Method for Skid Resistance of Paved Surfaces Using a Full-Scale Tire. doi:10.1520/E0274.

[24] FAA AAS-100, 150/5370-10G-Standards for Specifying Construction of Airports, (2014).

[25] ASTM-C150, Standard Specification for Portland Cement. 1–8. doi:10.1520/C0150.

[26] ASTM Standard C33, Standard Specification for Concrete Aggregates. doi:10.1520/C0033.

[27] M.A. Ahammed, S.L. Tighe, Concrete pavement surface textures and multivariables frictional performance analysis: a North American case study, Can. J. Civ. Eng. 35 (2008) 727–738. doi:10.1139/L08-025.

[28] T. J. Young, J. Jackson, S. Roy, H. Ceylan, S. Sundararajan, Tribological behavior and wettability of spray-coated superhydrophobic coatings on aluminum, Wear. (2017) in press.

[29] D. V. Petrović, C.B. Mitrović, N.R. Trišovic, Z.Z. Golubović, On the particles size distributions of diatomaceous earth and perlite granulations, Stroj. Vestnik/Journal Mech. Eng. 57 (2011) 843–850. doi:10.5545/sv-jme.2010.050.

[30] G. Polizos, K. Winter, M.J. Lance, H.M. Meyer, B.L. Armstrong, D.A. Schaeffer, J.T. Simpson, S.R. Hunter, P.G. Datskos, Scalable superhydrophobic coatings based on fluorinated diatomaceous earth: abrasion resistance versus particle geometry, Appl. Surf. Sci. 292 (2014) 563–569. doi:10.1016/j.apsusc.2013.12.009.

[31] S. Srinivasan, G.H. McKinley, R.E. Cohen, Assessing the accuracy of contact angle measurements for sessile drops on liquid-repellent surfaces., Langmuir. 27 (2011) 13582–9. doi:10.1021/la2031208.

[32] X. Feng, L. Jiang, Design and creation of superwetting/antiwetting surfaces, Adv. Mater. 18 (2006) 3063–3078. doi:10.1002/adma.200501961.

[33] B. Kulakowski, J. Henry, C. Lin, Aclosed-loop calibration procedure for a british pendulum tester, Surf. Charact. of Roadways: International Research and Technologies ASTM Internationl (1990).

[34] Y. Liu, T.F. Fwa, Y.S. Choo, Effect of surface macrotexture on skid resistance measurements by the british pendulum test, J. Test. Eval. 32 (2004) 304–309.

[35] ASTM, Standard Test Method for Measuring Surface Frictional Properties Using the British Pendulum Tester, ASTM Int. 93 (2013) 1–5. doi:10.1520/E0303-93R13.2.

[36] R.Y.M. Huang, P. Shao, C.M. Burns, X. Feng, Sulfonation of poly(ether ether ketone)(PEEK): kinetic study and characterization, J. Appl. Polym. Sci. 82 (2001) 2651–2660. doi:10.1002/app.2118.

[37] S. Muzenski, I. Flores-Vivian, K. Sobolev, Hydrophobic engineered cementitious composites for highway applications, Cem. Concr. Compos. 57 (2015) 68–74. doi:10.1016/j.cemconcomp.2014.12.009.

[38] T. Hoerner , K. Smith , R. Larson , M. Swanlund , Current practice of Portland cement concrete pavement texturing, Transp. Res. Rec. 1860 (2003) 178–186.

CHAPTER 5. ELECTRICALLY-CONDUCTIVE ASPHALT MASTIC: TEMPERATURE DEPENDENCE AND HEATING EFFICIENCY

To be re-submitted to the journal of Materials and Design

Ali Arabzadeh[1], Halil Ceylan[2], Sunghwan Kim[3], Alireza Sassani[4], Kasthurirangan Gopalakrishnan[5] and Mani Mina[6]

Abstract

Asphalt mastic, a pitch-matrix composite, consists of bitumen and mineral fillers (very fine aggregates) that fill the voids created by coarser aggregates in asphalt concrete. In this study, asphalt mastic was modified with carbon fiber (CF) and graphite powder (GP) to produce single-phase (containing only CF) and two-phase (containing both CF and GP) electrically-conductive asphalt mastic (ECAM) to fill the aggregate system in asphalt concrete and impart ice and snow melting capabilities to asphalt concrete. Volume resistivities were measured at two different temperatures, and the influence of temperature on electrical conductivity was evaluated, revealing that reduction in temperature enhances ECAM electrical conductivity. After analyzing the volume resistivity data for both single-phase and two-phase ECAM specimens, heat generation efficiency of single-phase ECAM was investigated at a conductive material dosage slightly higher than the optimum level. The heat generation efficiency was evaluated at below-freezing temperatures by performing active infrared thermography (IRT). Based on the active IRT analysis results, it was found that single-phase ECAM at the selected CF content is capable

[1] Graduate Research Assistant, Civil, Construction and Environmental Engineering (CCEE), Iowa State University (ISU), Ames, IA, E-mail: arab@iastate.edu
[2] Professor, Director, Program for Sustainable Pavement Engineering and Research (PROSPER), CCEE, ISU, Ames, IA, E-mail: hceylan@iastate.edu
[3] Research Scientist, Institute for Transportation, ISU, Ames, IA, E-mail: sunghwan@iastate.edu
[4] Graduate Research Assistant, CCEE, ISU, Ames, IA, E-mail: asassani@iastate.edu
[5] Research Associate Professor, CCEE, ISU, Ames, IA, E-mail: rangan@iastate.edu
[6] Associate Professor, College of Design, Departments of Industrial Design and Electrical and Computer Engineering, ISU, Ames, IA, E-mail: mmina@iastate.edu

of generating enough heat for melting ice and snow or preventing accumulation of snow and formation of ice.

Introduction

Electrically-conductive asphalt concrete (ECAC) can be a promising material for anti-icing or de-icing purposes to mitigate winter maintenance problems in critical paved areas such as airports, bridge decks, etc. ECAC can be produced by adding conductive aggregates or fillers to asphalt concrete. Asphalt concrete consists of bitumen, aggregates, and fillers, with aggregates providing a skeleton that needs to be covered while the filler combined with bitumen forms a mastic that fills the interstitial voids created by aggregates [1]. A common way for producing ECAC is incorporating conductive fillers into asphalt concrete [2], [3], i.e., producing an electrically-conductive asphalt mastic (ECAM) that fills the voids created by an aggregate system. Because of the key role that ECAM can play in generating a desired amount of heat through resistive heating in asphalt concrete, its resistivity and heat generation capability should be studied in a more isolated way, i.e., when there are no aggregates present [4] to interfere with ECAM performance.

García, et al., [5] who studied the heating efficiency of electrically-conductive asphalt mortar (ECAM + sand) for self-healing applications, investigated the heat-generation capacity of asphalt mortar through induction heating. They used eddy currents produced by a magnetic field [3] for increasing the temperature in asphalt mortar. Generation of eddy currents requires closed-loop conductive material circuits [5] locally present in asphalt-based materials, but in conduction heating, for ice-and snow-free pavement applications [6], there is a need for presence of continuous conductive material network(s) in asphalt-based materials connecting one electrode to another, so that the electric current can flow between the electrodes when they are subjected to an electric potential difference.

Material-related factors, including types, combinations, and amounts of conductive fillers can influence the volume resistivity of ECAM. García, et al., [7], were the first to investigate the influence of steel fibers on enhancing the electrical conductivity of asphalt mastic for self-healing applications. They produced an ECAM with a volume resistivity of 200 Ω-cm at an optimum fiber content of 6% by volume of mastic. Although conductive powders can enhance electrical conductivity, it is believed that addition of conductive powders to asphalt concrete containing conducting fibers has no appreciable influence on enhancing electrical conductivity [2]. With advancement in production of conductive fibers and fillers, it seems possible to produce highly-conductive asphalt-based materials capable of generating sufficient heat for ice- and snow-free heated pavement applications.

In addition to material-related factors, external stimuli can influence the electrical conductivity of a composite material such as ECAM [8]. Wu, et al., [9], first to investigate the influence of temperature change on electrical resistance of dense-graded ECAC, found that while reducing the temperature from 30°C to 24°C did not result in any change in resistance of ECAC, they observed a 12% reduction in resistance when they subjected the same ECAC to a temperature reduction from 38°C to 30°C. Resistivity of polymers (such as bitumen) not containing conducting materials is temperature-dependent [10], and above the glass transition temperature ($T_{g\infty}$), which for bitumen can occur at temperatures as low as -25°C [11], the volume resistivity of polymers gradually increases with decreasing temperature [12], i.e., polymers exhibit a negative thermal coefficient (NTC) for $T > T_g$ when they are not modified with electrically-conducting materials. As a result, investigating the effect of temperature on volume resistivity of ECAM at below-freezing temperatures (but still higher than T_g) is of

paramount importance, since ECAM would not be a good candidate for ECAC-heated pavement applications if it were not able to maintain its electrical conductivity at low temperatures.

The objective of this study was to produce an electrically-conductive asphalt mastic (ECAM) with efficient heat generation capability, so that when it fills voids created by aggregates, the result is an anti-icing or de-icing electrically-conductive asphalt concrete (ECAC) for heated pavement applications. To achieve the objective of this study, asphalt mastic was modified with carbon fiber (CF) and graphite powder (GP) to produce both single-phase (containing only CF) and two-phase (containing CF and GP) ECAM specimens. Volume resistivities were measured at two different temperatures, and when the influence of temperature on electrical conductivity was evaluated, percolative behaviors were observed and low resistivity regions were identified. After analyzing the volume resistivity data for both single-phase and two-phase ECAM specimens, it was decided to investigate heat generation efficiency only for single-phase ECAM at a certain conductive material dosage slightly higher than the optimum content. The heat generation efficiency was evaluated at a below-freezing temperature by performing active infrared thermography (IRT). Finally, based on the active IRT analysis results, it was found that single-phase ECAM at the selected CF content is capable of generating enough heat at the selected below-freezing temperature for anti-icing and deicing purposes. Figure 5.1 presents more information regarding the procedure followed for accomplishing this study.

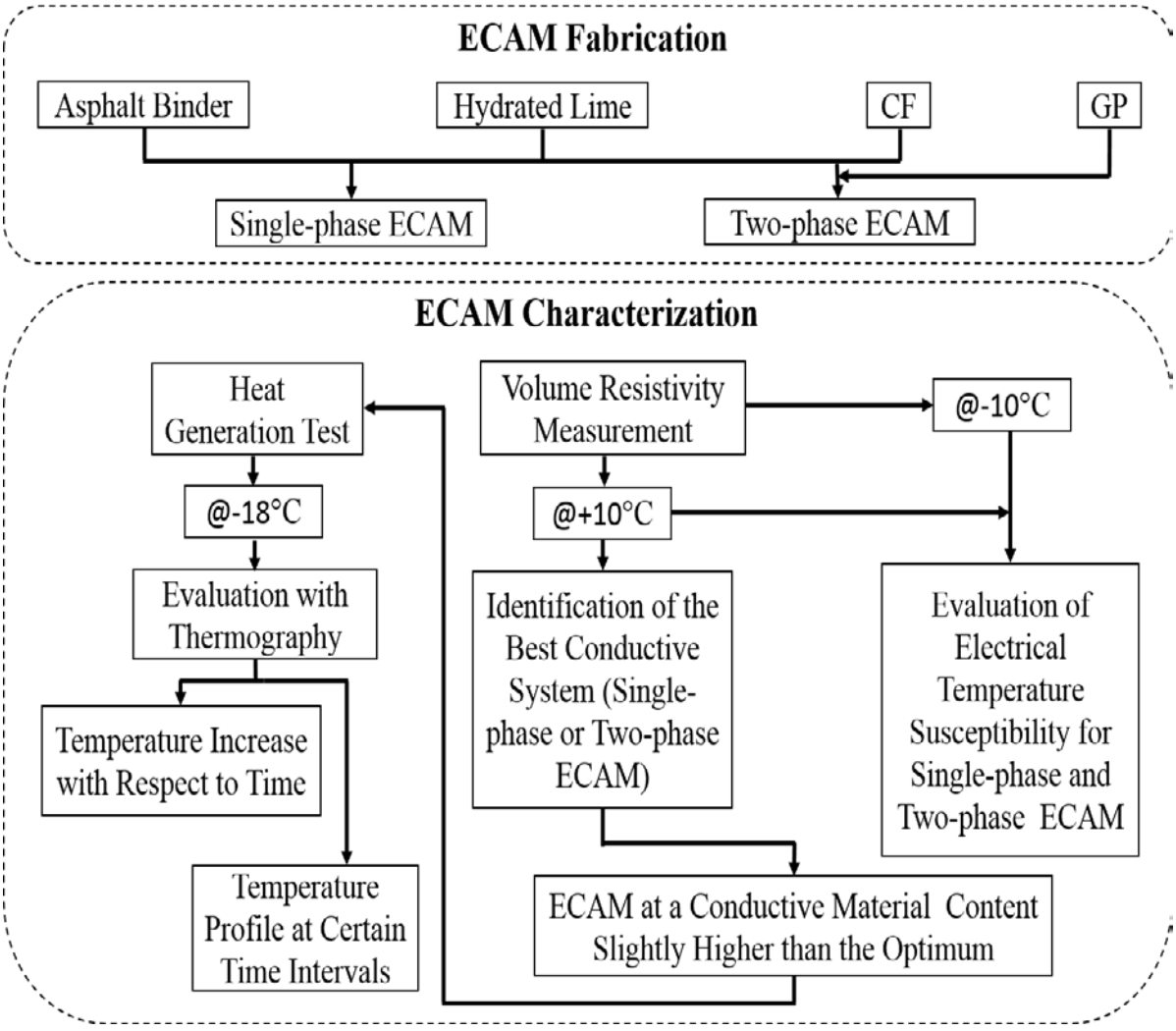

Figure 5.1 *Flowchart laying out the research steps.*

Experimental

Materials

The ECAM specimens prepared for this study were composed of performance grade (PG) bitumen with both non-conductive and conductive fillers. The bitumen, PG 58-28, was obtained from Jebro Inc. The non-conductive filler was hydrated lime (HL), and the conductive fillers, obtained from Asbury Carbons Inc., were flake-type graphite powder (GP) and carbon fiber (CF). The properties of each component type are presented in Table 5.1.

Electrical conductivity in a composite material such as ECAM depends on (in order of importance) [13], [14]: (a) intrinsic conductivity of conductive additives, (b) the degree of direct contact of conductive additives in an insulating matrix such as asphalt mastic, and (c) the hopping of electrons between the conductive materials in close proximity but not in direct contact. As a result, as can be easily interpreted from Table 5.1, CF, with the lowest volume resistivity, is the best conductivity enhancement filler, followed by GP. The resistivity values reported for CF and GP were obtained from Asbury Carbons Inc., and the resistance of CF, according to Asbury Carbons Inc., was determined by measuring the voltage drop along a single fiber or a fiber bundle, after which the resistivity was calculated based on the geometry of the single fiber or the fiber bundle. Resistivity measurement based on voltage drop is thoroughly explained in the ASTM D4496-13 standard. According to Asbury Inc., the resistivity of powdered carbonaceous materials such as GP can be measured by filling a nonconductive hollow cylinder with GP between two metallic pistons and forming a pressure chamber by applying a pressure of 200 Mpa; these pistons are connected to an ohmmeter for measuring the resistance and calculating the resistivity. HL and PG 58-28 are insulating materials, so their resistivity values are not reported in Table 5.1. SG values (see Table 5.1) are necessary for converting each component's volume to weight and vice versa which helped in developing the mastic design information in Table 5.2. Sizes of GP, CF and HL can provide an understanding about the spatial dominance of CF's when blocked by HL particles and can also be an indicator of the ability of CFs to bridge between the GP clusters in an insulating matrix (asphalt mastic), enhancing the overall composite's electrical conductivity. Although copper electrodes have SG and size values, it was decided not to report them, because they were not used in this study.

Specimen Fabrication

To identify suitable approaches for enhancing electrical conductivity of asphalt-based materials, ECAM specimens were prepared using two different methods: (a) using CF to produce a single-phase electrically-conductive material system, and (b) using combined CF and GP to produce a two-phase electrically-conductive material system. To alleviate mechanical problems associated with presence of GP in asphalt concrete [15], GP volume was limited to 5% of mastic volume. GP, because of its intrinsic lubricating characteristic and its tendency to absorb oil, if incorporated into asphalt concrete beyond a certain limit, about 20%, can substantially reduce indirect tensile strength [16], Marshall stability [15], resilient modulus [15], and rutting dynamic stability of asphalt concrete [15]. Since it is believed that incorporation of GP into asphalt concrete at a dosage rate range in the range 3% - 7% does not significantly influence its mechanical properties [15], [17], the median of the range 3% - 7%, i.e., 5%, was selected for incorporation of GP for enhancing the electrical conductivity of ECAM while not compromising the mechanical performance of asphalt concrete. The high tensile strength of CFs does contribute to increased tensile strength of asphalt concrete [18] and its resistance to thermal cracking [19], [20]. With regard to stiffening effects, CFs increase the fatigue life of asphalt concrete [18]. It has been reported that presence of CF can increase the fatigue life of asphalt concrete by approximately 10-25 orders of magnitude [21] and that CF is the best conductivity enhancement material for use in asphalt concrete [2]. The reason for this good performance stems from the fact that high aspect ratio CFs produce the longest conductive paths compared with other types of conductive fillers [2]; the fiber-to-fiber contact mechanism facilitates the conductive network formation and hence increases the electron transmission rate through the asphalt concrete [2]. Although CF can considerably increase the electrical conductivity of asphalt-based materials, it has one major drawback, i.e., poor dispersion, causing CF to have a

high tendency to agglomerate into small or large clusters [2]. Before producing the ECAM specimens in this study, some trial mixes were prepared to investigate the distribution quality of CFs in the asphalt mastic, and it was found that while 2.75% CF was the maximum volume content at which the fibers would uniformly disperse in the mastic, for the sake of maintaining the accuracy of test results it was decided to use CF up to 2.5%. All percentages reported in this paper are representative of volume fractions of asphalt mastic.

Table 5.1 *Material properties.*

Material Type	**Properties**		
	SG	**Resistivity (Ω.cm)**	**Size (μm)**
GP	1.9	0.05, measured along the compaction axis of particles compacted at 200 MPa	44 - 75
CF	2.26	6×10^{-3}, measured along the fiber axis	Length = 3500 and Diameter= 13
HL	2.3	NA	< 75
PG 58-28	1.035	NA	NA
Copper Electrode	NA	$\sim2\times10^{-6}$	NA

Note: SG = specific gravity, GP = graphite powder, CF = carbon fiber, HL = hydrated lime, PG = performance grade and NA= not applicable.

For enhancing the conductivity of asphalt-based materials, it is possible to either substitute conductive fillers for non-conductive fillers [2] or to just incorporate the conductive fillers with no substitution [7]. The first approach, filler substitution, was implemented in this study (see Table 5.2), and a bitumen-to-filler weight ratio of 1:1 was held constant for preparation of all the mastic specimens. According to the Superpave method of mix design, the maximum amount of filler (particles smaller than 0.075mm) to be used in an asphalt concrete was 10% by weight of aggregate [22]. In addition to limiting the maximum amount of filler incorporated into asphalt concrete, the current design standard requires incorporation of mineral filler be limited to a ratio in a range of 0.6-1.2 by mass of filler to bitumen [23], [24], and, simultaneously, the gradation of the overall aggregate (including fillers) must fall within the

specification limits [25]. For producing ECAC, Wu, et al., [2] maintained a bitumen-to-filler ratio of approximately 1:1 and their asphalt concrete specimens were composed of 6.5-7.5% bitumen, 7.4% fillers (limestone powder and conductive fillers) and 85.6% basalt aggregates. García, et al, [7] investigated induction heating of asphalt mastic containing sand for self-healing applications and thoroughly studied the influence of sand-to-bitumen ratio; they found that a sand-to-bitumen ratio of 1:1 resulted in the lowest volume resistivity for a mastic containing steel wool and graphite. For all these reasons, a bitumen-to-filler weight ratio of 1:1 was maintained in all the fabricated specimens in this study. Moreover, Park et al., [26], who investigated the conductivity of asphalt mastic containing graphite powder, used this same filler-to-bitumen weight ratio in their investigations. It is worth noting that all the weights presented in Table 5.2 were calculated using SG values provided in Table 5.1.

Table 5.2 *Detailed mastic design information for ECAM conductive systems.*

Single-phase Conductive System				**Two-phase Conductive System**					
CF		**HL (g)**	**PG 58-28 (g)**	**CF**		**HL (g)**	**GP**		**PG 58-28 (g)**
V (%)	**W (g)**			**V (%)**	**W (g)**		**V (%)**	**W (g)**	
0.00	0.00	321.20	321.20	0.00	0.00	270.40	5.00	50.9	321.20
0.25	2.10	319.10	321.20	0.25	2.10	268.20	5.00	50.9	321.20
0.50	4.30	316.90	321.20	0.50	4.30	266.10	5.00	50.9	321.20
0.75	6.40	314.80	321.20	0.75	6.40	263.90	5.00	50.9	321.20
1.00	8.60	312.70	321.20	1.00	8.60	261.80	5.00	50.9	321.20
1.25	10.70	310.50	321.20	1.25	10.70	259.70	5.00	50.9	321.20
1.50	12.80	308.40	321.20	1.50	12.80	257.50	5.00	50.9	321.20
1.75	15.00	306.20	321.20	1.75	15.00	255.40	5.00	50.9	321.20
2.00	17.10	304.10	321.20	2.00	17.10	253.30	5.00	50.9	321.20
2.25	19.20	302.00	321.20	2.25	19.20	251.10	5.00	50.9	321.20
2.50	21.40	299.80	321.20	2.50	21.40	249.00	5.00	50.9	321.20

Note: GP = graphite powder, CF = carbon fiber, HL = hydrated lime and PG = performance grade.

According to the literature, conductive fillers can be incorporated into asphalt-based materials through either dry [7], [27] or wet [28], [29] mixing methods. In a dry mixing method, all components, including the conductive filler, are mixed within a temperature range of 150-160°C [7], [27], while in a wet mixing method, the conductive fillers are first blended with

bitumen at an elevated temperature range of 170-180°C [28], [29], after which the modified bitumen is mixed with other components. Increasing the mixing temperature increases the oxidation of bitumen [30], so as a result, to reduce bitumen oxidation, a dry mixing method was utilized in this study. Using a rotational viscometer - and following the ASTM D4402 standard [31] - the minimum mixing temperature of PG 58-28 was determined to be 145°C. Mixing the mastic components at 145°C was attempted, but the conductive fillers - especially CFs at high dosage rates, e.g., 2.5% - did not become evenly distributed in the mastic. It was therefore decided to decrease the bitumen viscosity by increasing the mixing temperature, so mixing was attempted at 150 °C, 155 °C, 160 °C and 165°C. With increase in mixing temperature, CF dispersion quality improved, with the best result obtained at 165°C. It is worth noting that mixing at higher temperatures was not attempted due to an increased chance of bitumen oxidation in the mastic. Moreover, using HL as non-conductive filler in this study worked towards our benefit, because the HL particles applied shear during the mixing process, enhancing the conductive material dispersion quality. The absence of non-conductive fillers and aggregates is the reason for using an elevated mixing temperature range of 170-180°C in a wet mixing method [28], [29]. Our claim is consistent with the findings of Liu, et al., [27], who mixed steel wool in asphalt concrete (ECAM + aggregates) at 160 °C to produce electrically conductive porous asphalt concrete for self-healing applications; the applied shear by aggregates during the mixing process helped enhance the conductive material distribution and thereby avoided the need for using a high mixing temperature. Based on the results obtained during the mixing process, it is anticipated that producing ECAC (ECAM + aggregates) will require a mixing temperature less than165°C but higher than 145°C.

Based on the results obtained from all the trial mixes, all the mastic components were conditioned in an oven set to 165 °C (this does not reflect the temperature at which asphalt concrete would be produced in an asphalt plant) for 1 h. This conditioning time window allowed the bitumen viscosity to increase while bringing the temperature of bitumen, hydrated lime, and conductive fillers to the mixing temperature of 165°C. The components were then mixed for 5 minutes at 60 rpm using a Hobart mixer, and the mixtures were then conditioned (cured) again in the oven at 165 °C for 15 m. Such conditioning time allowed the specimens to attain sufficient workability, after which they were hand-compacted in wooden molds (the hand-compaction method does not represent the way that mastic would be compacted in the field in the presence of aggregates). There is no standard that details the preparation of ECAM or even asphalt mastic specimens; Park, et al., [26] previously used a hand-compaction method for placing self-sensing ECAM in wooden molds, and Liu [32] and García, et al., [7] also used a hand-compaction method for placing ECAM in silicon molds. However, to increase test result accuracy, ECAM was cured in the oven (facilitating ECAM placement in the molds) and the specimen weights were measured after the compaction then compared with the calculated design values to decrease introduction of operator-related errors during the specimen preparation; such a weight control method was also practiced by Liu [32]. It is worth noting that, due to the absence of aggregates, ECAM tended to slightly deform during the demolding process at room temperature, so in this study, the resulting asphalt mastic specimens were conditioned for 2 h in a freezer set at 0°C so they could be easily detached from the molds (Figure 5.2 (a)), achieving virtually no deformation during the demolding process.

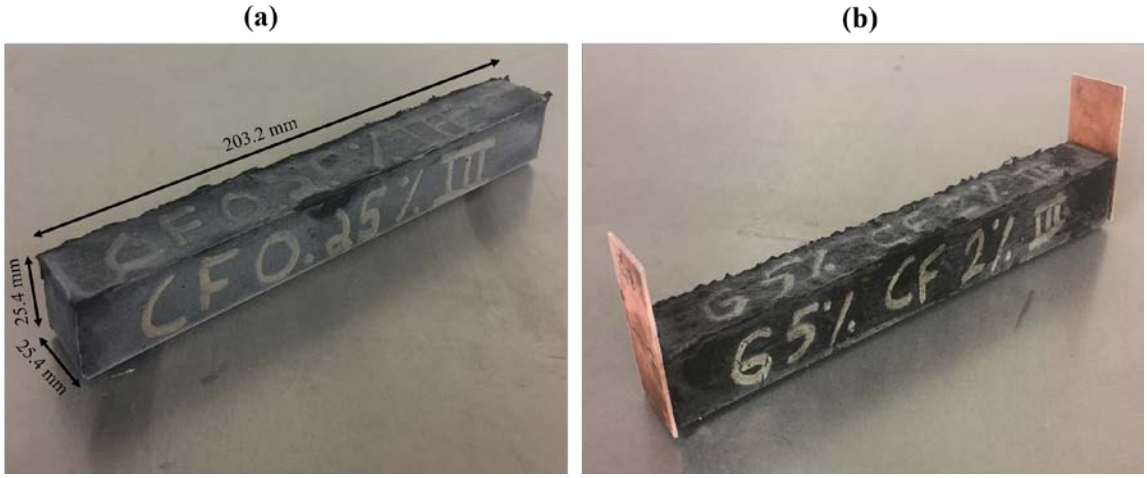

Figure 5.2 *Preparation of prismatic asphalt mastic specimens: (a) demolded asphalt mastic specimen, and (b) asphalt mastic specimen with attached copper electrodes.*

To ensure perfect contact between the electrodes and each asphalt mastic specimen, dispersed graphite [2], graphite powder [5], or silver paint could be used to fill cavities on the specimen and enhance electrical conductivity at the electrode-specimen interface. However, since the bitumen used in asphalt-based materials is temperature-dependent and can become tacky at temperatures above 60°C [33], to take advantage of this adhesive behavior of bitumen, the asphalt mastic specimens were slightly warmed up using a blowtorch at the electrode-specimen contact areas, followed by placing the electrodes into contact with the resulting tacky surfaces of the asphalt mastic specimens (Figure 5.2 (b)). The electrodes were forced tightly against the specimens, permitting the bitumen to flow and fill the small cavities, thereby ensuring that the electrode-specimen contact area was pore-free; there were no pores visible to the naked eye. It is worth noting that this method of attaching electrodes to ECAM specimens is operator-dependent and its accuracy was evaluated through calculating relative standard errors (RSEs) from the volume resistivity values obtained from the ECAM specimens' replicates. Such use of the bitumen adhesive property for connecting electrodes to the mastic specimens closely represents what is likely to happen during the actual process of ECAC paving, because it is the

mastic that would form the adhesive portion of asphalt concrete binding the aggregates together [34] as well as helping ECAC adhere to electrodes, although the electrode material and configuration (including type and spacing) can vary according to the design requirements and field environmental conditions where the ECAC is to be placed. In other studies [35], [36], the authors provided detailed discussion on the field requirements of heated pavement systems made of electrically-conductive portland cement concrete.

Volume Resistivity Characterization

Resistance is defined as the ratio of applied voltage to the resulting electric current, and an object's resistance depends on its dimensions and material composition [5]. To eliminate the effect of shape and size of an object, one can instead consider resistivity, an intrinsic material property. The electrical resistivity of asphalt-based materials, like other materials, can be obtained using Ohm's law [5] for a specimen of length L and uniform cross-sectional area S:

$$\rho = \frac{RS}{L} \quad (1)$$

where ρ is electrical resistivity measured in Ω-cm, R is electrical resistance measured in Ω, S is electrode-specimen contact area measured in cm^2 (in this study 2.54 cm × 2.54 cm), and L is the distance between electrodes measured in cm (in this study 20.32 cm).

All resistivity values were measured using a two-probe method, a common approach for measuring electrical resistivity of asphalt-based materials [2], [5], [28], [37], [16]. Unlike hydrophilic portland cement-based materials [38], asphalt-based materials are hydrophobic [39], and there is no concern regarding the presence of capillary water in the asphalt mastic. Since we are investigating the electrical properties of a water-free matrix (i.e., mastic), there is no concern about ionic conduction and hence no need for resistivity measurement using a four-probe method [40].

The electrical resistivity of asphalt mastic specimens was characterized using two probes (i.e., copper electrodes) attached to each specimen (see Figure 5.2 (b)). A FLIR DM62 digital multimeter was used for measuring resistance values below 40 MΩ, and a DC Hipot Tester was used for measuring resistance values above 40MΩ. To evaluate temperature-dependent properties of asphalt, resistivity measurements were performed at both -10 °C and +10 °C. A of novel feature of this study was to measure the resistivity at a temperature below the freezing point of water (-10 C). If an ECAM matrix cannot maintain low resistivity at temperatures below 0°C, it would be unable to generate sufficient heat and therefore unable to increase the asphalt concrete temperature sufficiently to melt ice/snow in an efficient manner.

All resistivity measurements were performed in an environmental chamber with two fans and a dehumidifier unit, with the fans constantly recirculating the air to ensure a uniform temperature distribution. At each test temperature, the dehumidifier unit maintained the relative humidity (RH) at the lowest possible limit to guarantee measurement accuracy. RH values were maintained at 10% and 35%, respectively, when measurements were performed at -10 °C and +10 °C. If vapor condensation the environmental chamber made it impossible to adequately decrease the RH, a thin layer of ice (at -10°C) or a thin layer of water (at +10°C) could form around the specimens, resulting in inaccurate and erroneous determination of resistivity values, especially in specimens containing smaller amounts of conductive materials. Volume resistivity of pure water at 25°C is approximately 18E+06 Ω.cm [41] and it increases with a decrease of temperature, e.g., the volume resistivity of frozen pure water is about 86E+06 Ω.cm. If the resistivity of ice/water on the boundaries of specimen is lower than that of ECAM, during the resistivity measurements some number of electrons will pass through ice/water causing a false reduction in measured ECAM resistivity values. Observation of the same behavior is expected

for ECAC implemented in the field, but presence of different ions (at variable concentrations), PH levels, etc., can influence the volume resistivity of water, so there is a need to consider the influence of non-pure water/ice on ECAC, if ECAC is to be produced using very low dosage rates of conductive material contents, i.e., for applications other than melting ice or snow.

Before performing resistivity measurements, all asphalt mastic specimens were preconditioned at each specified temperature (either -10 °C or +10 °C) for at least three hours to achieve thermal equilibrium [20]. The resistivity vs. conductive material volume content data were analyzed so that resistivity zones/stages, optimum conductive material contents, and effect of temperature on volume resistivity could be determined.

Heating Characterization

A FLIR T650sc IR camera with a resolution of 640 × 480 pixels was used to evaluate the heat generation efficiency of only the asphalt mastic specimen at 1 % CF volume content. Analyses on the volume resistivity data showed that ECAM with 1% CF provides a sufficiently low volume resistivity value for anti-icing and de-icing applications, and this CF content is also above the percolation transition zone. According to Wang, et al., [28], operating close to the percolation transition zone is not recommended, because safety and energy efficiency are of paramount importance for de-icing and anti-icing purposes, and operation in the percolation transition zone with its intrinsic high rate of resistivity change [28] should be avoided in design procedures. Also, analyses on volume resistivity data obtained from single-phase and two-phase ECAM revealed that utilizing GP does not substantially decrease the volume resistivity for anti-icing and de-icing applications. A self-heating material, unlike a self-sensing one [42], requires a highly conductive composite, so it is better to avoid using GP – considering its negative influence on mechanical properties of asphalt concrete – when it does not significantly enhance the electrical conductivity at high CF dosage rates, i.e., equal to or greater than 1% CF.

Before performing the thermography, all specimen replicates were preconditioned at -18 °C, the lowest range at which the IR camera could operate, for at least three hours to achieve thermal equilibrium [20]. Performing the thermography on ECAM at a below freezing temperature (i.e., -18 °C) was one of the novel features of this study, and this also prevented excessive deformation of mastic (due to absence of aggregates) at higher temperatures produced by resistive heating. Since ECAM can be heated by applying an electric current, i.e., an external stimulus, the heat generation efficiency of all specimens used in this study were evaluated by performing active infrared thermography (IRT) [43]. An AC voltage of 60 V at a frequency of 64 Hz was applied to each specimen for a duration of 10 minutes, after which the top surface temperature of each specimen was measured and recorded using an IR camera that produced data in the form of radiometric video. The acquired data were then analyzed using the ResearchIR Max® software package, and the heat generation efficiency was evaluated.

Results and Discussion

Evaluation of Volume Resistivity

Specimen volume resistivities were measured, and the values obtained from the replicates (each specimen had three replicates) were averaged for each specimen type. Figure 5.3 presents the change trends in volume resistivity of asphalt mastic specimens, measured at +10 °C, as a function of CF content. Additional information regarding the volume resistivity values of single-phase and two-phase ECAMs, respectively, are presented in Table 5.3 and Table 5.4.

As expected [27], three stages can be observed in the curves of Figure 5.3: high resistivity, transit, and low resistivity – all of which are proof of the percolative behavior [44] of ECAM. In the context of electrical conductivity, percolative behavior is defined as a sudden decrease (by orders of magnitude) in volume resistivity, resulting in an insulator-conductor transition, with addition of conductive materials such as CF at small dosage rates; the transition

stages in Figure 5.3 are proof of such behavior [44], [45]. It is worth noting that the ECAM specimens had to be prepared over a wide enough range of conductive material additive to capture such percolative behavior.

In the high resistivity stage, both single-phase and two-phase ECAM specimens exhibited resistivity values higher than 2.43×10^5 Ω.cm and 4.55×10^5 Ω.cm, respectively. In the second stage, for specimens modified by CF and CF&GP, the volume resistivities drop sharply from 2.43×10^5 Ω.cm and 4.55×10^5 Ω.cm to 1.44×10^2 Ω.cm and 8.65×10^2 Ω.cm, respectively. This stage, associated with a large change in resistivity, is known as the percolation transition zone [27]. In the low resistivity stage, starting immediately after the percolation transition zone, i.e., at optimum conductive material contents, the resistivity values gradually decrease [2] until the curves become essentially flat [5]. Optimum content is defined as the value beyond which increasing the dosage of conductive materials does not appreciably decrease the volume resistivity [2]. The optimum content values for single-phase and two-phase specimens are 0.75% and 0.5%, respectively [27].

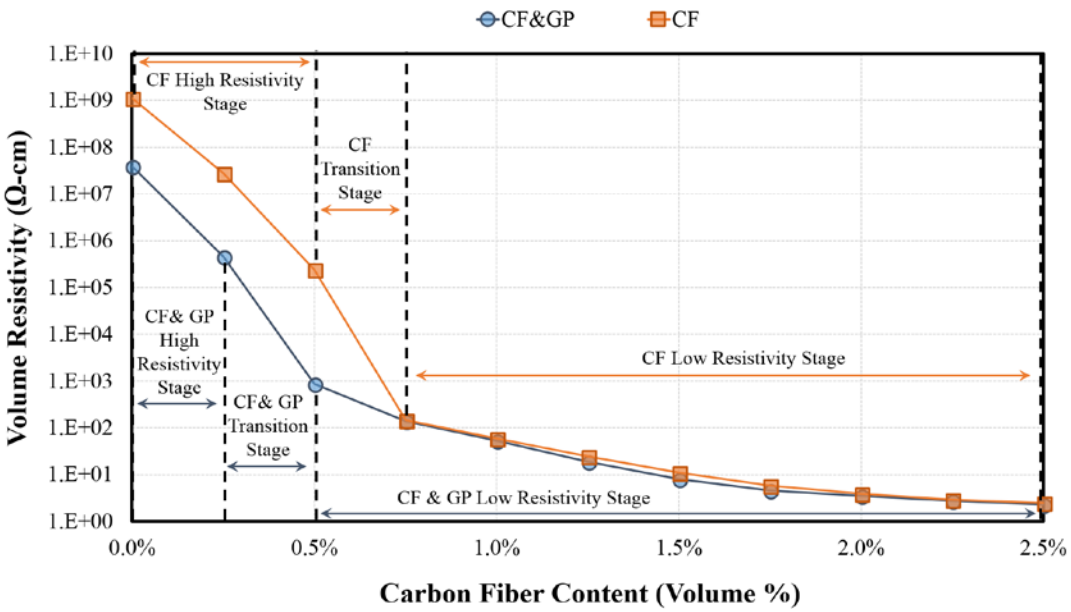

Figure 5.3 *Relationship between electrical resistivity and CF content in single-phase and two-phase ECAM specimens.*

According to Weber, et al., [46], the sudden insulator-to-conductor transition in polymer composites such as ECAM is evidence of existence of a percolation threshold [46]. When small amounts of CF are added to asphalt mastic, they tend to be completely electrically isolated, and electrons cannot easily travel between and within the CFs. Increasing the amount of CFs allows the fibers to become closer or even contact one another, i.e., the greater the amount of CFs, the greater the conductivity. When the CF volume content reaches a threshold value, a value within the transition zone (see Figure 5.3), the first few continuous conductive paths will be formed, enabling easy movement of electrons through the asphalt mastic and an associated substantial drop in volume resistivity [46]. Beyond the percolation transition zone (i.e., at optimum conductive material content), addition of conductive materials results in gradual development and spreading of a purely conductive network in all three dimensions. A similar insulator-to-conductor behavior was observed by Liu, et al., [27], in a study performed on electrically-conductive porous asphalt concrete for self-healing applications. Based on their findings, adding conductive materials to porous asphalt concrete can continue until an optimum value at which the conductive materials are in extensive contact with one another in all directions, forming many conductive networks and electron passages. As a result, above such an optimum value, addition of conductive materials to asphalt mastic would not significantly decrease the resistivity, nor would it be economical (see low resistivity regions in Figure 5.3). According to García, et al., [5], expected curve shapes for volume resistivity versus conductive material would be S-shaped for conductive asphalt mortar (i.e., a mixture of bitumen, fillers, fine aggregate, and electrically conductive materials), and this was confirmed for the single-phase ECAM specimens of this study (see Figure 5.3). However, the curves obtained for asphalt mastic specimens made of two-phase conductive materials (i.e. CF&GP) are only slightly S-shaped because GP particles

make the percolation transition smoother, enabling more precise manipulation of volume resistivity over a wider range of conductive materials [28]. Wang, et al., [28], observing this behavior in dense-graded asphalt concrete modified with electrically-conductive materials, claimed that such a concave shape is desirable, and that the same principle can be applied for two-phase ECAM. In addition to making the curve more concave, adding 5% of GP causes the percolation transition and optimum conductive material content to be achieved, compared to single-phase ECAM at lower volume dosage rates of CF. Moreover, between 0% and 0.5% values of CF volume content, addition of GP causes a huge decrease - virtually 100% - in volume resistivity (see Figure 5.3).

When resistivity values become lower than 1,000 Ω.cm, a CF-based conductive network has already been established and the bridging effect [2] cannot further enhance the conductivity substantially. The bridging effect - defined as the capability of fibers to form bridges between isolated GP clusters to enhance passage of electrons [2] - is more effective when there are fewer CFs present in the specimens, e.g., in the range from 0% to 0.5 % CF (see Figure 5.3). Because of lack of bridging effect efficiency in the low resistivity region (see Figure 5.3), presence of 5% GP in asphalt-based materials is not significantly helpful for self-heating applications, because CFs by themselves can result in achieving sufficiently low resistivity values.

Evaluation of Temperature Effect on Volume Resistivity

Table 5.3 and Table 5.4 present averaged volume resistivity values at +10°C and -10°C. These averaged values are the arithmetic means of the resistivity values measured for each asphalt mastic type for the three replicates. Standard error (SE) and relative standard error (RSE) values were calculated. RSE is obtained as SE divided by the arithmetic mean and is then reported as a percentage quantifying the size of the standard error relative to the averaged measurements. Excluding the RSE calculated for single-phase specimen tested at -10°C, the

largest RSE values calculated for single-phase ECAM belong to the specimens containing the optimum CF content of 0.75%; this can be attributed to the large volume resistivity fluctuations within the percolation transition zone [12], [44]. Also, the largest RSE values calculated for the two-phase ECAM specimens are associated with the specimen containing the optimum CF content of 0.5%, and this again can be attributed to the large resistivity fluctuations within the percolation transition zone [12], [44]. The reason for large RSE values in single-phase and two-phase ECAM specimens containing no CF can be water condensed or ice formed on the surface of specimens. As mentioned earlier, presence of condensed water/ice on specimens with high resistivity values can influence volume resistivity measurements and when the temperature decreases (i.e., from +10°C to -10°C) the amount of condensed/frozen water will increase, accounting for even higher RSE values at -10°C. It is worth noting that while the environmental chamber equipped with dehumidifying units used in this study decreased the relative RH values, these values were still 35% and 10% at +10°C and -10°C, respectively.

Table 5.3 *Measured resistivity values for the specimens modified with CF only.*

CF (Vol %)	Resistivity (Ω.cm)					
	+10 °C			-10 °C		
	Ave	SE	RSE (%)	Ave	SE	RSE (%)
0.00	1.12E+09	2.43E+08	20.9	1.15E+09	3.94E+08	34.4
0.25	2.73E+07	2.33E+06	8.5	2.46E+07	2.27E+06	9.2
0.50	2.43E+05	2.80E+03	1.2	2.12E+05	4.42E+03	2.1
0.75	1.44E+02	3.30E+01	22.9	8.62E+01	2.20E+01	25.5
1.00	5.85E+01	7.41E-01	2.0	3.75E+01	1.81E+00	4.5
1.25	2.43E+01	4.55E-01	16.2	1.66E+01	4.61E-01	18.4
1.50	1.08E+01	3.78E-01	3.5	7.26E+00	2.98E-01	4.1
1.75	5.85E+00	4.04E-01	9.5	4.62E+00	3.50E-01	10.4
2.00	3.87E+00	2.29E-01	5.9	3.15E+00	2.28E-01	7.2
2.25	2.87E+00	8.27E-02	2.9	2.28E+00	1.06E-01	4.7
2.50	2.50E+00	7.63E-02	3.0	2.05E+00	4.23E-02	2.1

Note: Ave = Average, SE = Standard Error and RSE = Relative Standard Error.

According to Table 5.3 and Table 5.4, except for ECAMs prepared at 0% CF or the ECAMs produced at CF contents falling within the percolation transition zone, the RSE values are relatively small, confirming the reproducibility capability of ECAM specimens using the provided mixing and compaction procedures and following the method utilized for attaching the electrodes to ECAM specimens.

Table 5.4 *Measured resistivity values for the specimens modified with both CF and GP.*

CF (Vol %)	Resistivity (Ω.cm)					
	+10 °C			-10 °C		
	Ave	SE	RSE (%)	Ave	SE	RSE (%)
0.00	3.90E+07	1.11E+07	28.4	3.81E+07	1.14E+07	30.0
0.25	4.55E+05	2.80E+04	6.2	3.92E+05	1.06E+04	2.7
0.50	8.65E+02	3.04E+02	35.1	5.39E+02	3.01E+02	55.9
0.75	1.37E+02	2.83E+01	20.6	9.30E+01	1.70E+01	18.3
1.00	5.30E+01	8.09E+00	15.3	3.57E+01	6.68E+00	18.7
1.25	1.89E+01	7.16E-01	15.2	1.46E+01	5.96E-01	21.5
1.50	7.93E+00	2.92E-01	2.6	6.29E+00	4.24E-01	5.4
1.75	4.54E+00	3.68E-01	8.1	3.78E+00	3.39E-01	9.0
2.00	3.51E+00	1.84E-01	5.2	2.92E+00	5.50E-02	1.9
2.25	2.75E+00	1.06E-01	3.9	2.17E+00	5.29E-02	2.4
2.50	2.28E+00	6.94E-02	3.0	1.91E+00	3.67E-02	2.0

Note: Ave = Average, SE = Standard Error and RSE = Relative Standard Error.

The electron conduction mechanisms in polymeric materials such as asphalt mastic modified with conductive materials depends on [13], [14] (a) the intrinsic conductivity of the conductive fillers, (b) the degree of direct contact between conductive fillers, and (c) the tunneling/hopping of electrons between the conductive fillers not in contact with one another. Tunneling, a quantum-mechanical effect, occurs when electrons pass through an insulating material or barrier. In the quantum-mechanical world, unlike in classical physics, electrons possess wavelike properties, and these waves taper off quickly rather than merely ending abruptly when they encounter a wall or barrier. It is believed that the distance between conductive materials has a very significant influence on electrons' ability to tunnel [47], [48].

Because of the effect of a negative thermal coefficient (NTC), while the resistivity of the specimen with no conducting materials increases 2.4% with respect to a 20°C decrease in temperature (Figure 5.4), the presence of conducting materials can be a game-changer because volumetric contraction of an insulating polymer-based matrix (such as asphalt mastic) enhances the continuity of the conducting networks of conducting materials, thereby decreasing the volume resistivity [49]. Note that in Figure 5.3 small amounts of conductive materials, such as 5% GP in a two-phase ECAM at 0% CF content, and 0.25% CF content in a single-phase ECAM (with no GP), respectively, cause 2.2% and 10.1% reductions in resistivity values for a temperature decrease of 20°C.

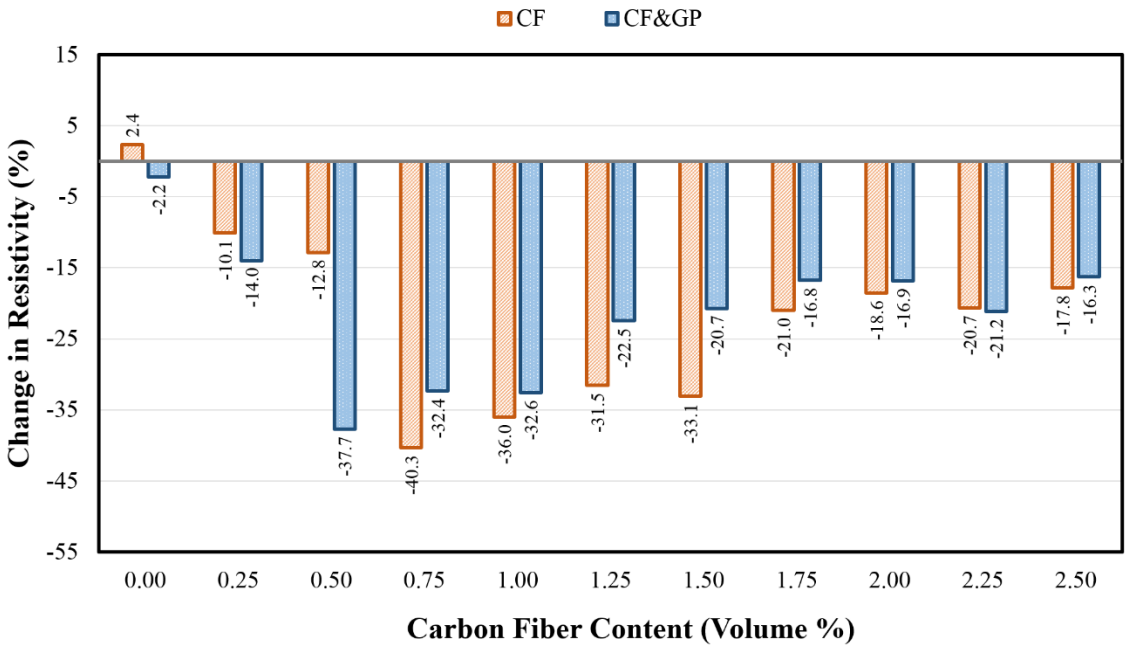

Figure 5.4 *Reduction in volume resistivity, because of a 20°C reduction in temperature, at variable CF contents.*

Within the percolation transition zone, electrical conductivity of composite materials is dominated by charge tunneling between the conducting materials [50] because the majority of conducting material components are not in contact. When such components become closer due to thermal contraction of asphalt mastic, the conductivity is enhanced, and such enhancement

may increase the chance of electron “hopping” that is highly dependent on tunneling distance [47], [48]. As a result of such decreased tunneling distance, both ECAM specimen types (single-phase and two-phase) will show improved conductivity as the temperature drops by 20°C. It is worth noting that asphalt-based materials exhibit different behaviors at different temperatures [33]. Based on the literature, an asphalt-based material’s volume thermal contraction/expansion is greatest above its glass transition temperature [51], [52], a temperature at which a thermoset polymer such as bitumen transforms from an amorphous rigid state to a more flexible state. Within the percolation transition zone, the temperature-related reduction in resistivity increases with addition of CF content up to 0.5% and 0.75% (i.e., optimum conductive material contents), respectively, in two-phase and single-phase specimens. Such reduction can be explained by presence of more conductive material contents and an increased chance of electron tunneling due to thermal volume contraction.

At the optimum level of conductive material contents, the reduction in volume resistivity values reach their maximums (see Figure 5.3) for both ECAM specimen types, i.e., a reduction of 40.3% and 37.7%, respectively, in resistivity values of single-phase and two-phase specimens. Such enhancement in conductivity can be attributed to simultaneous effects of electron tunneling and contact resistance conduction mechanisms. It is worth noting that the optimum conductive material content occurs at the beginning of formation of many conductive networks in which fibers are touching one another in many directions, resulting in enhancement of conductivity through contact resistance. As a result of such behavior at the optimum conductive material content level, and because of asphalt mastic’s thermal contraction, many fibers can rapidly be brought into contact, causing the collective common contact areas to grow; moreover, the chance

of electron tunneling can increase, so the reduction in resistivity values will reach a maximum value at optimum conductive material contents.

Note that Figure 5.3 shows that the 20°C temperature reduction causes a greater reduction in electrical resistivity in two-phase ECAM specimens at CF contents of 0.25% and 0.5%. Such a substantial reduction in volume resistivity associated with presence of GP particles can be explained by the dominance of the bridging effect of CFs caused by thermal contraction when there are fewer CFs present in the mastic. However, in the CF content range of 0.75%-1.75%, the presence of GP particles makes the two-phase ECAM volume resistivity less susceptible to a 20°C reduction in temperature compared to that of single-phase ECAM. This feature can be useful in increasing accuracy in strain-related self-sensing applications in pavements exposed to recurrent thermal variation.

In the low-resistivity region (see Figure 5.3), at a CF content level equal to or greater than 1.75% used in both single-phase and two-phase ECAM, the conducting networks are gradually saturated with conductive materials [5], resulting in more stable behavior in response to external stimuli such as a 20°C temperature decrease. In support of this statement, Jovic, et al., [53] and Yi, et al., [54] observed the same behavior in polymer-based materials when they investigated the effect of temperature change on volume resistivity of polymer-based materials at high conductive material dosage rates.

Based on the observed behavior of ECAM, i.e., its improved volume resistivity when exposed to a temperature reduction of 20°C, it can be concluded that asphalt mastic containing conductive fillers such as CF and GP can act as posistors, materials exhibiting a positive thermal coefficient (PTC) effect, within the temperature range -10°C to +10°C. When a material's resistivity decreases with decreased temperatures, it is referred to as a PTC resistor.

Resistive heating for de-icing and anti-icing purposes requires a material with high electrical conductivity [40], i.e., the ECAM's volume resistivity must fall within a low resistivity region (see Figure 5.3). ECAM design should not be based on optimum conductive material content, especially when ECAM binds the aggregates together to produce ECAC, because according to Wang, et al., [28], operating close to the percolation transition zone is not recommended. For de-icing and anti-icing purposes, since safety and energy efficiency are of paramount importance, the percolation transition zone with its intrinsic high rate of resistivity change [28] must be avoided in design procedures. Along with basing the design on a low resistivity region, the selection of an appropriate conductive material system could also be cost-saving. For example, this study suggests that the single-phase ECAM modified by 1% CF might be a good candidate for resistive heating. First, its CF is still low and, second, addition of GP (i.e., switching from a single-phase conductive system to a two-phase conductive system) does not substantially improve the resistivity, and addition of GP decreases the resistivity by only 9.4%. As a result, it was decided to evaluate the heat generation efficiency for single-phase ECAM containing 1% CF.

Evaluation of Heat Generation

It is worth noting that the heating test was conducted in an environmental chamber set at a constant temperature of -18°C, and the surface temperature of ECAM was measured and recorded (in the form of radiometric data with the aid of FLIR T650sc IR camera) within a time window of 10 minutes. Figure 5.6 presents four frames (thermographs) extracted from the recorded radiometric video data. The data was further processed in a ResearchIR Max® software environment and only the pixels within the polygon (see Figure 5.6) were selected for further analysis. The selected pixels (each pixel represents a data point or temperature) were then averaged and reported as a function of time for each ECAM replicate (Figure 5.5). Figure 5.5

shows the heat generation performance of single-phase ECAM with a CF volume content of 1%, and it was found that the ECAM's average surface temperature (see Figure 5.6) was increased by about 46 °C within 10 minutes.

The temperature increase rate is variable in different regions of the developed curves (Figure 5.5). During the first 30 seconds, the temperature increases at a decreasing rate for each replicate; this can be attributed to the lower volume resistivity of ECAM at lower temperatures, i.e., the volume resistivity increased in the temperature range -18°C to -10°C. It is worth noting that, although the rate of temperature increase is decreasing in the range between -18°C and -10°C, the fastest temperature increase - considering the average rate - occurs in the first 30 seconds for all the replicates, an effect that can be attributed to high temperature-susceptibility of ECAM during the first 30 seconds.

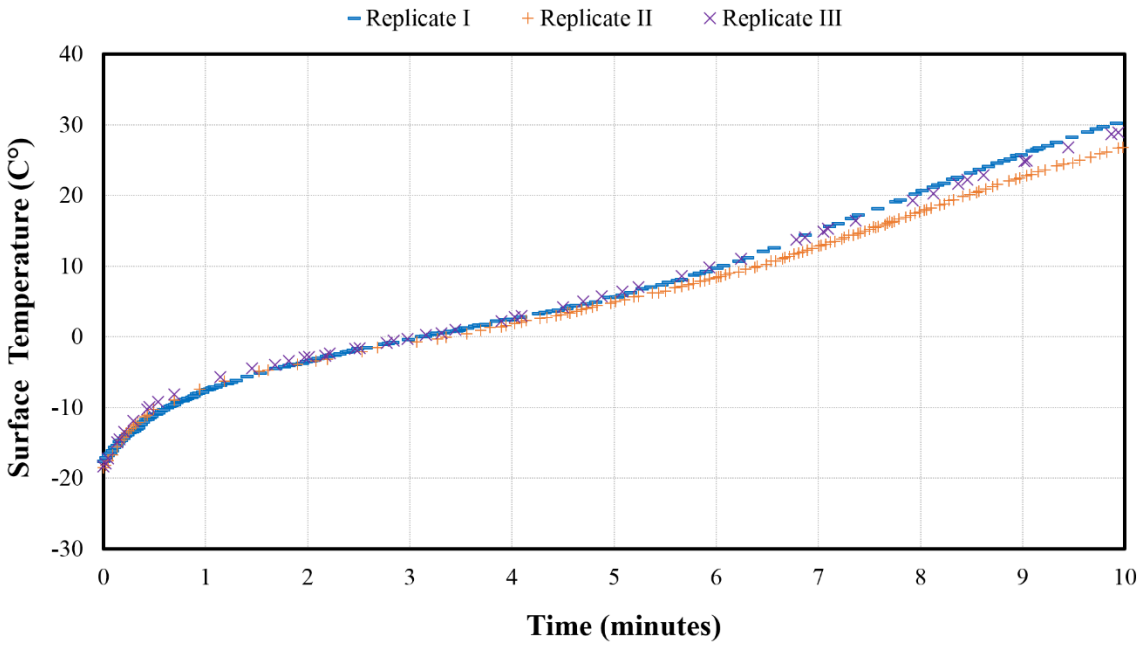

Figure 5.5 *Temperature plot quantifying the heat generation in ECAM specimen's replicates modified with 1% CF.*

After 30 seconds, the temperature of each replicate begins to increase at a constant rate until it reaches 4.5°C. Such a steady temperature increase can be a result of moderate ECAM

temperature susceptibilities in the temperature range -10 to +4.5°C. After 252 seconds (i.e., 4 minutes and 12 seconds), the temperature increase rate increases because of switching the behavior of asphalt-based materials from PTC to NTC at 4.5ºC, i.e., at a "turning point" [55]. Wu, et al., [55] who investigated properties of self-sensing ECAC, also observed a PTC behavior (i.e., increase in resistivity with increase in temperature) at temperature increases ranging from-20 to +25ºC and observed NTC behavior (i.e., decrease of resistivity with increase of temperature) at temperature increases ranging from +25 ºC to 70 ºC, so as a result they referred to +25 ºC as a turning point. It is worth noting that the reason for observing a lower "turning point" in this study can be attributed to absence of an aggregate system in ECAM, because aggregates act as a skeleton in decreasing the excessive deformation of asphalt concrete, and hence the temperature-related volume resistivity variations, at elevated temperatures, resulted in prevention of excessive deformation of ECAM and movement of fibers.

Presence of randomly-developed warm regions inside the ECAM replicates can account for the curve divergences that begin after 252 seconds (or 4.5°C). In these regions, at temperatures close to 60°C, bitumen can behave like a Newtonian fluid [56], allowing it to become less viscous and provide larger and better contact areas between fibers already in contact. It is worth mentioning that none of the ECAM replicates tested at -18°C and subjected to the potential difference of 60V deformed within the test duration of 10 minutes. The reason for selecting 10 minutes as a time window for performing heating tests is that ECAM containing 1% CF started to deform – as was visible by the naked eye – after 12 minutes, so it was decided to discard the acquired data after ten minutes to ensure that tests were performed when specimen replicates were not deformed.

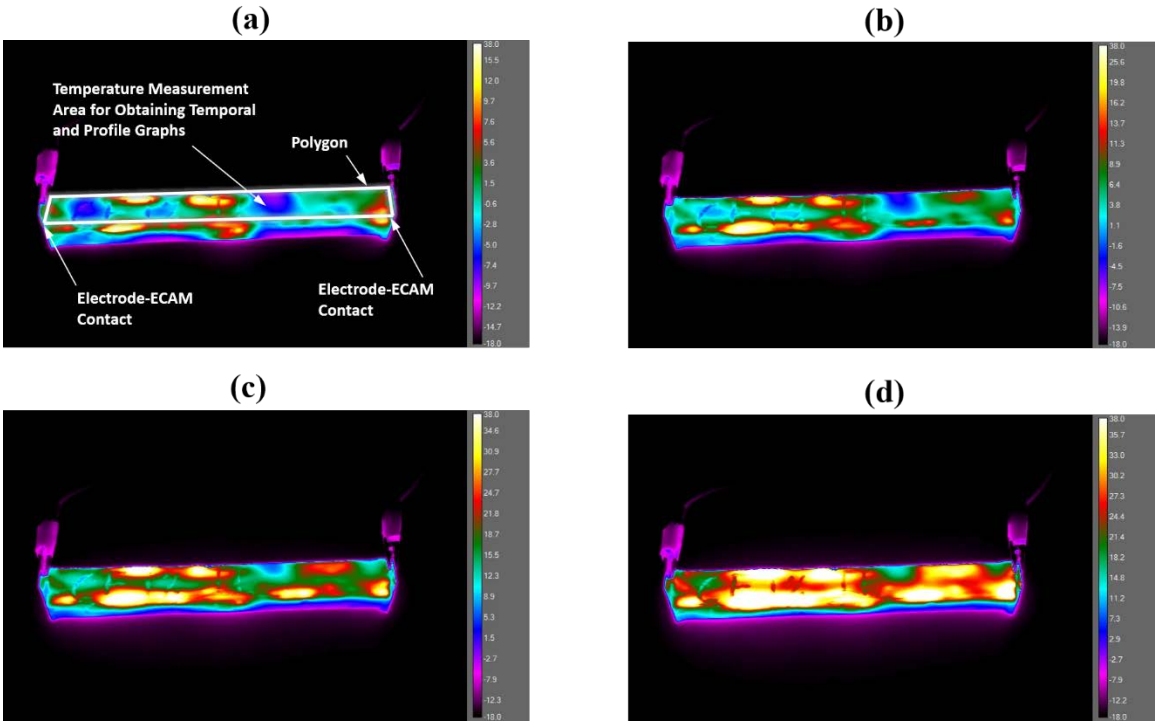

Figure 5.6 *Thermographs obtained from an ECAM specimen containing 1% CF: at: (a) 00:02:30, (b) 00:05:00, (c) 00:07:30 and (d) 00:10:00.*

Figure 5.7 quantifies the uniformity of heat generation presented in Figure 5.6 at different times within the time window of 10 minutes. Note that Figure 5.7 also represents data analysis conducted in the ResearchIR Max® software environment and only the pixels within the polygon (see Figure 5.6) were selected for further analysis. While this analysis is virtually the same as that performed when obtaining the graph presented in Figure 5.5, in Figure 5.7, instead of drawing temporal graphs, i.e., plots presenting temperature change with respect to time (see Figure 5.5), the data analysis results are presented in the form of temperature profile graphs, i.e., plots presenting temperature variation within the specimen length. For obtaining the profile graphs, the data (i.e., pixels) across the width of polygon were averaged then presented with respect to the length of the specimen (or polygon).

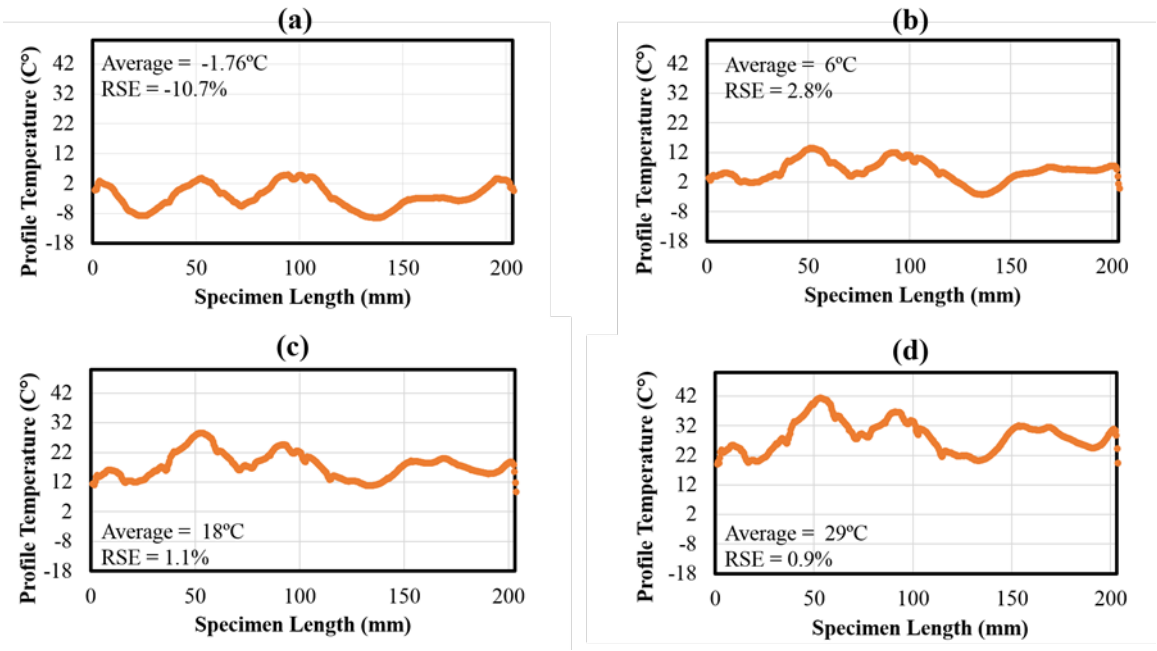

Figure 5.7 *Temperature profiles presenting the uniformity of heat generation within 10 minutes along the ECAM specimen containing 1% CF at: (a) 00:02:30, (b) 00:05:00, (c) 00:07:30 and (d) 00:10:00.*

According to Figure 5.7, while ECAM profile temperature increases with respect to time, there is a decreasing trend in temperatures in proximity to electrodes, and this phenomenon can be explained through the Joule Heating law as investigated in another study [57] by the authors of this study. ECAM containing 1% CF has higher resistivity, i.e. 5.85E+01 Ω.cm, compared to electrodes made of copper whose volume resistivity is approximately 2E-06 Ω.cm. Because of such differences between resistivity values, according to the Joule Heating law, the amount of heat generated in the electrodes will always be lower than the amount produced in ECAM, considering that the current is instantaneously constant within the whole system. As a result, the electrodes have a lower temperature than the ECAM. Lower temperatures in electrodes can also explain lower temperatures in ECAM in proximity to electrodes by producing a thermal gradient - with a high rate of temperature decrease within the narrow area including the electrode, the ECAM interface.

According to Figure 5.6(a) Figure 5.6 (b), Figure 5.6 (c) and Figure 5.6 (d), obtained, at 150, 300, 450 and 600 seconds, respectively, the homogeneity increases with time, and enhancement in homogeneity of temperature values obtained on the surface enclosed by the polygon (see Figure 5.6) can also be observed in Figure 5.7. Note that in Figure 5.7 the variation in temperature profile is largest, as can be proved with the RSE value obtained for the data presented in the graph, i.e., -10.7%, and the RSE value decreases with respect to time until it reaches the minimum absolute value of 0.9%.

A thermal camera detects the temperature only on the surface of objects, while the conductive network, when formed, is distributed both on the surface and within (inside) the specimen. As a result of such distribution, during the beginning of heating test, e.g., during the first 2-3 minutes, the conductive paths in regions touching the surface begin to quickly warm up, possibly explaining the existence of color heterogeneity, i.e., having warmer regions (see Figure 5.6). As time passes, heat generated from embedded portions of conductive networks deeper inside the specimen begins to transfer through the non-conductive portion of asphalt mastic (i.e., HL and bitumen), so that the thermal camera then becomes able to detect the temperature increase above the conductive paths, providing a reason for temperature homogeneity to increase with respect to time (see Figure 5.6 and Figure 5.7). It is worth noting that presence of aggregates in ECAC can change the electrical and thermal properties of ECAM, and that aggregates can block conductive paths or make them more tortuous, making the ECAC less electrically-conductive compared with ECAM. Moreover, aggregates can increase the thermal conductivity and make the temperature distribution more uniform within the ECAC, resulting in the potential difference and heating duration for warming up the ECAC possibly being different from that observed at laboratory scale in ECAM. Moreover, in the field, performance of ECAC

is dependent on environmental conditions such as temperature, wind, snow fall rate, etc., all of which can result in changing the amount of voltage applied and the heating duration for reaching a target surface temperature value [35]. It is worth mentioning that there is no need for temperatures to reach a level exceeding the freezing point of water if the central purpose of an electrically-conductive asphalt-based material is just to melt ice and snow. For example, while maintaining the surface temperature at 5°C will allow an ice melting process to occur, and an ECAM containing 1% CF and starting at -18°C can reach this temperature after 300 s with an applied AC voltage of 60V, as mentioned earlier, the presence of aggregates in ECAC can influence the performance of ECAM.

Conclusions

The objective of this study was to produce single-phase and two-phase electrically-conductive asphalt mastics (ECAMs) with efficient heat generation capabilities, so that when they fill the voids within mineral aggregates, the results are production of anti-icing or de-icing electrically-conductive asphalt concretes (ECACs) for heated pavement applications. To this end, ECAM specimens were prepared, their volume resistivities measured, and their low-resistivity regions identified; moreover, electrical temperature-susceptibility of ECAM specimens was investigated. After identifying and analyzing low-resistivity regions for both single-phase and two-phase ECAMs, it was decided to investigate heat generation efficiency for only single-phase ECAM at a certain of level carbon fiber (CF) content, and at a below-freezing temperatures. The results obtained from the heating test showed that single-phase ECAM at the selected CF content can generate sufficient heat for anti-icing and deicing purposes. The results of this study led to the following specific conclusions:

- The optimum CF contents for single-phase and two-phase ECAM were found to be 0.75% and 0.5%, respectively, and the presence of 5% GP results in an optimum CF content being achieved at a lower volume content of CF, i.e., the optimum CF of single-phase ECAM is lower than that of two-phase ECAM.
- Presence of GP particles at a volume content of 5% causes a huge reduction in volume resistivity when CF contents are low, e.g., 0.25 % and 0.5%. Addition of 5% GP has little influence on volume resistivity reduction in the low resistivity region – 0.75 to 2.5% CF content – of single-phase ECAM.
- Addition of very small amounts of conductive materials to asphalt mastic changes its behavior from NTC to PTC. For example, in this study, a GP of only 5% or a CF of only 0.25% in asphalt mastic exposed to a 20°C temperature drop causes reductions in resistivity values of 2.2% and 10.1%, respectively.
- The PTC behavior of ECAM, i.e., reduction in resistivity value due to a temperature reduction of 20°C, reaches its maximum value at optimum CF contents of 0.75% and 0.5%, respectively, for single-phase and two-phase specimens.
- All the temperature versus time curves obtained from the ECAM replicates prepared with only 1% carbon fiber nearly coincided during the first 4 minutes when the temperature increased from -18°C to 4.5°C.
- While ECAM specimens modified with carbon fiber content of 1% have potential for melting ice and snow, the selected volume content of 1% might be changed if the mastic is considered as a component of asphalt concrete.

Acknowledgments

This paper was prepared from a study conducted at Iowa State University under the Federal Aviation Administration (FAA) Air Transportation Center of Excellence Cooperative Agreement 12-C-GA-ISU for the Partnership to Enhance General Aviation Safety, Accessibility and Sustainability (PEGASAS). The authors would like to thank the current project Technical Monitor, Mr. Benjamin J. Mahaffay, and the former project Technical Monitors, Mr. Jeffrey S. Gagnon (interim), Mr. Donald Barbagallo, and Dr. Charles A. Ishee for their invaluable guidance on this study. The authors also would like to thank the PEGASAS Industry Advisory Board members for their valuable support and feedback. The assistance and efforts of Mr. Robert F. Steffes, ISU PCC Lab Manager, with the lab investigations are greatly appreciated. The authors would like to express their sincere gratitude to Mr. Paul Kremer, ISU CCEE Program Manager for his significant assistance with lab accessibility. The assistance of Nathan Ross, an ISU undergraduate student research assistant, with the lab work is greatly appreciated. The authors would like to thank Asbury Carbons Inc. and Jebro Inc. for kindly donating the materials used in this study. Although the FAA sponsored this project, it neither endorses nor rejects the findings of this research. The presentation of this information is in the interest of invoking comments by the technical community on the results and conclusions of the research. The authors would also like to thank the anonymous reviewers for their constructive discussions and valuable comments from which this work greatly benefited.

References

[1] S. Bressi, A. G. Dumont, and M. N. Partl, “An advanced methodology for the mix design optimization of hot mix asphalt,” Mater. Des., vol. 98, pp. 174–185, 2016.

[2] S. Wu, L. Mo, Z. Shui, and Z. Chen, “Investigation of the conductivity of asphalt concrete containing conductive fillers,” Carbon N. Y., vol. 43, no. 7, pp. 1358–1363, 2005.

[3] J. Norambuena-Contreras and Á. García, “Self-healing of asphalt mixture by microwave and induction heating,” Mater. Des., vol. 106, pp. 404–414, 2016.

[4] A. Bozorgzad, S. F. Kazemi, and F. Moghadas Nejad, “Evaporation-induced moisture damage of asphalt mixtures: Microscale model and laboratory validation,” Constr. Build. Mater., vol. 171, pp. 697–707, 2018.

[5] Á. García, E. Schlangen, M. Van De Ven, and Q. Liu, “Electrical conductivity of asphalt mortar containing conductive fibers and fillers,” Constr. Build. Mater., vol. 23, no. 10, pp. 3175–3181, 2009.

[6] A. Sassani, H. Ceylan, S. Kim, A. Arabzadeh, P. C. Taylor, and K. Gopalakrishnan, “Development of carbon fiber-modified electrically conductive concrete for implementation in Des Moines International airport,” Case Stud. Constr. Mater., vol. 8, pp. 277–291, 2018.

[7] Á. García, E. Schlangen, M. Van De Ven, and D. Vliet, “Induction heating of mastic containing conductive fibers and fillers,” Mater. Struct., vol. 44, no. 2, pp. 499–508, 2011.

[8] D. S. McLachlan, M. Blaszkiewicz, and R. E. Newnham, “Electrical resistivity of composites,” J. Am. Ceram. Soc., vol. 73, no. 8, pp. 2187–2203, 1990.

[9] S. Wu, P. Pan, M. Chen, and Y. Zhang, “Analysis of characteristics of electrically conductive asphalt concrete prepared by multiplex conductive materials,” J. Mater. Civ. Eng., vol. 25, no. 7, pp. 871–879, 2012.

[10] R. W. Warfield and M. C. Petree, “A study of the polymerization of thermosetting polymers by electrical resistivity techniques,” Polym. Eng. Sci., vol. 1, no. 1, pp. 3–8, 1961.

[11] D. Anderson and M. Marasteanu, “Physical hardening of asphalt binders relative to their glass transition,” Transp. Res. Rec. J. Transp. Res. Board, vol. 1661, pp. 27–34, 1999.

[12] Y. Chekanov, R. Ohnogi, S. Asai, and M. Sumita, “Positive temperature coefficient effect of epoxy resin filled with short carbon fibers,” Polymer Journal, vol. 30, no. 5. pp. 381–387, 1998.

[13] S. Paschen, M. N. Bussac, L. Zuppiroli, E. Minder, and B. Hilti, “Tunnel junctions in a polymer composite,” J. Appl. Phys., vol. 78, no. 5, pp. 3230–3237, 1995.

[14] W. S. Bao, S. A. Meguid, Z. H. Zhu, and G. J. Weng, “Tunneling resistance and its effect on the electrical conductivity of carbon nanotube nanocomposites,” J. Appl. Phys., vol. 111, no. 9, 2012.

[15] X. Liu and S. Wu, “Study on the graphite and carbon fiber modified asphalt concrete,” Constr. Build. Mater., vol. 25, no. 4, pp. 1807–1811, 2011.

[16] B. Huang, X. Chen, and X. Shu, “Effects of electrically conductive additives on laboratory-measured properties of asphalt mixtures,” J. Mater. Civ. Eng., vol. 21, no. 10, pp. 612–617, 2009.

[17] J. Wu, J. Liu, and F. Yang, “Three-phase composite conductive concrete for pavement deicing,” Constr. Build. Mater., vol. 75, pp. 129–135, 2015.

[18] S. M. Abtahi, M. Sheikhzadeh, and S. M. Hejazi, “Fiber-reinforced asphalt-concrete - a review,” Constr. Build. Mater., vol. 24, no. 6, pp. 871–877, 2010.

[19] A. Arabzadeh, “The influence of different mixture design variables on thermal fatigue cracking of asphalt concrete pavements,” Middle East Tecnical University, 2015.

[20] A. Arabzadeh and M. Güler, “Influence of mixture design variables on thermal coefficient of asphalt concrete,” in Proceedings of Conference on Advances in Civil Engineering, 2014, pp. 1–6.

[21] S. J. Lee, J. P. Rust, H. Hamouda, Y. R. Kim, and R. H. Borden, “Fatigue cracking resistance of fiber-reinforced asphalt concrete,” Text. Res. J., vol. 75, no. 2, pp. 123–128, 2005.

[22] E. R. Brown, P. S. Kandhal, F. L. Roberts, Y. R. Kim, D. Y. Lee, and T. W. Kennedy, Hot mix asphalt materials, mixture design, and construction. Lanham, MD: NAPA Research and Education Foundation, 2009.

[23] R. Moraes and H. U. Bahia, “Effect of mineral filler on changes in molecular size distribution of asphalts during oxidative ageing,” Road Mater. Pavement Des., vol. 16, no. sup2, pp. 55–72, 2015.

[24] A. A. S. H. T. O. M323-07, “Standard specification for Superpave volumetric mix design,” 2008.

[25] A. Diab and M. Enieb, “Investigating influence of mineral filler at asphalt mixture and mastic scales,” Int. J. Pavement Res. Technol., vol. 11, no. 3, pp. 213–224, 2018.

[26] P. Park, Y. Rew, and A. Baranikumar, “Controlling conductivity of asphalt concrete with graphite,” Southwest Region University Transportation Center, 2014.

[27] Q. Liu, E. Schlangen, and M. Van De Ven, “Induction Healing of Porous Asphalt,” Transp. Res. Rec. J. Transp. Res. Board, vol. 2305, pp. 98–101, 2012.

[28] H. Wang, J. Yang, H. Liao, and X. Chen, “Electrical and mechanical properties of asphalt concrete containing conductive fibers and fillers,” Constr. Build. Mater., vol. 122, pp. 184–190, 2016.

[29] H. V. Vo and D. W. Park, “Application of conductive materials to asphalt pavement,” Adv. Mater. Sci. Eng., vol. 2017, 2017.

[30] M. Guo, A. Motamed, Y. Tan, and A. Bhasin, “Investigating the interaction between asphalt binder and fresh and simulated RAP aggregate,” Mater. Des., vol. 105, pp. 25–33, 2016.

[31] A. D4402, “Standard test method for viscosity determination of asphalt at elevated temperatures using a rotational viscometer,” 2015.

[32] Q. Liu, “Induction Healing of Porous Asphalt,” Wuhan University of Technology, 2012.

[33] H. E. Schweyer and R. L. Davis, “Asphalt rheology in the near-transition temperature range,” Highw. Res. Rec, vol. 468, pp. 1–15, 1973.

[34] M. Zeng and C. Wu, “Effects of type and content of mineral filler on viscosity of asphalt mastic and mixing and compaction temperatures of asphalt mixture,” Transp. Res. Rec. J. Transp. Res. Board, vol. 2051, no. -1, pp. 31–40, 2008.

[35] H. Abdualla, H. Ceylan, S. Kim, K. Gopalakrishnan, P. C. Taylor, and Y. Turkan, “System requirements for electrically conductive concrete heated pavements,” Transp. Res. Rec. J. Transp. Res. Board, vol. 2569, pp. 70–79, 2016.

[36] H. Abdualla, H. Ceylan, S. Kim, M. Mina, K. Gopalakrishnan, A. Sassani, P. C. Taylor, and K. Cetin, “Configuration of electrodes for electrically conductive concrete heated pavement systems,” in Airfield and Highway Pavements, 2017, pp. 1–9.

[37] P. Cong, P. Xu, and S. Chen, “Effects of carbon black on the anti aging, rheological and conductive properties of SBS/asphalt/carbon black composites,” Constr. Build. Mater., vol. 52, pp. 306–313, 2014.

[38] A. Arabzadeh, H. Ceylan, S. Kim, K. Gopalakrishnan, A. Sassani, S. Sundararajan, and P. C. Taylor, "Superhydrophobic coatings on Portland cement concrete surfaces," Constr. Build. Mater., vol. 141, pp. 393–401, 2017.

[39] A. Arabzadeh, H. Ceylan, S. Kim, K. Gopalakrishnan, and A. Sassani, "Superhydrophobic coatings on asphalt concrete surfaces," Transp. Res. Rec. J. Transp. Res. Board, vol. 2551, pp. 10–17, 2016.

[40] S. Wen and D. D. L. Chung, "The role of electronic and ionic conduction in the electrical conductivity of carbon fiber reinforced cement," Carbon N. Y., vol. 44, no. 11, pp. 2130–2138, 2006.

[41] T. S. Light and S. L. Licht, "Conductivity and resistivity of water from the melting to critical points," Anal. Chem., vol. 59, no. 19, pp. 2327–2330, 1987.

[42] A. D'Alessandro, F. Ubertini, A. L. Materazzi, S. Laflamme, A. Cancelli, and L. Micheli, "Carbon nanotube cement-based sensors for dynamic monitoring of concrete structures," in International Conference on Environment and Electrical Engineering (EEEIC2016), 2016.

[43] X. Maldague and S. Marinetti, "Pulse phase infrared thermography," Appl. Phys, vol. 79, no. 5, pp. 2694–2698, 1996.

[44] C. C. Chen and Y. C. Chou, "Electrical-conductivity fluctuations near the percolation threshold," Phys. Rev. Lett., vol. 54, no. 23, pp. 2529–2532, 1985.

[45] K. S. Deepa, M. S. Gopika, and J. James, "Influence of matrix conductivity and Coulomb blockade effect on the percolation threshold of insulator-conductor composites," Compos. Sci. Technol., vol. 78, pp. 18–23, 2013.

[46] M. Weber and M. R. Kamal, "Estimation of the volume resistivity of electrically conductive composites," Polym. Compos., vol. 18, no. 6, pp. 711–725, 1997.

[47] F. P. Zamborini, L. E. Smart, M. C. Leopold, and R. W. Murray, "Distance-dependent electron hopping conductivity and nanoscale lithography of chemically-linked gold monolayer protected cluster films," Anal. Chim. Acta, vol. 496, no. 1–2, pp. 3–16, 2003.

[48] C. Yeh and K. Najafi, "A low-voltage tunneling-based silicon microaccelerometer," IEEE Trans. Electron Devices, vol. 44, no. 11, pp. 1875–1882, 1997.

[49] J. Fournier, G. Boiteux, and G. Seytre, "Positive temperature coefficient effect in carbon black/epoxy polymer composites," J. Mater. Sci. Lett., vol. 16, no. 20, pp. 1677–1679, 1997.

[50] S. Barrau, P. Demont, A. Peigney, C. Laurent, and C. Lacabanne, “DC and AC conductivity of carbon nanotubes-polyepoxy composites,” Macromolecules, vol. 36, no. 14, pp. 5187–5194, 2003.

[51] H. Bahia and D. A. Anderson, “Glass transition behavior and physical hardening of asphalt binders (with discussion),” J. Assoc. Asph. Paving Technol., vol. 62, 1993.

[52] C. S. Clopotel, R. Velasquez, H. U. Bahia, F. Perez-Jimenez, R. Miro, and R. Botella, “Relationship between binder and mixture damage resistance at intermediate and low temperatures,” Transp. Res. Rec., no. 2293, pp. 39–47, 2012.

[53] N. Jović, D. Dudić, A. Montone, M. V. Antisari, M. Mitrić, and V. Djoković, “Temperature dependence of the electrical conductivity of epoxy/expanded graphite nanosheet composites,” Scr. Mater., vol. 58, no. 10, pp. 846–849, 2008.

[54] X. S. Yi, L. Shen, and Y. Pan, “Thermal volume expansion in polymeric PTC composites: a theoretical approach,” Compos. Sci. Technol., vol. 61, no. 7, pp. 949–956, 2001.

[55] S. P. Wu, L. T. Mo, and Z. H. Shui, “Piezoresistivity of graphite modified asphalt-based composites,” Key Eng. Mater., vol. 249, pp. 391–395, 2003.

[56] Á. García, J. Norambuena-Contreras, M. Bueno, and M. N. Partl, “Single and multiple healing of porous and dense asphalt concrete,” J. Intell. Mater. Syst. Struct., vol. 26, no. 4, pp. 425–433, 2015.

[57] S. S. Sadati, K. Cetin, and H. Ceylan, “Numerical modeling of electrically conductive pavement systems,” in Congress on Technical Advancement, 2017, pp. 111–120.

CHAPTER 6. ELECTRICAL AND THERMAL PROPERTIES OF CEMENT PASTE AND ASPHALT MASTIC MODIFIED BY ELECTRICALLY-CONDUCTIVE CARBON-BASED MATERIALS

To be submitted to the journal of Carbon

Ali Arabzadeh[1], Alireza Sassani[2], Halil Ceylan[3], Sunghwan Kim[4], Kasthurirangan Gopalakrishnan[5] and Peter C. Taylor[6]

Abstract

Asphalt mastic and cement paste are matrices filling voids between aggregates in hot mix asphalt (HMA) and portland cement concrete (PCC). In this study, asphalt mastic and cement paste were modified with carbon fiber (CF) - at variable volume contents - and graphite powder (GP) - at a constant volume content - to produce electrically conductive asphalt mastic (ECAM) and electrically-conductive cement paste (ECCP) capable of generating heat through resistive heating sufficient to increase the temperature in the aggregate systems for anti-icing and de-icing purposes. Optimum CF contents were identified and potential temperature-related volume resistivity changes studied at CF contents equal to or greater than the optimum value, and heat generation efficiency was analyzed by performing active infrared thermography (IRT) for a few CF content values equal to or greater than the optimum. Based on the results obtained from volume resistivity measurements, it was found that ECCP with higher conductivity has a stable electrical behavior when exposed to a temperature change, while ECAM' volume resistivity drops as the temperature decreases. Moreover, the results obtained from conducting active IRT

[1] Graduate Research Assistant, Civil, Construction and Environmental Engineering (CCEE), Iowa State University (ISU), Ames, IA, E-mail: arab@iastate.edu
[2] Graduate Research Assistant, CCEE, ISU, Ames, IA, E-mail: asassani@iastate.edu
[3] Professor, Director, Program for Sustainable Pavement Engineering and Research (PROSPER), CCEE, ISU, Ames, IA, E-mail: hceylan@iastate.edu
[4] Research Scientist, Institute for Transportation, ISU, Ames, IA, E-mail: sunghwan@iastate.edu
[5] Research Associate Professor, CCEE, ISU, Ames, IA, E-mail: rangan@iastate.edu
[6] Director, National Concrete Pavement Technology Center, SU, Ames, IA, E-mail: ptaylor@iastate.edu

revealed that both ECAM and ECCP are capable of generating heat sufficient for melting ice/snow or preventing their formation/accumulation.

Introduction

Asphalt mastic is a mixture of asphalt binder and fillers (particles with diameters less than 75μm), and cement paste is a mixture of portland cement, water, and possibly chemical admixtures. Asphalt mastic and cement paste are matrices binding aggregate system to produce hot-mix asphalt (HMA) and portland cement concrete (PCC). There are different types of electrically-conductive additives such as powders, fibers, and solid particles that can be added to concrete to produce electrically-conductive asphalt concrete (ECAC) [1] or electrically-conductive portland cement concrete (ECON) [2]. If such conductive additives are powders or fibers, it will be the matrix that becomes electrically-conductive and the aggregate system will act as either a skeleton or a non-conducting component. Such a matrix in ECAC can be referred to as electrically-conductive asphalt mastic (ECAM) and one used in ECON can be referred to as electrically-conductive cement paste (ECCP).

Carbon fibers (CFs) when added to HMA or PCC result in composites with multifunctional properties [3]. CF decreases drying shrinkage age and increases flexural strength, flexural toughness, tensile strength, and tensile ductility of PCC and simultaneously enhances the electrical conductivity of concrete [4]–[7]. Similar to the way it enhances the mechanical and electrical properties of PCC, CF, with a melting point of approximately 1000°C, increases tensile strength [8], fatigue life [9], and rutting resistance [10] of asphalt concrete, and it is believed that CF is the best conductivity enhancement material when used in asphalt concrete [11]. If only a single type of conductive powder or fiber is used in HMA or PCC, e.g., only CF, the modified matrix, would be referred to as single-phase ECAM or single-phase ECCP [1]. For increasing

conductivity, it is also possible to add other conductive material types such as graphite powder (GP) to a single-phase system containing CF to produce two-phase ECAM or two-phase ECCP [1].

GP, because of its intrinsic lubricating characteristics, if incorporated beyond a certain limit into HMA, approximately 20%, can substantially reduce indirect tensile strength, Marshall stability, resilient modulus, and rutting dynamic stability of asphalt concrete [10], [12]. GP has a similar effect on PCC [2] because of its hydrophilic nature, like that of portland cement [13]. It therefore has a high tendency to absorb water, and if incorporated at a high dosage rate, 20% or so, into PCC, it can substantially decrease its compressive strength, e. g., to as low as 2Mpa [14]. However, it still seems worthwhile to investigate its influence, at a relatively low volume content, on enhancing the conductivity of ECAM and ECCP already modified with CF for self-heating purposes, i.e., anti-icing and de-icing purposes. It is believed that incorporation of GP into HMA and PCC at dosage rates in the range of 3% - 7% does not significantly influence such mechanical properties [12], [14].

Temperature change can influence the volume resistivity of composite materials such as ECAM and ECCP. For the first time, Wu, et al., [1] found that changing temperature from 38°C to 24°C causes a 12% reduction in resistivity of ECAC produced for self-heating applications. They also found that temperature changies from 24°C to 30°C had no influence on the volume resistivity of ECAC. Wen, et al. [15], the first to investigate the influence of temperature change on volume resistivity of cement paste produced for self-sensing applications, observed increases in resistivity of ECCP for temperature decreases occurring in a temperature range of +1°C - +45°C. To make an analogous comparison between ECAC and ECON in terms of resistivity-related temperature susceptibility, it would be better to study the volume resistivity of their

matrices (i.e., ECAM and ECCP) under similar test conditions and for identical conductive material contents, and, most importantly, when aggregates are not present.

It is believed that volume resistivity has a reciprocal relationship with temperature increase achieved through resistive heating in ECAC. While Liu, et al., [16] proved existence of such relationship in self-healing ECAC modified with steel wool at room temperature [16], there has been no such investigation relating volume resistivity of electrically-conductive cement-based materials (i.e., ECCP or ECON) to induced temperature increase achieved through resistive heating. As a result, it would be beneficial to compare and identify such relationships between self-heating ECCP and self-heating ECAM modified with the same conductive materials at the same dosage rates and under the same test conditions.

The objective of this study was to produce self-heating ECAM and self-heating ECCP so that, when they fill the voids in aggregate systems, the result would be concretes with engineered anti-icing and de-icing performance for heated pavement applications. To this end, asphalt mastic and cement paste reflecting the same dosage rates were modified with CF and GP to produce single-phase and two-phase electrically-conductive systems. Volume resistivities were measured at a temperature above water freezing temperature, and to investigate temperature susceptibility, resistivity measurements only for the specimens containing content equal to or greater than optimum CF were repeated at a temperature below that of water freezing. Use of active infrared thermography (IRT) to determine heat generation efficiency of ECAM and ECCP at certain CF volume contents was then evaluated by measuring temperature increase within a certain time window and calculating its rate of increase.

Experimental

Materials

Asphalt binder (i.e., bitumen), performance grade (PG) 58-28 obtained from Jebro Inc., was used together with hydrated lime for preparing ECAM specimens. Thep cement used for preparing ECCP specimens was type I/II, a general application cement. The specimens (both ECAM and ECCP) were made conductive by using CF and GP obtained from Asbury Carbons Inc. The chopped and unsized CF had a carbon content greater than 95% (by mass), length of 3 mm, diameter of 7.2 microns, and resistivity of 6×10^{-3} Ω.cm. The GP, a flake-type graphite, had a specific gravity (SG) of 2.26, carbon content greater than 95% (by mass), and a resistivity range of 0.03 Ω.cm – 0.05 Ω.cm [17]. Silver paste, a two-part conductive epoxy with electrical resistivity of 7×10^{-2} Ω.cm, was obtained from MG Chemicals®, and used for attaching the copper plates (electrodes) to ECCP specimens.

Fabrication of ECAM and ECCP specimens

Two types of ECAM specimens were prepared: (I) single-phase (containing only CF at variable volume dosage rates ranging from 0% to 2.5%), and (II) two-phase (containing GP at a constant volume content of 5% and CF at variable volume dosage rates like those for single-phase). For fabricating ECAM specimens, conductive materials (CF or GP&CF), bitumen, and hydrated lime were conditioned for 1 h in an oven set at 165 °C. After the conditioning time was over, the components were mixed for 5 m at 60 rpm using a planetary (Hobart) mixer. The mixtures were then conditioned once again in the oven, at 165 °C, for 15 m. After the conditioning time, the mixtures were hand-compacted in wooden molds, and cured for 24 h in room temperature to obtain prismatic beam specimens, with each specimen type having three

replicates. After curing time, the ends of specimens were warmed up and copper electrodes attached to the tacky warm surfaces (Figure 6.1a).

ECPCP specimens comprised of water, portland cement, and conductive materials were prepared using the same conductive materials at volume dosage rates identical to those for which the ECAM specimens were fabricated. The mixtures had a constant water-to-cement ratio of 0.5, and were prepared by mixing the components for 5 m at 60 rpm in a Hobart mixer. After mixing time, the fresh pastes were poured into steel molds and consolidated by tamping. The fresh specimens were cured in the molds for 24 hours, then demolded and cured in a moist room at 23°C for 28 days. ECCP specimens were then brought to a dry condition by placing them in an oven set at 105°C for 24 h to minimize the influence of moisture and pore solution on the volume resistivity of ECCP [18]. It is also widely believed that under dry conditions electronic conduction becomes more dominant than ionic conduction in ECCP [18], [19]. The dimensions of ECCP specimens were the same as for the ECAM specimens and the copper electrodes were attached to the ECCP specimens using silver paste (Figure 6.1b).

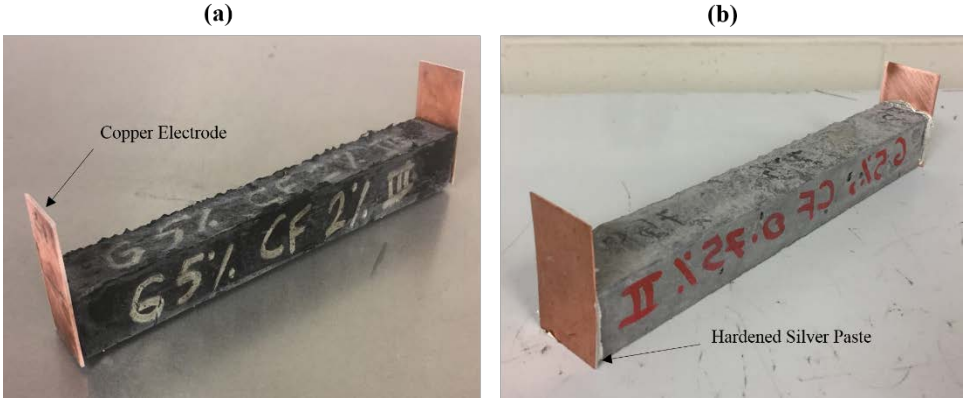

Figure 6.1 *Electrically-conductive specimens: (a) ECAM and (b) ECCP.*

Characterization of conductivity and heat generation efficiency

Conductivity of ECAM and ECCP specimens can be characterized through volume resistivity measurements according to Ohm's law:

$$\rho = \frac{RS}{L} \quad (1)$$

where ρ is electrical volume resistivity (calculated in Ω-cm), R is electrical resistance (measured in Ω), S is electrode-specimen contact area (measured in cm^2), 2.54 cm × 2.54 cm, and L is the distance between electrodes (measured in cm), 20.32 cm.

The two-probe method [11], [20], a reliable and accurate approach for resistance measurement, was utilized in this study, and the reliability and accuracy of this method is thoroughly described in the authors' previous studies [21], [22]. A FLIR DM62 digital multimeter and a DC Hipot Tester were used for measuring resistance values below and exceeding, respectively, 40 MΩ. It is worth noting that the resistivity measurements were conducted using DC current over a very short time (virtually 1 second) to avoid polarization [18]. All measurements were performed in an environmental chamber at +10°C (and some repeated at -10°C), using copper electrodes (i.e., probes) attached to the specimens (Figure 6.1). The environmental chamber was equipped with fans and a dehumidifier unit to ensure a uniform temperature distribution and a minimum and constant amount of humidity in the air. Performing measurements at two temperatures allowed investigating the temperature susceptibility of self-heating ECAM and self-heating ECCP when exposed to a temperature decrease of 20°C (i.e., from +10°C to -10°C). The reason for referring to ECAM and ECCP as self -heating is that their temperature susceptibilities were evaluated at CF contents equal to or greater than optimum to enable generation of a sufficient amount of heat through resistive heating. It is worth noting that, if CFs are incorporated into the matrices at dosage rates less than the optimum content, the

resulting ECAM and ECCP would be suitable for self-sensing applications [18], [23], although evaluating temperature susceptibility of such matrices in the context of electrical conductivity is beyond the scope of this study.

To evaluate ice and snow melting capability of the specimens, heat generation efficiency of self-heating ECAM and self-heating ECCP specimens was characterized through active IRT measurement [24] at a temperature below water freezing temperature, a novel feature of this study. To this end, all the specimens were preconditioned at -20 °C for at least three hours so they could achieve thermal equilibrium [25] and an AC voltage of 40 V at a frequency of 64 Hz then applied to each specimen for a duration of 4 minutes while the surface temperature of each specimen was measured and recorded using a FLIR T650sc camera with a resolution of 640 × 480 pixels. The acquired radiometric data were then analyzed using the ResearchIR Max® software package and heat generation evolution with respect to time.was quantified for each specimen

Results and discussion

Electrical volume resistivity data analysis

As can be seen in Figure 6.2, the selected range of CF contents resulted in capturing percolative behavior [26]. The curve for two-phase ECAM is less S-shaped compared with the one drawn for single-phase ECAM, and it is believed that presence of GP makes the insulator-to-conductor transition smoother [27]. As was expected, when there are no conductive materials in the mastic, e.g., in single-phase ECAM at 0% CF, the volume resistivity is very high, 1.12E+09 Ω.cm (see Figure 6.2), signifying that asphalt mastic is electrically insulating.

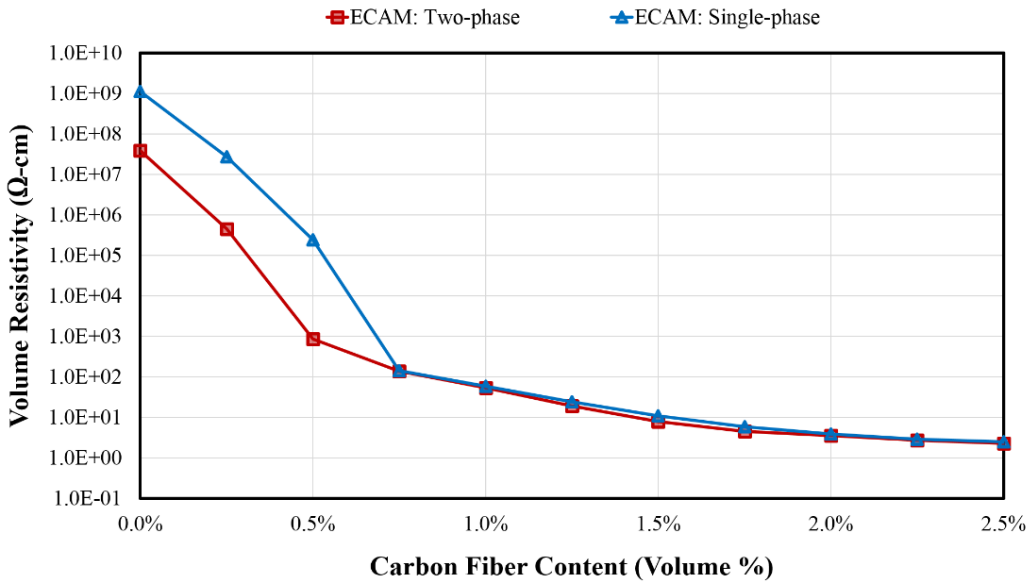

Figure 6.2 *Volume resistivity as a function of CF content measured for ECAM specimens.*

Note that, in Figure 6.2, the volume resistivity drops gradually with addition of CF, except for CF dosage rate ranges of 0.25%-0.50% and 0.50%-0.75%, respectively, in two-phase and single-phase ECAM specimens. The aforementioned ranges represent percolation transition stages at which resistivity values drop at very high rates and in orders of magnitude with addition of CFs at very small amounts [26]. For example, the resistivity decreases from 2.73E+07 Ω.cm to 2.43E+05 Ω.cm and from 4.55E+05 Ω.cm to 8.65E+02 Ω.cm, respectively, in single-phase and two-phase ECAM with addition of only 0.25% CF. For two-phase and single-phase ECAMs, respectively, 0.5% and 0.75% CF contents were found to be optimum values of conductive materials above which resistivity values do not drop at drastic rates [28]. If the purpose for production of ECAM, to fill voids in aggregates to produce ECAC to achieve an anti-icing and deicing pavement surface, its conductive material content should be equal to an optimum or greater than optimum content so that it can generate sufficient heat through resistive heating and cause the ECAM to behave like a self-heating material [1]. However, it should be kept in mind

that factors such as mixture workability and cost also govern the maximum percentage of fibers used in ECAC.

Figure 6.3 presents data gathered from resistivity measurements performed on single-phase and two-phase ECCP specimens. As expected, the volume resistivity decreases with increase in CF content [18] and for the selected range of CF dosage rates percolative behavior [26] was captured in ECCP. Compared to asphalt mastic, incorporation of conductive materials into cement paste results in the smoother insulator-to-conductor transition that can be easily noticed in Figure 6.3. The reason for such smooth behavior, i.e., curves that are not S-shaped [29], stems from the fact that cement paste is more conductive than asphalt mastic, e.g., according to Figure 6.5, volume resistivity of hardened virgin cement paste is 1.80E+07 Ω.cm, two orders of magnitude smaller than for virgin asphalt mastic, 1.12E+09 Ω.cm. Such behavior in cement paste (including both single-phase and two-phase ECCP) is comparable with that of asphalt mastic having only 5% graphite powder (Figure 6.2) because, unlike single-phase ECAM, two-phase ECAM has a smoother insulator-to-conductor transition due to the lower resistivity of the mastic containing 5% GP. In other words, having a matrix (such as cement past or containing a conductive powder like GP) with higher conductivity results in a smoother insulator-to-conductor transition.

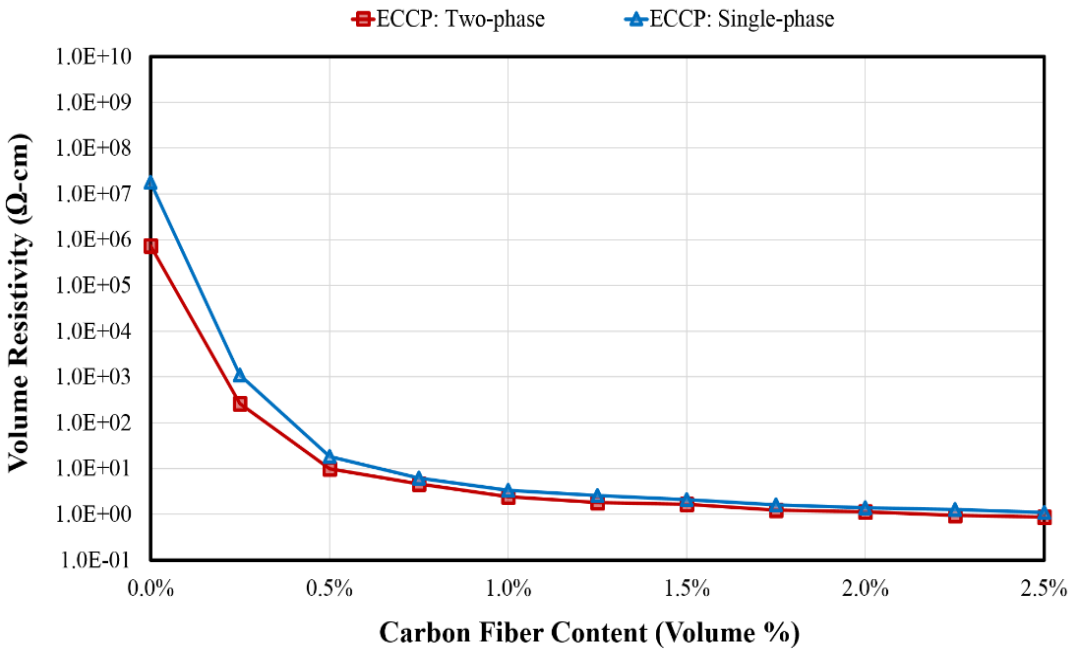

Figure 6.3 *Volume resistivity as a function of CF content measured for ECCP specimens.*

Percolation transition zones for both single-phase and two-phase ECCP occur in the CF content range 0.0%-0.25%, because resistivity values drop with the highest rates in this range, e.g., the volume resistivity of single-phase ECCP drops by as much as 4 orders of magnitude (from 1.8E+07 Ω.cm to 1.12E+03 Ω.cm) and that of two-phase ECCP drops by about 3 orders of magnitude (from 7.91E+05 Ω.cm to 2.61E+02 Ω.cm). The optimum CF content of both ECCP types is 0.25%, because above this volume dosage rate there are no such drastic drops in volume resistivity values. As explained for ECAM, if the purpose for ECCP production, to fill the voids between aggregates for producing ECON, is for self-heating purposes, its conductive material content should be beyond the percolation transition zone, i.e., the CF content should be equal to or greater than optimum content [18]. However, here again there are factors such as mixture workability and cost that govern the maximum amount of fibers to be used in self-heating ECON.

As it is seen in Figure 6.2 and Figure 6.3, while presence of 5% GP in the matrix causes a huge reduction in volume resistivity in ECAM and ECCP specimens at CF volume contents less than optimum for single-phase systems, presence of graphite powder becomes less influential as CF content increases (see Figure 6.2 and Figure 6.3). Improved conductivity, because of the presence of GP, at low CF dosage rates makes both ECAM and ECCP suitable for self-sensing applications [18], [23]. Such substantial influence of graphite powder on reducing volume resistivity at low volume dosage rates of CF can be attributed to a bridging effect (Figure 6.4) [11]. While this effect reflects the ability of CFs to bridge between remote GP clusters, as the CF content increases the bridging influence becomes less and less effective due to saturation of matrices (both ECAM and ECCP) with CFs.

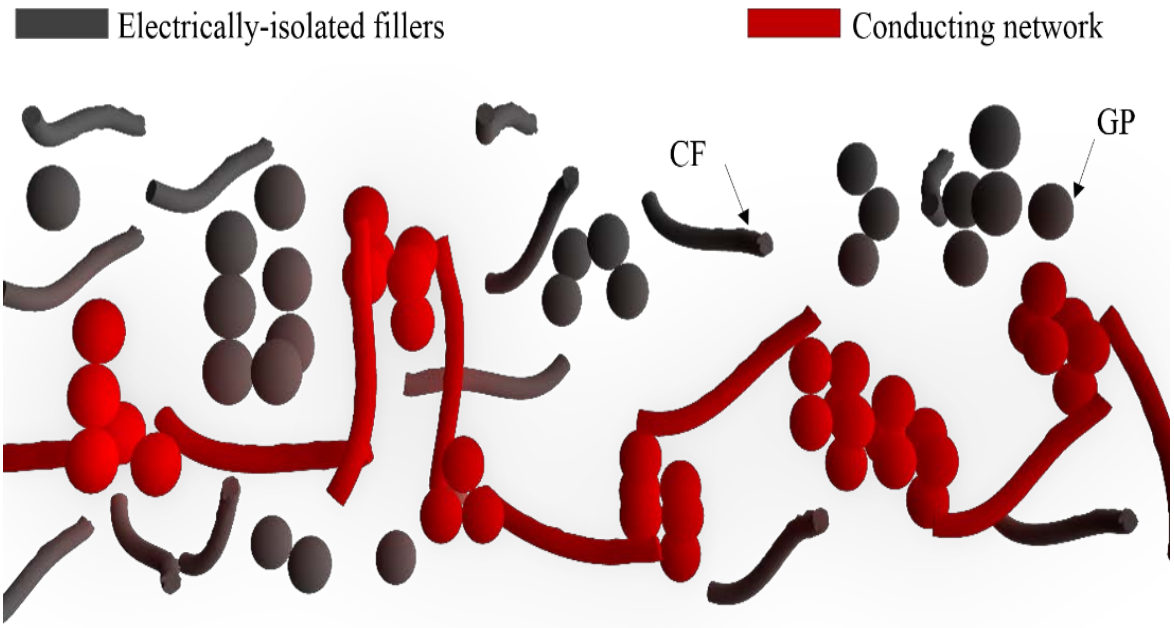

Figure 6.4 *Bridging effect and its influence on conductivity enhancement.*

Figure 6.5 juxtaposes volume resistivity values of single-phase ECAM and single-phase ECCP as a function of CF volume content. As explained earlier, the resistivity of ECCP is two orders of magnitude smaller than that of ECAM when they are not modified with conductive

materials. Addition of a small CF content of 0.25% (i.e., from 0.0% to 0.25%) causes the resistivity of single-phase ECCP to drop from 1.80E+07 Ω.cm to 1.12E+03 Ω.cm, a drop of virtually four orders of magnitude in single-phase ECCP. However, addition of the same amount of CF causes the resistivity of single-phase ECAM to drop by up to virtually two orders of magnitude, i.e., from 1.12+E09 Ω.cm to 2.73E+07 Ω.cm. As can easily be observed in Figure 6.5, while the overall resistivity of single-phase ECCP is less than that of single-phase ECAM at variable CF contents, addition of the first 0.25% CF causes a more drastic drop in resistivity of single-phase ECCP. This phenomenon can be explained by noting the lower resistivity of cement paste compared with asphalt mastic that results in a very large resistivity reduction in single-phase ECCP when CFs are added in even small amounts. For the same reason, the lower conductivity of cement paste can explain occurrence of a percolation transition zone at a lower CF content range, from 0.0% to 0.25%, in single-phase ECCP, compared to the percolation transition zone in single-phase ECAM that occurs at a 0.5% to 0.75% CF content range (see Figure 6.5). Note that in Figure 6.5, with addition of CF, especially for values equal to or greater than 0.25%, the differences between resistivity values of single-phase ECAM and single-phase ECCP become smaller (Figure 6.5 and Table 6.1), and the smallest difference (or reduction) of 56% occurs at 2.5% CF. The reason for such behavior can be explained by saturation of matrices at higher-volume dosage rates of CF, i.e., the more saturated the matrices the less the influence of matrix material on electrical conductivity.

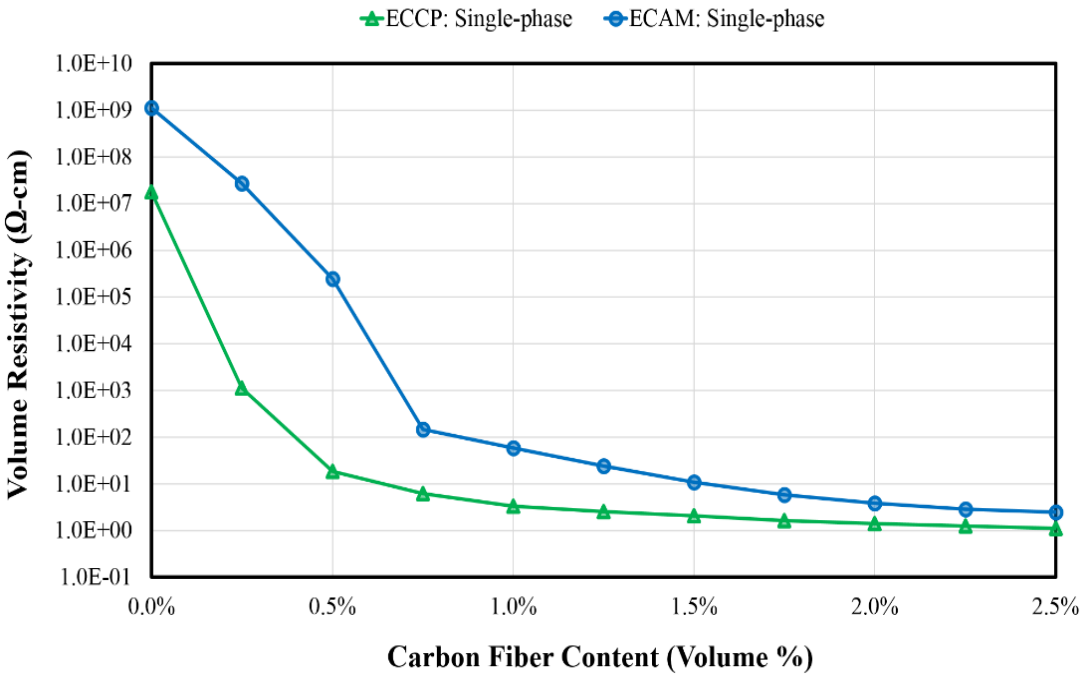

Figure 6.5 *Volume resistivity of single-phase ECAM and ECCP specimens as a function of CF content.*

Similar to what was observed in single-phase systems, addition of CF, especially for values equal to or greater than 0.25%, decreases the difference between resistivity values of two-phase ECAM and two-phase ECCP (Figure 6.6 and Table 6.1). According to Table 6.1, the measured volume resistivity at 0.25% for two-phase ECCP is about 100% smaller than that for two-phase ECAM, and this difference becomes smallest (i.e., 61.86%) at 2.5% CF content, again because of saturation of two-phase matrices (ECAM and ECCP) at high volume dosage rates of CF. The influence of matrix electrical conductivity therefore becomes less significant as CF content increases.

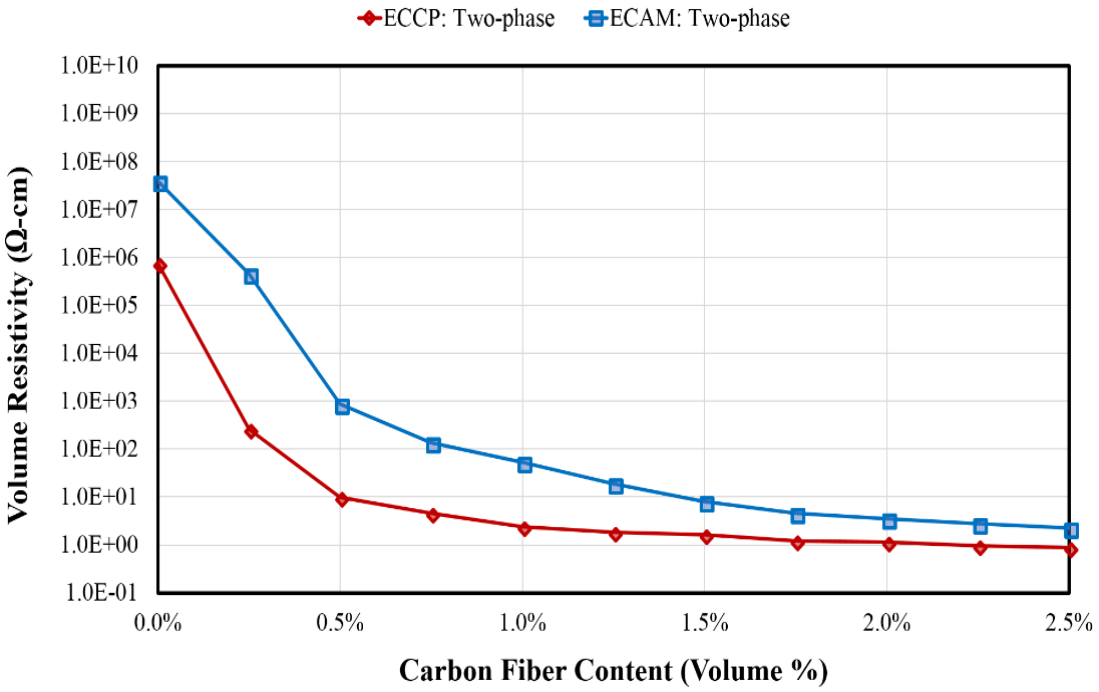

Figure 6.6 *Volume resistivity of two-phase ECAM and ECCP specimens as a function of CF content.*

Table 6.1 *Reduction in resistivity when cement paste matrix is hypothetically replaced with asphalt mastic.*

CF Volume Content	Single-phase System	Two-phase System
0.00%	98.39%	98.10%
0.25%	100.00%	99.94%
0.50%	99.99%	98.87%
0.75%	95.74%	96.64%
1.00%	94.25%	95.49%
1.25%	89.45%	90.42%
1.50%	80.88%	79.17%
1.75%	72.33%	73.19%
2.00%	63.93%	67.47%
2.25%	56.09%	65.38%
2.50%	55.93%	61.86%

Saturation of matrices (both asphalt mastic and cement paste) with CF at high volume dosage rates should cause the curves to coincide at 2% or higher CF contents (see Figure 6.5 and Figure 6.6), similar to the way curves pertaining to single-phase and two-phase systems coincided in Figure 6.2 and Figure 6.3; however, since the curves remain parallel at high dosage

rates (Figure 6.5 and Figure 6.6), there must be another reason beyond higher conductivity of cement paste compared with that of asphalt mastic. The electron conduction mechanism in electrically-insulating matrices such as asphalt mastic and cement paste, in order of dominance, depends on [30], [31]: (a) intrinsic conductivity of conductive additives, (b) the degree of direct contact of conductive additives, and (c) the hopping of electrons between the conductive additives not in direct contact but still at very close proximity. As mentioned earlier in the methodology section, the same conductive materials are used in both ECAM and ECCP, so the intrinsic conductivity of conductive additives would not be responsible for the difference observed in electrical behavior of ECAM and ECCP at high dosage rates of CF. We hypothesize that presence of an intrinsic pore structure in cement paste (Figure 6.7b) may cause a major portion of CFs to directly come into contact with one another, resulting in improved conductivity, while in asphalt mastic such micro-sized pores are scarce, decreasing the dominating effect of contact conduction in ECAM and merely encouraging the transmission of electrons with the aid of electron hopping/tunneling through thin asphalt films (Figure 6.7a) if the films are thin enough. As a result, the resistivity values of ECAM and ECCP at high dosage rates of carbon fibers do not coincide (see Figure 6.5 and Figure 6.6), although these matrices are already saturated with CFs at high volume contents.

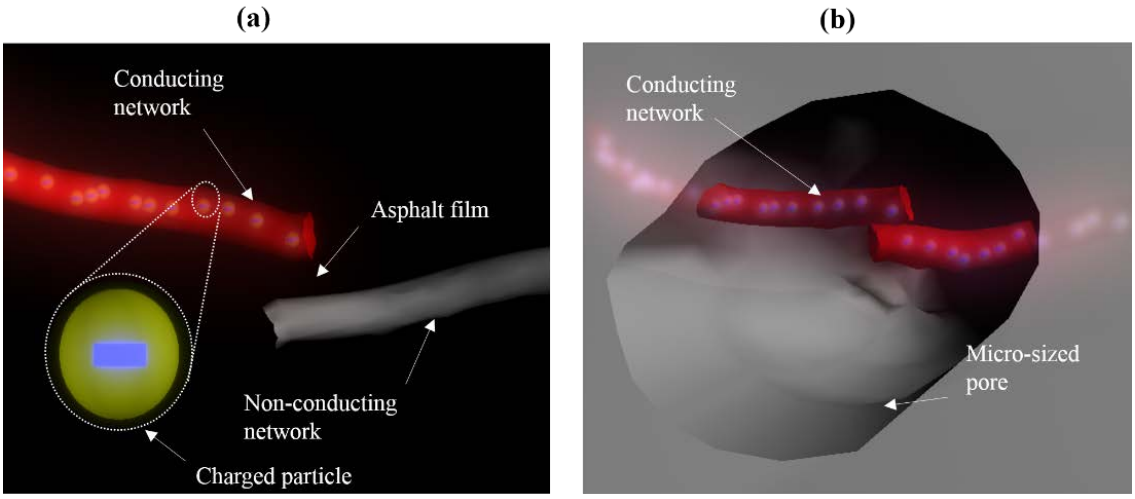

Figure 6.7 *Visualization of asphalt film and pore influence on degrading and enhancing conductivity in: (a) asphalt mastic and (b) cement paste.*

Temperature susceptibility evaluation

With regard to material behavior, increase in resistivity with increase of temperature can be described by a positive thermal coefficient (PTC) phenomenon, and decrease in resistivity with increase of temperature can be described by a negative thermal coefficient (NTC) phenomenon [32]. It would be of paramount importance to study the temperature-related electrical behavior of self-heating ECAM and self-heating ECCP at CF contents above the percolation transition zone, if the ultimate reason for studying ECAM and ECON is to produce concretes suitablefor heated pavement applications. The volume resistivity measurements were therefore repeated at -10°C for matrices containing CF contents equal to and greater than optimum, to determine PTC/NTC behaviors of self-heating ECAM and self-heating ECCP when they are exposed to a thermal change of 20°C – i.e., from -10°C to +10°C (see Figure 6.8, Table 6.2 and Table 6.3).

Figure 6.8a and Figure 6.8b, respectively, provide volume resistivity versus CF content data for single-phase and two-phase self-heating ECAMs, another novel feature of this research.

Note that in Figure 6.8a and Figure 6.8b CF contents of 0.75 and 0.5, respectively, are the optimums for single-phase and two-phase systems. As mentioned earlier, these values (i.e., 0.75 and 0.5) are the minimums for producing a conductive system capable of generating enough heat for anti-icing and de-icing purposes, and this can be easily interpreted as implying that ECAM acts as a PTC material when exposed to a temperature change of 20°C, i.e., from -10°C to +10°C, so it can potentially serve its purpose (anti-icing and de-icing) when it is used in ECAC, because its resistivity decreases as the temperature decreases.

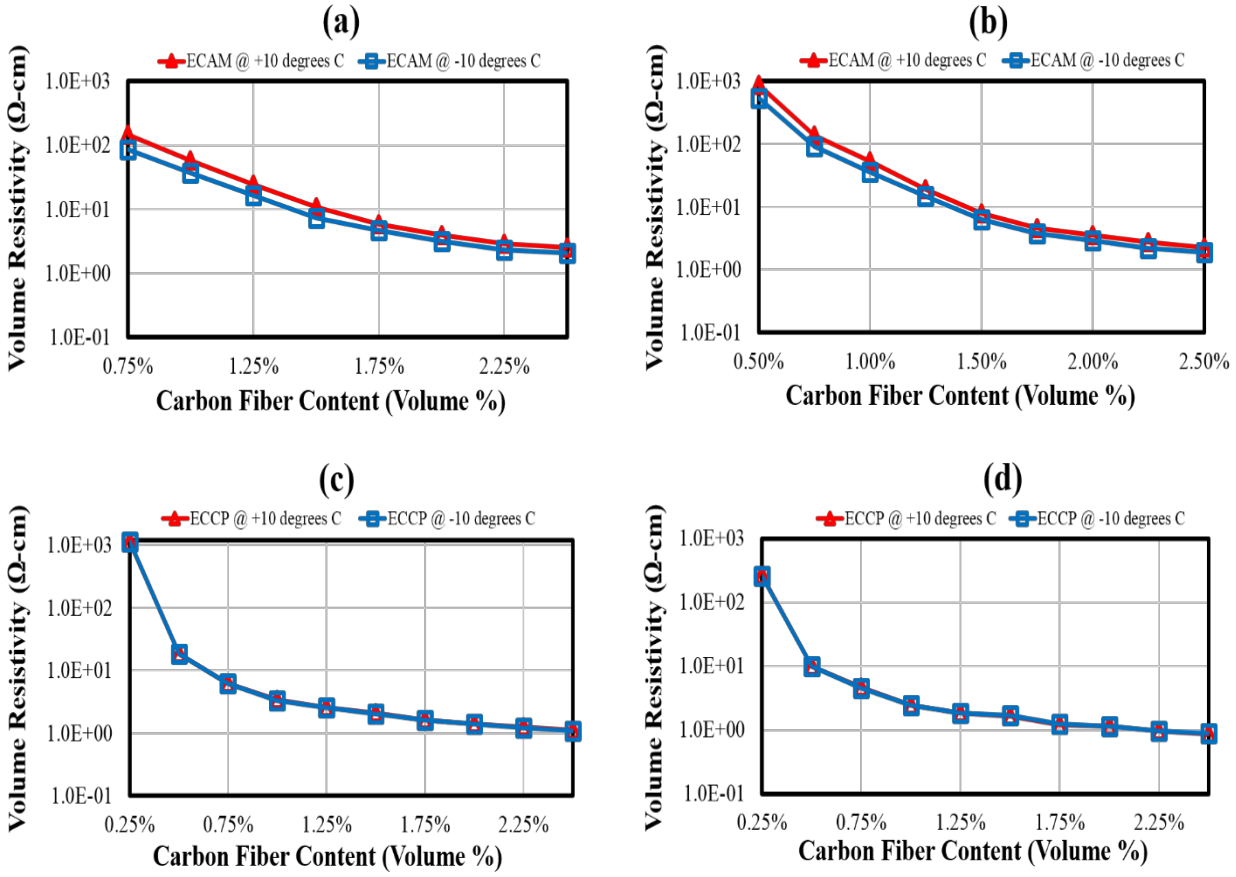

Figure 6.8 *Temperature influence on volume resistivity of: (a) single-phase ECAM, (b) two-phase ECAM, (c) single-phase ECCP a, and (d) two-phase ECCP.*

Table 6.2 presents more detail regarding temperature-related changes in ECAM volume resistivity as a function of CF content - all the selected CF contents are equal to or greater than the optimum content. According to Table 6.2 and Figure 6.8a, the volume resistivity of single-phase ECAM containing 0.75% CF, at -10°C, is 8.62E+01 Ω, virtually 60% of its value at +10°C (i.e., 1.44E+02 Ω.cm), and the temperature-related difference between the resistivity of single-phase ECAM decreases with increase in CF content. Note that in Table 6.2 this difference reaches its minimum value at a CF content of 2.5, i.e., the volume resistivity of single-phase ECAM containing 2.5% CF at -10°C (i.e., 2.05 Ω.cm) is virtually 82% of its value at +10°C (i.e., 2.5 Ω.cm).

Identical behavior was observed in two-phase ECAM (see Table 6.2 and Figure 6.8b). The volume resistivity of two-phase ECAM containing 0.5% CF was measured as 5.39E+02 Ω.cm at -10°C; this measured value is virtually 62% of the result obtained at +10°C, 8.65E+02 Ω.cm. Again the behavior observed in single-phase ECAM is that the temperature-related difference between the resistivity of two-phase ECAM decreases with an increase of CF content. According to Table 6.2 and Figure 6.8b, this difference reaches its smallest value at the CF content of 2.5, e.g., the volume resistivity of two-phase ECAM containing 2.5% CF at -10°C is virtually 84% of its value at +10°C. The reduction in temperature-susceptibility with respect to increase in CF content can potentially assist in the automation of ECAC heated pavement systems by reducing temperature-related noise in the acquired data and consequently increase system precision when ECAC is produced with high dosage rates of CF.

Table 6.2 *Volume resistivity of ECAM specimens measured in Ω.cm.*

CF Volume Content	Single-phase				Two-phase			
	-10		+10		-10.0		+10	
	Avg.	SE	Avg.	SE	Avg.	SE	Avg.	SE
0.50%	NA	NA	NA	NA	5.39E+02	3.01E+02	8.65E+02	3.04E+02
0.75%	8.62E+01	2.20E+01	1.44E+02	3.30E+01	9.30E+01	1.70E+01	1.37E+02	2.83E+01
1.00%	3.75E+01	1.81E+00	5.85E+01	7.41E-01	3.57E+01	6.68E+00	5.30E+01	8.09E+00
1.25%	1.66E+01	4.61E-01	2.43E+01	4.55E-01	1.46E+01	5.96E-01	1.89E+01	7.16E-01
1.50%	7.26E+00	2.98E-01	1.08E+01	3.78E-01	6.29E+00	9.17E-02	7.93E+00	2.92E-01
1.75%	4.62E+00	3.50E-01	5.85E+00	4.04E-01	3.78E+00	3.39E-01	4.54E+00	3.68E-01
2.00%	3.15E+00	2.28E-01	3.87E+00	2.29E-01	2.92E+00	5.50E-02	3.51E+00	1.84E-01
2.25%	2.28E+00	1.06E-01	2.87E+00	8.27E-02	2.17E+00	5.29E-02	2.75E+00	1.06E-01
2.50%	2.05E+00	4.23E-02	2.50E+00	7.63E-02	1.91E+00	3.67E-02	2.28E+00	6.94E-02

Unlike the behavior that observed in ECAM, ECCP's behavior is not significantly influenced by a 20°C temperature change (see Figure 6.8c and Figure 6.8d). Table 6.3, presenting the gathered data in a tabular format, proves the conclusion drawn from Figure 6.8c and Figure 6.8d. , that ECCP proves exhibits insensitivity when exposed to a temperature change of 20°C (changing from -10°C to +10°C or vice versa). Such behavior is in contradiction with the findings of Wen, et al., [15] who investigated the electrical thermal susceptibility of ECCP at low dosage rates of CF for self-sensing applications. According to Wen et al., self-sensing ECCP acts as a thermistor, i.e., exhibiting NTC behavior, when exposed to temperature increases above 0°C. The reason for the discrepancy may stem from the fact that Wen, et al., used CF contents below the percolation threshold and conducted their experiments at a temperature range of 1°C-45°C, unlike the temperature range of -10°C - +10°C used in this study. Also, according to McCarter, et al., [33], portland cement mortar, containing no conductive materials, exhibited NTC behavior when exposed to temperature increases above 10°C. Based on the findings of this study, it is possible to conclude that having CF contents above the percolation transition zone stabilizes the volume resistivity behavior of ECCP when exposed to a 20°C temperature range at temperatures close to 0°C.

Table 6.3 *Volume resistivity of ECCP specimens measured in Ω.cm.*

CF Volume Content	Single-phase				Two-phase			
	-10		+10		-10.0		+10	
	Avg.	SE	Avg.	SE	Avg.	SE	Avg.	SE
0.25%	1.13E+03	7.49E+02	1.12E+03	7.40E+02	2.54E+02	7.82E+01	2.61E+02	8.04E+01
0.50%	1.83E+01	6.66E-01	1.85E+01	6.47E-01	9.86E+00	5.24E-01	9.79E+00	5.33E-01
0.75%	6.15E+00	2.19E-01	6.15E+00	2.12E-01	4.52E+00	1.25E-01	4.62E+00	1.35E-01
1.00%	3.33E+00	9.70E-02	3.37E+00	7.99E-02	2.39E+00	1.10E-01	2.39E+00	1.10E-01
1.25%	2.57E+00	7.99E-02	2.56E+00	8.47E-02	1.83E+00	2.80E-02	1.81E+00	1.83E-02
1.50%	2.01E+00	6.44E-02	2.07E+00	9.23E-02	1.66E+00	3.82E-02	1.65E+00	3.67E-02
1.75%	1.63E+00	2.12E-02	1.62E+00	0.00E+00	1.23E+00	7.41E-02	1.22E+00	6.44E-02
2.00%	1.40E+00	1.83E-02	1.40E+00	1.83E-02	1.12E+00	3.82E-02	1.14E+00	1.83E-02
2.25%	1.23E+00	2.80E-02	1.26E+00	1.06E-02	9.53E-01	1.83E-02	9.53E-01	1.83E-02
2.50%	1.07E+00	3.82E-02	1.10E+00	2.80E-02	8.89E-01	1.83E-02	8.68E-01	3.82E-02

Heat generation data analysis

Recall that the optimum CF content values in single-phase ECAM and two-phase ECAM were 0.75% and 0.5%, respectively, and the optimum CF content in both single-phase and two-phase ECCP was 0.25%. Thus, to support an analogous heating performance comparison between ECAM and ECCP, it was decided to perform active thermography on each matrix type and conductive system at 0.5%, 0.75%, 1% and 1.25% CF values. The reason for selecting 0.5% as the minimum for performing thermography stems from the fact that single-phase and two-phase ECAMs modified with amounts of CF as low as 0.25% were not capable of generating enough heat for the conditions under which the heating tests were performed, i.e., applied voltage of 40V and an environmental temperature of -20°C.

According to Garcia, et al., [28], heat generation has a reciprocal relationship with volume resistivity; the lower the resistivity, the higher the heat generation rate and the greater the amount of heat generated within a specific time window. Figure 6.9 presents the generated heat – in terms of temperature increase within a 4-minute interval for both ECAM conductive systems. The resistivity values of single-phase ECAM at 0.5%, 0.75%, 1% and 1.25% CF are,

respectively, 2.43E+05 Ω.cm, 1.44E+02 Ω.cm, 5.85E+01 Ω.cm and 2.43E+01 Ω.cm. Since these values change in descending order with an increase of CF the hence amount of heat generated increases in ascending order. The reason for no heat generated for single-phase ECAM is first because of its high resistivity (2.43E+05 Ω.cm) and then because the applied voltage was only 40V. If the voltage were tripled to 120V, it would be possible to obtain a higher temperature value at the 4^{th} minute. It was also possible to extend the test time window beyond 4 minutes so that the very slow rate of heat generation for single-phase ECAM at CF content, 0.5%, could possibly be compensated for. However, a 4-minute heating time allows a 15°C temperature increase in single-phase ECAM modified with 1.25% (see Figure 6.9). Note that in Figure 6.9 the overall performance of two-phase ECAM, in terms of heat generation, is better than that of single-phase because of lower resistivity values of two-phase ECAM (due to presence of GP) at CF contents of 0.5%, 0.75%, 1%, and 1.25% that are, respectively, 8.65E+02 Ω.cm, 1.37E+02 Ω.cm, 5.30E+01 Ω.cm and 1.89E+01 Ω.cm. The volume resistivity of two-phase ECAM at 0.5% CF (i.e., 8.65E+02 Ω.cm) is virtually 0.003 of single-phase ECAM volume resistivity at 0.5% CF, but still not low enough to enable transmitting enough current for generating sufficient heat through resistive heating with an applied voltage of 40V. Since there was a 1°C increase in temperature in two-phase ECAM with a volume resistivity of 8.65E+02 Ω.cm, it can be hypothetically concluded that the maximum volume resistivity value for generating heat in a matrix should be close to 800 Ω.cm if the aim were to heat up the matrix with a voltage of only 40V at a low temperature such as -20°C (the ambient temperature at which the heating tests were performed).

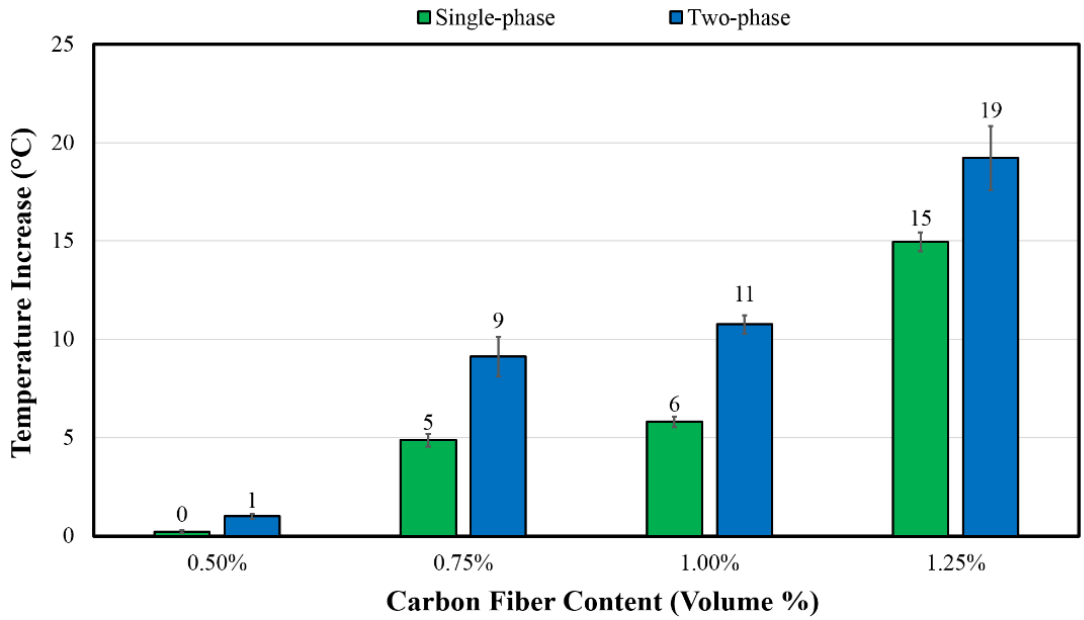

Figure 6.9 *Averaged surface temperature of ECAM specimens after 4 minutes.*

Comparing Figure 6.9 to Figure 6.10, one can easily notice that ECCP is able to produce a greater amount of heat within the test duration of 4 minutes. The reason for such behavior is again because of the lower resistivity of ECCP compared to that of ECAM due to lower resistivity and presence of pores in cement paste. Similar to ECAM, volume resistivity in ECCP has a reciprocal relationship with heat generation rate and the amount of heat produced within a selected time window. The resistivity values of single-phase ECCP at 0.5%, 0.75%, 1% and 1.25% CF are, respectively, 1.85E+01 Ω.cm, 6.15E+00 Ω.cm, 3.37E+00 Ω.cm and 2.56E+00 Ω.cm. Like an identical trend observed for ECAM, such ECCP resistivity values changes are in descending order with increase of CF, hence the amount of heat generated increases in ascending order. The temperature of single-phase ECCP containing 0.5% CF, the minimum CF content according to Figure 6.10, increased up to 26°C after 4 minutes with the applied voltage of 40V.

The largest amount of selected CF content, 1.2%, helped the single-phase ECCP temperature rise up to 124°C.

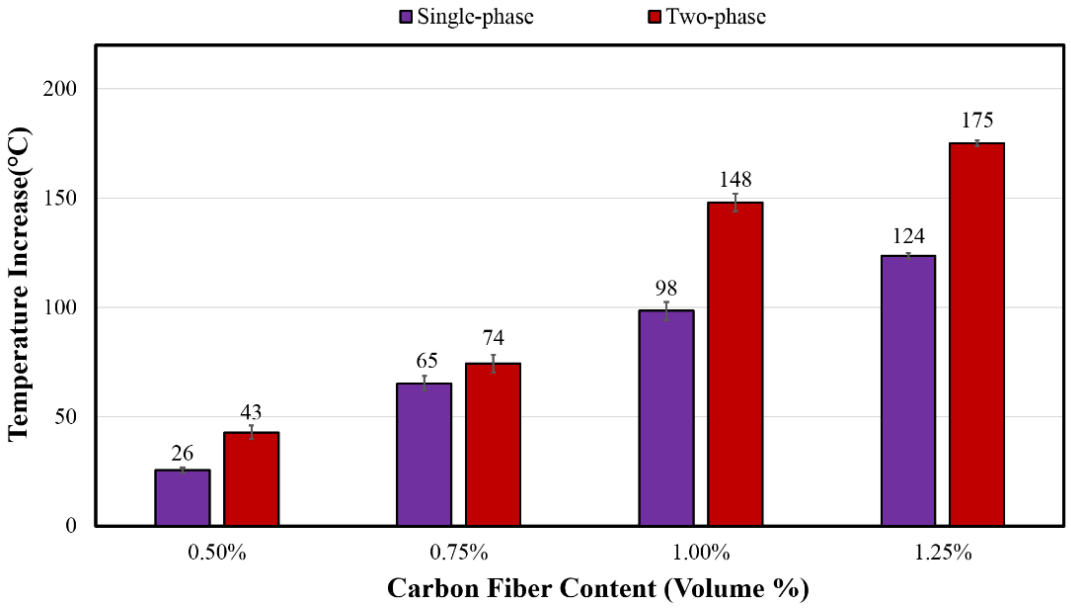

Figure 6.10 *Averaged surface temperature of ECCP specimens after 4 minutes.*

Note that in Figure 6.10 the overall performance of two-phase ECCP, in terms of heat generation, is better than that of single-phase because of lower resistivity values of two-phase ECCP (due to presence of GP) at CF contents of 0.5%, 0.75%, 1% and 1.25% that are, respectively, 9.79E+00 Ω.cm, 4.62E+00 Ω.cm, 2.39E+00 Ω.cm and 1.81E+00 Ω.cm.

Within the test time window of 4 minutes, the applied voltage of 40V caused a moderate temperature increase in both single-phase and two-phase ECAM at CF dosage rates of 1% and 1.25% (see Figure 6.9), while the same voltage of 40V caused a drastic increase in temperature for both single-phase and two-phase ECCP modified with the same CF dosage rates of 1% and 1.25% (see Figure 6.10). The self-heating behavior of ECAM and ECCP can be made more comparable, in terms of temperature increase within a certain time window, by applying a higher voltage on ECAM and applying a lower voltage on ECCP. The reason for not varying this

voltage in this study was because the authors' aim was to provide equal test condition resulting in analogous comparison.

Fig. 11a and Fig. 11b depict temperature versus time curves for, respectively, single-phase and two-phase ECAM. The selected CF content for single-phase ECAM and two-phase ECAM are, respectively, 1% and 0.75%, both 0.25% more than their identified optimum CF contents (see Fig. 1). Selecting CF contents slightly higher than optimum helps in heat generation and simultaneously prevents increased cost and degraded workability. Note that in Fig. 11a the heating rate is very slow because of the applied voltage of 40V; moreover, the test temperature condition of -20°C did not allow heat buildup on the specimen surfaces. It can be inferred that the rate of heat generated on the surface of single-phase ECAM containing 1% CF is only slightly higher than the amount lost and use of a higher voltage could obviously have increased the temperature increase rate. According to Fig. 11b, the average heating rate observed in two-phase ECAM is 2.5 °C/minute, virtually twice the value calculated for single-phase ECAM, i.e., 1.2°C/minute (see Fig. 11a). The superiority of two-phase ECAM over single-phase ECAM can be justified through their measured volume resistivity values, because the resistivity of two-phase ECAM is 5.30E+01 Ω.cm, virtually one-third of the value measured for single-phase ECAM, 1.44E+02 Ω.cm, so it can be concluded that the lower the resistivity the higher the rate of temperature increase in ECAM; it is worth noting that the same trend was observed in other ECAM specimens at different CF dosage rates, i.e., resistivity had a reciprocal relationship with the rate of temperature increase.

Fig. 11c and Fig. 11d depict temperature versus time curves obtained from, respectively, single-phase and two-phase ECCP. The selected CF content for both single-phase and two-phase ECCP is 0.5%, 0.25% more than their optimum CF contents (see Fig. 2). The heating rate of

single-phase ECCP is 6.4°C/minute and that of two-phase ECCP is 11°C/minute, about twice the rate measured for single-phase ECCP. The reason for such behavior is again due to the lower resistivity of two-phase ECCP, 9.79E+00 Ω.cm, half the value calculated for single-phase ECCP that, 1.85E+01 Ω.cm. In a similar way to that observed for ECAM, it can be concluded that the lower the resistivity of ECCP the higher the temperature rate increase.

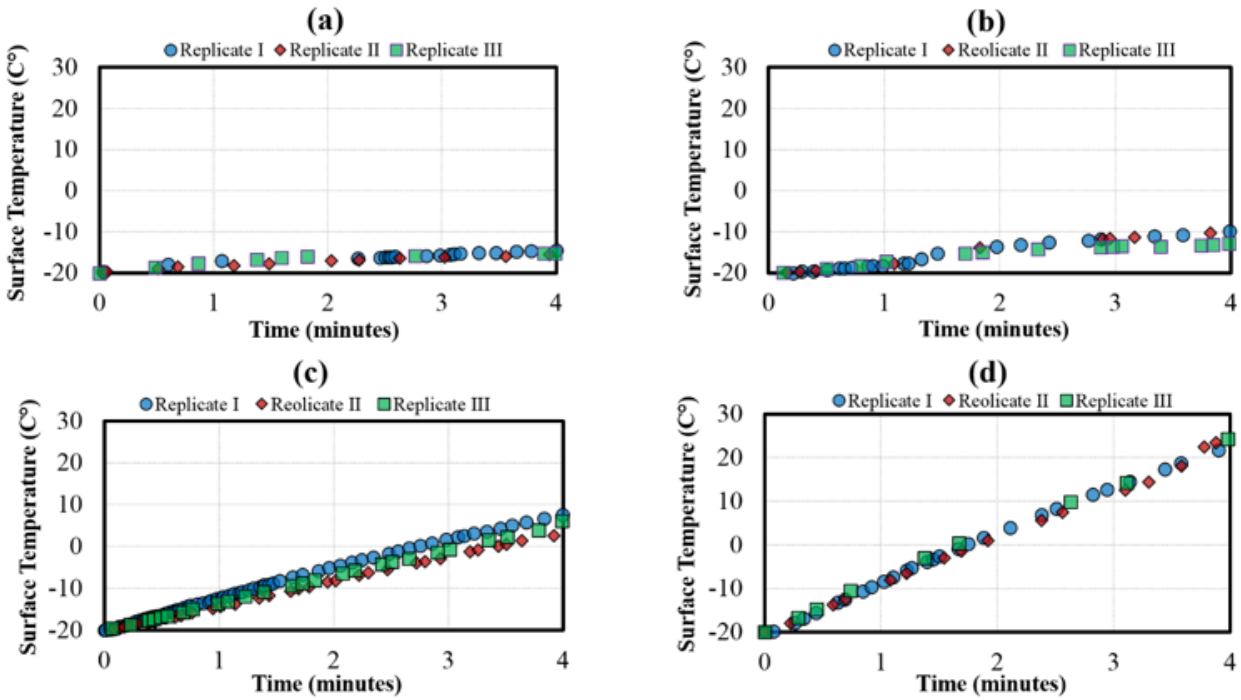

Figure 6.11 *Temperature plot quantifying the heat generation in: (a) single-phase ECAM at 1% CF, (b) two-phase ECAM at 0.75% CF, (c) single-phase ECCP at 0.5% CF, and (d) two-phase ECCP at 0.5% CF.*

Based on the conclusions drawn from Fig. 11, it can be stated that, to increase the heating rate in a matrix (ECAM or ECCP), the resistivity should be decreased. It is also worth noting that for melting ice/snow or curbing their formation/accumulation on the surface of a pavement paved with ECAC or ECON, it would be sufficient only to increase/keep the temperature to/at a temperature a few degrees Celsius above the freezing temperature point of water, i.e., about 3°C. Depending on the type of matrix (ECAM or ECCP) used for binding the aggregate together to

produce an electrically-conductive concrete (i.e., ECAC or ECON), one can arrive at an efficient mix design to produce a heated pavement system having efficient anti-icing and de-icing capabilities. For such design, there are a few factors that should be taken into account, including field ambient temperature history during the cold seasons of the year, the applied voltage, the matrix type, and the intended melting duration of ice or snow, especially for deicing purposes.

Fig.12 provides thermographs obtained from both single-phase and two-phase matrices (ECAM and ECCP) tdhat provide a more tangible understanding of heating performance of these matrices after 4 minutes of being exposed to an electrical potential difference of 40V.

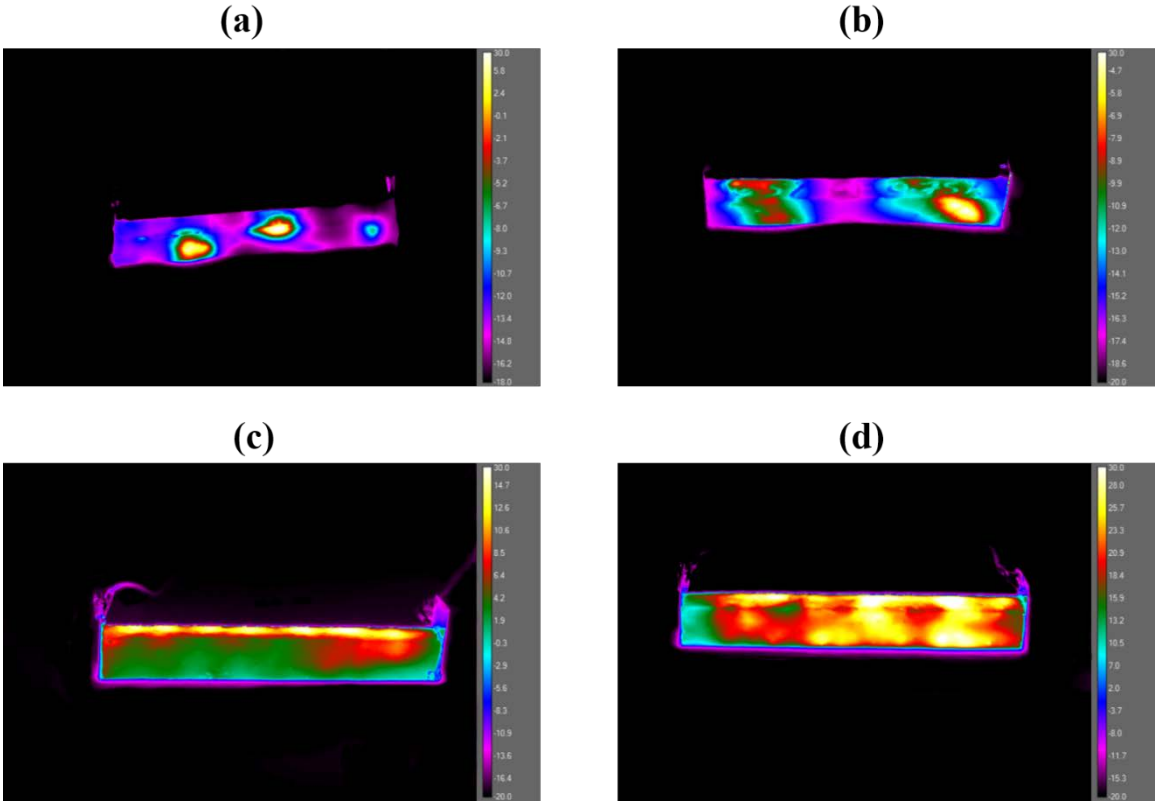

Figure 6.12 *Thermographs obtained at 4th minute from: (a) single-phase ECAM at 1% CF, (b) two-phase ECAM at 0.75% CF, (c) single-phase ECCP at 0.5% CF, and (d) two-phase ECCP at 0.5% CF.*

Findings and conclusions

The objective of this study was to produce electrically-conductive asphalt mastic (ECAM) and electrically-conductive cement paste (ECCP) so that when they fill the voids in an aggregate system the result would be either a highly-efficient electrically-conductive asphalt concrete (ECAC) or a highly-efficient electrically-conductive portland cement concrete (ECON) with application in heated pavement systems to anti-icing and deicing purposes. To this end, single-phase and two-phase matrices (both ECAM and ECCP) were prepared by modifying asphalt mastic and cement paste with addition of carbon fiber (CF) at variable contents and adding graphite powder (GP) at constant content. Volume resistivity of single-phase (containing only CF) and two-phase (containing CF and GP) matrices were measured at different CF contents. The optimum values of CF content were identified, and the influence of temperature change on volume resistivity of each matrix type was investigated for a few selected CF content values, i.e., optimum CF content value and a few CF content values above the optimum. The amount of temperature increase, i.e., heating efficiency, was measured and evaluated by performing active infrared thermography (IRT) at a below-freezing temperature for each matrix type modified with CF and GP for the aforementioned selected CF contents; moreover, the rate of temperature increase was calculated for each matrix type containing CF at a content slightly higher than optimum. Based on IRT results, it was shown that each matrix type is capable of generating heat, and this heat generation can be adjusted based on the design resistivity and the matrix type used. All the efforts in this study lead to the following outcomes:

- The optimum CF contents obtained for single-phase ECAM and two-phase ECAM were 0.75% and 0.5%, respectively, and for both single-phase ECCP and two-phase ECCP was 0.25%. The reason for obtaining the optimum CF at a lower value in ECCP stems from the

fact that volume resistivity of cement paste is two orders of magnitude smaller than that of asphalt mastic.

- Addition of GP to ECAM resulted in a much smoother insulator-to-conductor transition compared with the transition observed in ECCP. While presence of 5% graphite powder in the matrix causes a huge reduction in volume resistivity of ECAM and ECCP at CF volume contents less than the optimum identified for single-phase systems, presence of graphite powder becomes less influential as CF content increases and this is attributed to saturation of matrices at such high dosage rates dwarfing conductivity enhancement due to a bridging effect.
- Compared with asphalt mastic, incorporation of conductive materials into cement paste results in a smoother insulator-to-conductor transition. The reason for such smooth behavior, curves that are not S-shaped, stems from the fact that cement paste is two orders of magnitude more conductive than asphalt mastic.
- It was expected that, due to saturation of matrices (both asphalt mastic and cement paste), in CFs at high dosage rates, their volume resistivities become identical; however, due to presence of micro-structured pores in cement paste many CFs are in direct contact at high dosage rates while relative absence of a uniformly distributed pore structure in asphalt mastic matrix results in a smaller probability of fiber-fiber contact and such direct contact is usually interrupted by a very thin asphalt film. As a result, it would be possible to decrease the difference between the volume resistivities of ECAM and ECCP by saturation of the matrices with CF, but impossible to make their volume resistivity values identical to the high dosage rates of CF.

- When exposed to a temperature drop of 20°C the volume resistivity of self-heating ECAM (both single-phase and two-phase), at CF dosage rates above the optimum, dropped considerably while such a systematic tangible change was not observed in self-heating ECCP when exposed to the same temperature change at CF content equal to or greater than optimum. Such temperature susceptibility ensures enhanced heating performance of self-heating ECAM at lower temperatures, and it can be concluded that self-heating ECCP – containing high dosage rates of CF – is more stable in terms of volume resistivity when exposed to a temperature change of 20°C.
- If the purpose for production of ECAM and ECCP, to fill the voids in aggregates for producing ECAC and ECON, is for the purpose of achieving an anti-icing and deicing pavement surface, their conductive material contents should be equal to or greater than optimum content so that these matrices can generate enough heat through resistive heating to let ECAM and ECCP behave as self-heating materials.
- Heat generation has a reciprocal relationship with volume resistivity in both ECAM and ECCP; the lower the resistivity, the higher the heat generation rate and the greater the value of heat generated within a specific time window.
- In addition to matrix type and conductive material content, the energy conditioning of ECAM and ECCP such as applied voltage and test duration can influence heating performance. For example, it would be possible to increase the voltage for a matrix with lower resistivity and lower CF content, but still higher than optimum, to compensate for slow rate of temperature increase or within a selected time window. It also would be possible to extend the heating duration to compensate for lower temperature-increase rates and obtain higher temperatures at durations beyond 18 minutes.

Acknowledgments

This paper was prepared from a study conducted at Iowa State University under the Federal Aviation Administration (FAA) Air Transportation Center of Excellence Cooperative Agreement 12-C-GA-ISU for the Partnership to Enhance General Aviation Safety, Accessibility and Sustainability (PEGASAS). The authors would like to thank the current project Technical Monitor, Mr. Benjamin J. Mahaffay, and the former project Technical Monitors, Mr. Jeffrey S. Gagnon (interim), Mr. Donald Barbagallo, and Dr. Charles A. Ishee for their invaluable guidance on this study. The authors also would like to thank the PEGASAS Industry Advisory Board members for their valuable support and feedback. The assistance and efforts of Mr. Robert F. Steffes and Mr. Theodore Huisman, ISU Lab Managers, with the lab investigations are greatly appreciated. The authors would also like to express their sincere gratitude to Mr. Paul Kremer, ISU CCEE Program Manager for his significant assistance with lab and equipment accessibility. The assistance of Nathan Ross, an undergraduate student research assistant at ISU, with the lab work is greatly appreciated. The authors would like to thank Jebro Inc. and Asbury Carbons Inc. for kindly donating the materials used in this study. Although the FAA sponsored this project, it neither endorses nor rejects the findings of this research. The presentation of this information is in the interest of invoking comments by the technical community on the results and conclusions of the research.

References

[1] S. Wu, P. Pan, M. Chen, and Y. Zhang, “Analysis of Characteristics of Electrically Conductive Asphalt Concrete Prepared by Multiplex Conductive Materials,” J. Mater. Civ. Eng., vol. 25, no. 7, pp. 871–879, 2012.

[2] A. Sassani, H. Ceylan, S. Kim, A. Arabzadeh, P. C. Taylor, and K. Gopalakrishnan, “Development of Carbon Fiber-modified Electrically Conductive Concrete for

Implementation in Des Moines International Airport," Case Stud. Constr. Mater., vol. 8, no. October 2017, pp. 277–291, 2018.

[3] D. D. L. Chung, Multifunctional cement-based materials. CRC Press, 2003.

[4] D. D. L. Chung, "Electrical conduction behavior of cement-matrix composites," J. Mater. Eng. Perform., vol. 11, no. 2, pp. 194–204, 2002.

[5] P. W. Chen, X. Fu, and D. D. L. Chung, "Microstructural and mechanical effects of latex, methylcellulose, and silica fume on carbon fiber reinforced cement," Mater. J., vol. 94, no. 2, pp. 147–155, 1997.

[6] H. A. Toutanji, T. El-Korchi, and R. N. Katz, "Strength and reliability of carbon-fiber-reinforced cement composites," Cem. Concr. Compos., vol. 16, no. 1, pp. 15–21, 1994.

[7] P.-W. Chen and D. D. L. Chung, "Low-drying-shrinkage concrete containing carbon fibers," Compos. Part B, vol. 27B, no. 95, pp. 269–274, 1996.

[8] S. M. Abtahi, M. Sheikhzadeh, and S. M. Hejazi, "Fiber-reinforced asphalt-concrete - A review," Constr. Build. Mater., vol. 24, no. 6, pp. 871–877, 2010.

[9] P. Science, N. Carolina, N. Carolina, Y. R. I. K. Im, R. O. Y. H. B. Orden, E. Engineering, N. Carolina, and S. J. Lee, "Fatigue Cracking Resistance of Fiber-Reinforced Asphalt Concrete," Text. Res. J., vol. 75, no. 2, pp. 123–128, 2005.

[10] B. Huang, X. Chen, and X. Shu, "Effects of Electrically Conductive Additives on Laboratory-Measured Properties of Asphalt Mixtures," J. Mater. Civ. Eng., vol. 21, no. 10, pp. 612–617, 2009.

[11] S. Wu, L. Mo, Z. Shui, and Z. Chen, "Investigation of the conductivity of asphalt concrete containing conductive fillers," Carbon N. Y., vol. 43, no. 7, pp. 1358–1363, 2005.

[12] X. Liu and S. Wu, "Study on the graphite and carbon fiber modified asphalt concrete," Constr. Build. Mater., vol. 25, no. 4, pp. 1807–1811, 2011.

[13] A. Arabzadeh, H. Ceylan, S. Kim, K. Gopalakrishnan, A. Sassani, S. Sundararajan, and P. C. Taylor, "Superhydrophobic coatings on Portland cement concrete surfaces," Constr. Build. Mater., vol. 141, pp. 393–401, 2017.

[14] J. Wu, J. Liu, and F. Yang, "Three-phase composite conductive concrete for pavement deicing," Constr. Build. Mater., vol. 75, pp. 129–135, 2015.

[15] S. Wen and D. D. L. Chung, “Carbon fiber-reinforced cement as a thermistor,” Cem. Concr. Res., vol. 31, no. 4, pp. 665–667, 2001.

[16] Q. Liu, E. Schlangen, M. Van De Ven, and Á. García, “Induction Healing of Porous Asphalt,” Transp. Res. Rec. J. Transp. Res. Board, pp. 527–542, 2010.

[17] P. Park, Y. Rew, and A. Baranikumar, “Controlling conductivity of asphalt concrete with graphite,” Southwest Region University Transportation Center, 2014.

[18] S. Wen and D. D. L. Chung, “The role of electronic and ionic conduction in the electrical conductivity of carbon fiber reinforced cement,” Carbon N. Y., vol. 44, no. 11, pp. 2130–2138, 2006.

[19] V. H. Guerrero, S. Wang, S. Wen, and D. D. L. Chung, “Thermoelectric property tailoring by composite engineering,” J. Mater. Sci., vol. 37, no. 19, pp. 4127–4136, 2002.

[20] P. Cong, P. Xu, and S. Chen, “Effects of carbon black on the anti aging, rheological and conductive properties of SBS/asphalt/carbon black composites,” Constr. Build. Mater., vol. 52, pp. 306–313, 2014.

[21] A. Sassani, H. Ceylan, S. Kim, K. Gopalakrishnan, A. Arabzadeh, and P. C. Taylor, “Influence of mix design variables on engineering properties of carbon fiber-modified electrically conductive concrete,” Constr. Build. Mater., vol. 152, pp. 168–181, 2017.

[22] A. Sassani, H. Ceylan, S. Kim, K. Gopalakrishnan, A. Arabzadeh, and P. C. Taylor, “Factorial study on electrically conductive concrete mix design for heated pavement systems,” in Transportation Research Board 96th Annual Meeting, 2017, pp. 1–19.

[23] A. L. Materazzi, F. Ubertini, and A. D. Alessandro, “Carbon nanotube cement-based sensors for dynamic monitoring of concrete structures,” Res. Conf. Pap., no. November 2015, pp. 4–7, 2013.

[24] X. Maldague and S. Marinetti, “Pulse phase infrared thermography,” Appl. Phys, vol. 2694, no. 1996, 2013.

[25] A. Arabzadeh and M. Güler, “Influence of mixture design variables on thermal coefficient of asphalt concrete,” in Proceedings of Conference on Advances in Civil Engineering, 2014, pp. 1–6.

[26] C. C. Chen and Y. C. Chou, “Electrical-conductivity fluctuations near the percolation threshold,” Phys. Rev. Lett., vol. 54, no. 23, pp. 2529–2532, 1985.

[27] H. Wang, J. Yang, H. Liao, and X. Chen, “Electrical and mechanical properties of asphalt concrete containing conductive fibers and fillers,” Constr. Build. Mater., vol. 122, pp. 184–190, 2016.

[28] Á. García, E. Schlangen, M. Van De Ven, and Q. Liu, “Electrical conductivity of asphalt mortar containing conductive fibers and fillers,” Constr. Build. Mater., vol. 23, no. 10, pp. 3175–3181, 2009.

[29] S. Wen and D. D. L. Chung, “Double percolation in the electrical conduction in carbon fiber reinforced cement-based materials,” Carbon N. Y., vol. 45, no. 2, pp. 263–267, 2007.

[30] S. Paschen, M. N. Bussac, L. Zuppiroli, E. Minder, and B. Hilti, “Tunnel junctions in a polymer composite,” J. Appl. Phys., vol. 78, no. 5, pp. 3230–3237, 1995.

[31] W. S. Bao, S. A. Meguid, Z. H. Zhu, and G. J. Weng, “Tunneling resistance and its effect on the electrical conductivity of carbon nanotube nanocomposites,” J. Appl. Phys., vol. 111, no. 9, 2012.

[32] H. A. Tang, X. Chen, and Y. Lu, “Studies on the PTC/NTC effect of carbon black filled low density polyethylene composites,” Eur. Polym. J., vol. 33, no. 8, pp. 1383–1386, 1997.

[33] W. J. McCarter, “Effects of Temperature on Conduction and Polarization in Portland Cement Mortar,” J. Am. Ceram. Soc., vol. 78, no. 2, pp. 411–415, 1995.

CHAPTER 7. CONCLUSIONS AND RECOMMENDATIONS FOR FUTURE WORK

Summary

The goal of this study was to produce nano-engineered heated pavement systems (both flexible and rigid) for ice-and snow-free pavement applications. To this end, first the feasibility of producing nano-based superhydrophobic (super water-repellent) hot mix asphalt (HMA) and superhydrophobic portland cement concrete (PCC) with potential ice-repellent characteristics was investigated. Then the possibility of producing electrically conductive asphalt mastic (ECAM) and electrically-conductive cement paste (ECCP) was thoroughly studied to make sure that when either of these matrices (both ECAM and ECCP) bind an aggregate system together, the result would be either an electrically-conductive asphalt concrete (ECAC) or an electrically conductive portland cement concrete (ECON) that could efficiently melt ice/snow or prevent/curb their formation/accumulation.

For producing superhydrophobic HMA and PCC, a layer-by-layer (LBL) spray-deposition technique was developed and used for spraying fluorine or silane-based low surface energy materials on HMA and PCC surfaces to produce hierarchical water-repellent nano-based coatings; water repellency of these spray-coated surfaces was then characterized through static water contact angle measurements. Works of adhesion also were calculated based on the measured static water contact angles. After confirming the water-repellency of these surfaces with respect to potential ice-repellent characteristics, their skid resistance was evaluated by measurement of friction coefficients or determination of British pendulum numbers.

ECAM and ECCP were fabricated by incorporation of carbon-based electrically-conductive materials into either asphalt mastic or cement paste. Optimum conductive material contents and the conductive material dosage rates suitable for anti-icing and deicing purposes were identified through characterization of both ECAM and ECCP volume resistivities. The electrical temperature-susceptibility of ECAM and ECCP was evaluated to ensure that these matrices can generate enough heat when they are used in ECAC and ECON implemented in the field. Heat generation efficiency of these electrically-conductive matrices was then characterized by performing active infrared thermography (IRT) at below-freezing temperatures.

The research presented in this dissertation has led to multiple novel findings and innovations. In each chapter of this study, i.e., Chapters 1 through 6, a new finding, a new product or a new application of a material/method has been provided. Some of the main contributions of this research are:

- Proving the feasibility of using a LBL spray deposition technique for coating asphalt concrete and portland cement concrete surfaces with low surface energy materials.
- Demonstrating the effectiveness of fluorine-based and silane-based low surface energy materials for producing superhydrophobic coatings, with hierarchical roughness, on HMA and PCC surfaces.
- Enhancing skid-resistant superhydrophobic PCC by texturizing the surface of fresh concrete before coating the hardened concrete surfaces using an LBL method.
- Proving the efficiency of carbon-based electrically conductive materials such as CF and GP for enhancing the electrical conductivity of ECAM and ECCP.

- Discovering the electrical temperature-susceptibility of ECAM and demonstrating the improvement in ECAM electrical conductivity at lower temperatures.
- Investigating the heating efficiency of ECAM and ECCP at below-freezing temperatures, and comparing the heating performance of the matrices when exposed to the same electrical potential difference.

It is hoped that the findings of this study will contribute to production of hybrid heated pavement systems (i.e., pavement systems in which ice-repellent coating technology is merged with ECAM and/or ECON technology) for accelerating the ice/snow melting process or preventing accumulation of snow or formation of ice in critical areas such as airfield pavements, bridge decks, etc. where achieving ice-and snow-free surfaces is of paramount importance.

Conclusions

The following conclusions present the major findings of this study for helping achieve the goal of this research.

Superhydrophobic Coatings on Asphalt Concrete Surfaces: Toward Smart Solutions for Winter Pavement Maintenance

Superhydrophobic coated HMA surfaces were created, characterized, and evaluated. The layer by layer (LBL) method and the micro-tribometer based coefficient of friction measuring method were employed to create superhydrophobic coatings and to characterize skid resistance of superhydrophobic coated substrates at micro-texture level. A statistical design based experimental test program was developed and conducted to evaluate the effect

of different test variables, including spray times and dosage rates of PTFE. The major conclusions drawn from test procedures and results are summarized below:

- Using LBL method for spray depositing the PTFE particles seems to be a promising method for achieving ice-repellent surfaces having potential for mitigating problems associated with ice accretion or snow accumulation on the roadways or airfield areas paved with nano-coated asphalt concrete.
- The micro-tribometer-based coefficient of friction method designed and demonstrated in this study can be a promising method for characterizing skid resistance of nano-coated asphalt concrete at micro-texture level.
- Spray time is a significant factor affecting superhydrophobicity. Increasing the spray duration from 3 seconds to 6 seconds resulted in achieving contact angles greater than 150°, and at other spray times of 9 and 12 seconds, the superhydrophobicity still remained, even though super water-repellency did not uniformly increase for all of the specimens after 6 seconds. Increasing the amount of PTFE up to a certain level in nano-coating of asphalt concrete can also increase ice/snow repellency. Above that level, adding to the deposition amount of PTFE becomes uneconomical and does not significantly increase superhydrophobicity.
- In a manner similar to superhydrophobicity, spray time had a significant influence on the coefficient of friction. While increasing the spray time from 3 seconds to 6 seconds drastically increased skid resistance on the asphalt concrete samples, when PTFE is sprayed on epoxy in the field, it should be

kept in mind that if sufficient spraying deposition duration is not allowed, the epoxy not covered with PTFE could slightly decrease the skid resistance over the roadway/runway.

- In the context of micro-texture, PTFE results in obtaining comparable or even higher skid resistance measured on the nano-coated asphalt concrete at 6-second spray time for all PTFE dosages. If the spray time and dosage of PTFE are wisely selected, nano-coated pavements can provide high coefficients of friction at low speeds.
- In the context of macro-texture, the main contributors to improving skid resistance are shape, distribution, and angularities of the coarse aggregate present in the asphalt concrete. In other words, the physical properties of aggregate and their distribution should be the main concern in pavements coated at high speed with the super-ice/water repellent nanomaterials like PTFE. This issue is recommended for further study to implement the use of superhydrophobic coatings in actual snow and ice removal strategies for flexible pavement systems.

Superhydrophobic Coatings on Portland Cement Concrete Surfaces

The feasibility of producing super water/ice-repellent portland cement concrete was investigated in an laboratory environment. The LBL spray deposition technique was utilized for producing three different nano-based superhydrophobic coatings on concrete surfaces. A statistical design-based experimental test program was conducted on the measured responses (i.e., WCAs) to evaluate the effect of different test variables, including spray durations and coating types. A British pendulum tester was used for investigating the influence of different

concrete surface textures on enhancing the skid resistance of the surfaces coated with the most wear-resistant coating. The efforts made in this study led to the following conclusions:

- Low surface energy materials like PTFE, PEEK and silanized DE can help achieve water/ice-repellent surfaces with potential for mitigating winter maintenance issues on roadways and airfield areas paved with PCC.
- The Layer-by-layer (LBL) spray deposition technique was for the first time utilized to create superhydrophobic PCC for ice-and snow-free rigid pavement applications. The detailed procedure has been clearly documented in a step-by-step manner so that the researchers and practitioners can study and implement this technology.
- Spray duration significantly affects the superhydrophobicity. The WCA increased for all the specimens except for those coated with PTFE with the spray interval increasing from 4 to 10 seconds. The specimens coated with PTFE showed the same trend for intervals of 4 to 8 seconds, indicating that this type of coating reaches its best performance at the spray duration of 8 seconds among the spray durations selected for this study.
- Similar to the spray duration, the type of low surface energy material selected had an important impact on the degree of hydrophobicity. Within a spray duration range of 4-8 seconds, the PCC specimens coated with silanized DE were the most superhydrophobic, followed by the PTFE. The 4-second spray deposition of PTFE/PEEK resulted in obtaining an overhydrophobic, but not superhydrophobic, surface, although for this type of coating all other spray durations resulted in obtaining superhydrophobic PCC specimens. The silanized DE reached an excellent

degree of superhydrophobicity with a measured WCA greater than 160° at a spray duration of 10 seconds. This is the first time that a superhydrophobic PCC with such a high degree of superhydrophobicity has been engineered.

- Texturizing the surface of PCC can considerably enhance the skid resistance of super water/ice-repellent rigid pavements. Transverse turf drag texture and transverse and longitudinal-tined surface are good candidates for enhancing the skid resistance of superhydrophobic rigid pavements.

Electrically-conductive Asphalt Mastic: Temperature Dependence and Heating Efficiency

Single-phase and two-phase electrically-conductive asphalt mastics (ECAMs) were fabricated with efficient heat generation capabilities, so that when they fill the voids within mineral aggregates, the results produce anti-icing or de-icing electrically-conductive asphalt concretes (ECACs) for heated pavement applications. To this end, ECAM specimens were prepared, their volume resistivities measured, and their low-resistivity regions identified; moreover, electrical temperature-susceptibility of ECAM specimens was investigated. After identifying and analyzing low-resistivity regions for both single-phase and two-phase ECAMs, it was decided to investigate heat generation efficiency only for single-phase ECAM at a certain of level carbon fiber (CF) content, and at a below-freezing temperature. Based on the results obtained from the heating test, it was found that single-phase ECAM at the selected CF content can generate enough heat for anti-icing and deicing purposes. The results of this study led to the following conclusions:

- The optimum CF content values for single-phase and two-phase ECAM were found to be 0.75% and 0.5%, respectively, and the presence of 5% GP results in an optimum CF content at a lower volume content of CF, i.e., the optimum CF of single-phase ECAM is lower than that for two-phase ECAM.
- Presence of GP particles at a volume content of 5% causes a huge reduction in volume resistivity when CF content is low, e.g., 0.25 % and 0.5%. Addition of 5% GP has little influence on volume resistivity reduction in the low resistivity region, 0.75 to 2.5% CF content, of single-phase ECAM.
- Addition of very small amounts of conductive materials to asphalt mastic changes its behavior from NTC to PTC. For example, in this study contents of only 5% (GP) or 0.25% (CF) in asphalt mastic, exposed to a 20°C temperature drop, caused reductions in resistivity values by 2.2% and 10.1%, respectively.
- The PTC behavior of ECAM, i.e., reduction in resistivity value due to a temperature reduction of 20°C, reaches its maximum value at optimum CF contents of 0.75% and 0.5%, respectively, for single-phase and two-phase specimens.
- All the temperature versus time curves obtained from the ECAM replicates prepared with only 1% carbon fiber nearly coincided during the first 4 minutes after the temperature was increased from -18°C to 4.5°C.
- While ECAM specimens modified with carbon fiber content of 1% have potential for melting ice and snow, the selected volume content of 1% might be changed if the mastic is considered to be a component of asphalt concrete.

Electrical and Thermal Properties of Cement Paste and Asphalt Mastic Modified by Electrically-conductive Carbon-based Materials

Electrically-conductive asphalt mastic (ECAM) and electrically-conductive cement paste (ECCP) were fabricated in a laboratory environment, and it was expected that when they filled the voids in an aggregate system the result would be a highly efficient electrically-conductive asphalt concrete (ECAC) or a highly efficient electrically-conductive portland cement concrete (ECON) with applications in heated pavement systems for anti-icing and deicing purposes. To this end, single-phase and two-phase matrices (both ECAM and ECCP) were prepared by modifying asphalt mastic and cement paste with addition of carbon fiber (CF) at variable contents and adding graphite powder (GP) at a constant content. Volume resistivity of single-phase (containing only CF) and two-phase (containing CF and GP) matrices were measured at different CF contents. The optimum CF contents were identified, and the influence of temperature change on volume resistivity of each matrix type was investigated for a few selected CF contents, i.e., optimum CF content and a few CF contents above the optimum. The amount of temperature increase, i.e., heating efficiency, was measured and evaluated by performing active infrared thermography (IRT) at a below-freezing temperature for each matrix type modified with CF and GP at the aforementioned selected CF contents; moreover, the rate of temperature increase was calculated for each matrix type containing CF at a content slightly higher than optimum. Based on the IRT results, it was revealed that each matrix type is capable of generating heat, and this heat generation can be adjusted based on the design resistivity and the matrix type used. All the efforts in this study lead to the following outcomes:

- The optimum CF contents obtained for single-phase ECAM and two-phase ECAM were 0.75% and 0.5% respectively, and that obtained for both single-phase ECCP and two-phase ECCP was 0.25%. The reason for the lower optimum CF in ECCP stems from the fact that volume resistivity of cement paste is two orders of magnitude smaller than that of asphalt mastic.
- Addition of GP to ECAM resulted in a much smoother insulator-to-conductor transition compared to the transition observed in ECCP because of addition of GP. Presence of 5% graphite powder in the matrix causes a huge reduction in volume resistivity of ECAM and ECCP at CF volume content less than the optimum identified for single-phase systems. However, presence of graphite powder becomes less influential as CF content increases, and this is attributed to saturation of matrices at such high dosage rates dwarfing the conductivity enhancement due to bridging effects.
- Compared with asphalt mastic, incorporation of conductive materials into cement paste results in a smoother insulator-to-conductor transition. The reason for such smooth behavior, curves which are not S-shaped, stems from the fact that cement paste is two orders of magnitude more conductive than asphalt mastic.
- It was expected that, due to saturation of matrices (both asphalt mastic and cement paste) for CFs at high dosage rates, their volume resistivities become identical; however, due to presence of micro-structured pores in cement paste, many CFs are in direct contact at high dosage rates, while the absence of a uniformly distributed pore structure results in a smaller probability of fiber-fiber contact in asphalt mastic matrix, and such direct contact is usually interrupted by a very thin asphalt film. As a result, while it is possible to decrease the difference between the volume resistivities of

ECAM and ECCP by saturation of the matrices with CF, it is impossible to make their volume resistivity values identical at high dosage rates of CF.

- When exposed to a temperature drop of 20°C the volume resistivity of self-heating ECAM (both single-phase and two-phase), at CF dosage rates above the optimum, dropped considerably while such systematic tangible change was not observed in self-heating ECCP at CF content greater than optimum when exposed to the same temperature change. Such temperature susceptibility ensures enhanced heating performance of self-heating ECAM at lower temperatures, and it can be concluded that self-heating ECCP containing high dosage rates of CF is more stable in terms of volume resistivity when exposed to a temperature change of 20°C.
- If the purpose for production of ECAM and ECCP, filling the voids in aggregates to produce ECAC and ECON, is to achieve an anti-icing and deicing pavement surface, their conductive material contents should be equal to optimum or greater than optimum content so that these matrices can generate sufficient heat through resistive heating and let the ECAM and ECCP behave like self-heating materials.
- Heat generation has a reciprocal relationship with volume resistivity in both ECAM and ECCP; the lower the resistivity, the higher the heat generation rate and the greater the value of heat generated within a specific time window.
- In addition to the matrix type and conductive material content, the energy conditioning of ECAM and ECCP, such as applied voltage and test duration, can influence the heating performance. For example, it would be possible to increase the voltage for a matrix with lower resistivity and lower CF content, but still higher than optimum, to compensate for a slow rate of temperature increase or within a selected time window.

It also would be possible to extend the heating duration to compensate for lower temperature increase rates and obtain higher temperatures at durations beyond 18 minutes.

Recommendations for Future Studies

In addition to the conclusions drawn in this study, some recommendations will be presented, and it is hoped that they can help establish milestones for future studies.

Superhydrophobic Coatings on Asphalt Concrete Surfaces: Toward Smart Solutions

Contact angle and friction coefficient measurements were all performed at ambient temperature. Since flexible pavements coated with superhydrophobic PTFE must curb the formation of ice/snow in cold climatic conditions, it is recommended to perform these tests again at lower temperatures. In this way the effect of temperature on spray deposition, water/ice repellency, and skid resistance can be determined.

Superhydrophobic Coatings on Portland Cement Concrete Surfaces

There is a huge number of different types of water-repellent materials and spray deposition techniques that should be investigated in further studies related to finding smart solutions for winter pavement maintenance. Although, according to the reported literature, superhydrophobicity leads to ice-repellency, it is recommended that the force required to detach the ice from the surface of superhydrophobic concrete be directly measured to determine whether any ice will attach to this type of concrete. Another issue that needs investigation is the durability of nano-coatings on paved areas; there is a need for producing a standard test setup for measuring the wear resistance of these coatings on PCC surfaces. After performing this investigation, the appropriate materials resulting in the most economical approach should be utilized for spray deposition on PCC surfaces. Producing

superhydrophobic concrete is all about achieving a balance between cost and performance, i.e., one should decide between either increased lifespan and increased cost, or decreased lifespan and lower cost. It is also possible to nano-treat the surface of heated PCC pavements, then investigate the combined effect of these technologies on removing ice and snow.

Electrically-conductive Asphalt Mastic: Temperature Dependence and Heating Efficiency

Because presence of aggregates can change the electrical properties of ECAM, the findings of this study could be used for producing ECAC allowing the influence of the aggregate system on changes in ECAM electrical properties to be investigated. Moreover, different aggregate types have different thermal coefficients, so there is a need to find the best type with respect to improving the PTC effect of ECAM by further reducing the energy consumption of ECAC. The authors will also investigate electromagnetic interference shielding of ECAM at different volume dosage rates of CF, because electrically conductive materials are capable of reflecting radiation, suggesting applications for protection of transformers and electronic devices housed in underground concrete vaults.

Electrical and Thermal Properties of Cement Paste and Asphalt Mastic Modified by Electrically-conductive Carbon-based Materials

Aggregates can also alter the properties of ECAM and ECCP, so the findings of this study should be used for producing ECAC and ECON, and then investigating the influence of different aggregate types on changing the thermal and electrical properties of these types of concrete. Since PCC (because of the intrinsic hydrophilic property of portland cement) can absorb more water than HMA (because of the intrinsic hydrophobic property of bitumen), it

would be necessary to compare their heating performance at different degrees of saturation so that a more robust conclusion can be drawn.